Multi-scale analysis of soil erosion and its impact on soil organic carbon storage in agricultural landscapes

Sebastian Dötterl

Thèse présentée en vue de l'obtention du grade de

Docteur en Sciences

Université catholique de Louvain

Louvain-la-Neuve, Mars 2013

Content

Composition du Jury **5**
Acknowledgement **6**
List of abbreviations **7**
List of publications in peer-reviewed journals **10**

1 Introduction **11**
1.1 State of the art 11
1.1.1 Soil organic carbon 11
1.1.2 Mechanisms of SOC sequestration and stabilization 12
1.1.3 A landscape scale perspective on SOC 14
1.1.4 The role of soil redistribution 15
1.2 Problem statement 17
1.2.1 SOC in dynamic landscapes 17
1.2.2 Scales in SOC research 18
1.3 Thesis objectives 20
1.3.1 Hypothesis 20
1.3.2 Research questions 21
1.3.3 Framework and thesis outline 21

2 Towards constraining the magnitude of global agricultural sediment and soil organic carbon fluxes at the global scale **25**
2.1 Outline 25
2.2 Materials and Methods 27
2.2.1 NRI 27
2.2.2 Estimating erosion factors with global databases 28
2.2.3 Model implementation 29
2.2.4 Uncertainty assessment 31
2.3 Results 32
2.3.1 Identification of key factors controlling erosion in the US 32
2.3.2 Characterizing R, S and C with global datasets 32
2.3.3 Comparison with NRI soil erosion estimates 36
2.3.4 Uncertainty analysis 36
2.3.5 Global application 39
2.4 Discussion 41
2.4.1 Comparison with other global estimates 41
2.4.2 Soil erosion as a soil modifier 43

2.4.3 Caveats 45
2.5 Conclusion 47

3 Process understanding for SOC stock predictions at the regional scale 49
3.1 Outline 49
3.2 Material and Methods 50
3.2.1 Study area 50
3.2.2 Field sampling 51
3.2.3 Soil analysis 52
3.2.4 Environmental covariates 54
3.2.5 Model building, implementation and statistics 56
3.2.6 Regional SOC stock assessment using HRS topsoil SOC data 58
3.3 Results 58
3.3.1 Description of the soil profile data 58
3.3.2 LMM Model fit 60
3.3.3 Explanatory variables 61
3.3.4 Regional SOC stocks 63
3.4 Discussion 65
3.4.1 Control mechanisms of SOC distribution 65
3.4.2 Extrapolation and caveats for a regional application 69
3.5 Conclusion 71

4 Assessment of SOC dynamics using closed-tube sampling and Vis-NIR spectroscopy at the landscape scale 73
4.1 Outline 73
4.2 Material and Methods 74
4.2.1 Study area 74
4.2.2 Sampling design and sample preparation 75
4.2.3 Spectral measurements 77
4.2.4 Spectroscopic predictions 77
4.3 Results 79
4.3.1 Model performance and repeatability analysis 79
4.3.2 SOC distribution with depth 79
4.4 Discussion 81
4.4.1 Methodological improvements and limitations 81

4.4.2 Time and cost comparison 81
4.5 Conclusion 83

5 Re-sampling historical soil profiles – Caveats and opportunities 85
5.1 Outline 85
5.2 Material and methods 85
5.2.1 Sampling design and historical soil data 85
5.2.2 Analyzed parameters 86
5.3 Results 87
5.3.1 Soil texture and soil redistribution patterns 87
5.3.2 Spatio-temporal SOC patterns 88
5.3.3 Changes in plowing depth 89
5.4 Discussion 89
5.4.1 Representativeness of historical soil data 89
5.4.2 Spatio temporal SOC changes – Controls and uncertainties 90
5.5 Conclusion 93

6 SOC dynamics at the hillslope scale 95
6.1 Outline 95
6.2 Material and Methods 95
6.2.1 Site description 95
6.2.2 Field sampling 96
6.2.3 Soil analysis 97
6.2.4 SOC fractionation 97
6.2.5 Soil incubation 99
6.2.6 Implementation and statistical analyses 99
6.3 Results 100
6.3.1 Soil and total SOC patterns 100
6.3.2 Patterns of potential soil respiration 103
6.3.3 SOC fractions and stability 104
6.3.4 Spatial and vertical patterns of SOC fractions and pools 106
6.4 Discussion 109
6.4.1 SOC replacement at eroding positions 109
6.4.2 SOC deposition 109
6.4.3 SOC burial efficiencies 110
6.4.4 SOC budget in eroding vs. non-eroding landscapes 111

6.4.5 Controls on topsoil SOC respiration 111
6.4.6 Controls on subsoil SOC respiration 111
6.4.7 SOC mean residence time and geomorphic position 113
6.4.8 Effects of soil redistribution on SOC quality 114
6.4.9 Significance on larger scales and caveats 115
6.4.10 Soil aggregation vs. erosion 115
6.4.11 Integration of lateral soil fluxes into SOC models 117
6.5 Conclusion 117

7 Mineralogical and pedogenic controls on spatial explicit SOC pools 119
7.1 Outline 119
7.2 Material and methods 120
7.2.1 Study site and sampling 120
7.2.2 SOC fractionation 120
7.2.3 Soil physico-chemical characterization 121
7.2.4 Implementation and statistical analyses 123
7.3 Results 123
7.3.1 SOC fractions and SOC distribution 123
7.3.2 Total reserve in bases and soil weathering status 124
7.3.3 Reactive soil phases 125
7.3.4 Clay mineralogy 128
7.4 Discussion 130
7.4.1 Soil erosion as a soil rejuvenator 130
7.4.2 Interactions of the reactive soil phase with SOC 130
7.4.3 Importance of the abundance of clay types 133
7.4.4 Soil redistribution – A sink or source? 134
7.5 Conclusion 135

8 Synthesis and general conclusion 137
8.1 Main findings 137
8.2 Soils and SOC in the geomorphic pump 141
8.3 Final remarks – Scales, limitations and perspectives 144

9 Bibliography 149
10 List of figures 177
11 List of tables 183

Composition du jury

Président

Marie-Laurence De Keersmaecker, Professeur, Département de Géographie, Faculté des Sciences, Université Catholique de Louvain.

Promoteurs

Kristof van Oost, Promoteur, Professeur, Département de Géographie, Faculté des Sciences, Université Catholique de Louvain.

Johan Six, Co-promoteur, Professeur, Department of Plant Sciences, University of California at Davis.

Membres réguliers

Bas van Wesemael, Professeur, Département de Géographie, Faculté des Sciences, Université Catholique de Louvain.

Marnik Vanclooster, Professeur, Faculté d'ingénierie biologique, agronomique et environnementale, Université Catholique de Louvain.

Veerle Vanacker, Professeur, Département de Géographie, Faculté des Sciences, Université Catholique de Louvain.

Michael Sommer, Professeur, Institut für Bodenlandschaftsforschung, Leibniz-Zentrum für Agrarlandschaftsforschung e.V.

Acknowledgement

This thesis and the connected research was financed in the framework of the Action de Recherche Concerteé (Convention No. 09/14-022) of the Communauté Française de Belgique and the UC Louvain Fonds spécial de recherche (FSR). Further financial support for lab analysis and travel funding has been given by: UC Davis Department of Plant Sciences and the "Fonds de la Recherche Scientifique" (FNRS), Belgium. Part of the fieldwork to this study has been conducted and organized in cooperation with: "CONVIS Herdbuch Service Elevage et Génétique" and the "Service de pédologie", both based in Luxembourg. Thank you for your cooperation.

Special thanks goes to my promoter Kristof van Oost who always had time for my (sometimes) stupid questions, had patience with my slow learning, and who encouraged me to not give up in facing new challenges. Second is my co-promoter Johan who helped me by giving new directions, views and perspectives to my work. Many thanks also for fruitful discussions and help to Bas van Wesemael, Antoine Stevens, Tim Quine, Verena Dlugoß as well as Francois Wiaux and Francois Stevens. Throughout the PhD, many people gave me extraordinary help and support for conducting field and lab work: First of all the staff of the Soil Science and the TECLIM Lab at the UCL, with their great technicians Anne, Claudine and Marco, their smart post-docs Sophie, Antoine and Jean-Thomas as well as my great student helpers Sophie and Wei. Many thanks also to the staff of the Agroecology Lab at UC Davis who helped me with conducting my work as well as analysis and interpretation. Thank you, Bob, Jennifer, Ben and Charlotte for your warm welcoming, I had a great time! My time in Belgium would have been boring without you guys: Special thanks to my fellow PhD colleagues and friends Yann, Carole, Marie, Derek, Sen and Samuel. I hope we stay in contact!
Nachert gid's dou ja nu d'ganz'n Leit dahoam, ohne dei ih's dou herrumarrt garantdierd nird as'ghalt'n haid. Natürrle zerscht'amal Mamma, Papa, Oma u Kerstin. Oba vor all'm mei guad'n Freind, dei mi d'Distanz noa dahoam vergess'n loua hom: Nikki, Nadine, Mario, Mane, Flo, Christian u Matthias. Es wor a hoarte Zeit, oba ohne eich nu vül herta' ! Last but not least, the greatest thanks goes to Heather, my friend and heart. I could not have done it without you.

List of abbreviations

%	Percent
Ø	Diameter
δ	Delta
°C	Degrees in Celsius
1D	One-dimensional
3D	Three-dimensional
AIC	Aikake information criterion
Al	Aluminum
B	Basin
BC	Black carbon
Bq	Becquerel
C	Carbon
c	Clay associated SOC
Ca	Calcium
CB	Central Backslope
Cc	(R)USLE Crop cover factor
$CaCl_2$	Calcium dichloride
CF	Concave Footslope
cH	Non-hydrolyzable clay associated SOC
cm	Centimeter
cmi	Microaggregate clay associated SOC
cmiH	Non-hydrolyzable microaggregated clay associated SOC
CV	Coefficient of variation
CPOM	Coarse particulate organic matter
^{137}Cs	Radioactive Cesium 137 isotope
CS	Convex Shoulder
CSR	Cumulative soil redistribution
DEM	Digital elevation model
DOC	Dissolved organic carbon
DOM	Dissolved organic matter
EL	Mean elevation
ER	Range of elevation
Ew	Annual soil loss rate by water erosion
Fe	Iron
$FeCl_2$	Iron dichloride

FP	Flat Plateau
Fw	Annual soil flux
g	Gram
Gg	Gigagram
Gt	Gigatons
h	Hour
HCl	Hydrogen chloride
HRS	Hyperspectral remote sensing
imPOM	Intra-aggregate particulate organic matter
K	(R)USLE soil erodibility factor
kg	Kilogram
L	(R)USLE Slope length factor
LB	Lower Backslope
LMM	Linear mixed effect model
M	Mol
m	Meter
Ma	Macroaggregate associated SOC
Mg	Megagram
mi	Microaggregate associated SOC
ml	Milliliter
mM	SOC associated with Microaggregates within Macroaggregates
mm	Millimeter
Mn	Manganese
MRT	Mean residence time
MT	Model trees
Na	Natrium
NLRWA	Australian National Land and Water Resources Audit
NRI	National Resources Inventory
P	(R)USLE Crop management factor
p	Level of significance
Pg	Petagram
PLSR	Partial least square regression
POC	Particulate organic carbon
P_{seas}	Precipitation seasonality
PVC	Polyvinylchloride
R	(R)USLE Rainfall erosivity factor

r	Pearson’s correlation coefficient
RF	Random forest
(r)SE	(relative) Standard Error
(r)RMSE	(relative) Root mean square error
RPD	Ratio of Performance to Deviation
(R)USLE	(Revised) Universal soil loss equation
S	(R)USLE Slope steepness factor
s	silt associated SOC
SD	Standard deviation
SEL	Standard error of laboratory
sH	Non-hydrolyzable silt associated SOC
smiH	Non-hydrolyzable microaggregated silt associated SOC
smi	Microaggregated silt associated SOC
SOC	Soil organic carbon
SP	Sloping Plateau
SRI	Soil redistribution intensity
SVMR	Support Vector Machine Regression
t	Tons
TCI	Topographic convergence index
Tg	Teragram
TIN	Triangulated irregular network
TPI	Topographic position index
T_{seas}	Temperature seasonality
TSS	Total suspended sediment
UB	Upper Backslope
µg	Microgram
µm	Micrometer
WRB	World Reference Base
Yr	Year

List of publications in peer-reviewed journals

Published or accepted

Doetterl S., Six J., Van Wesemael B., Van Oost K. (2012b): Carbon cycling in eroding landscapes: geomorphic controls on soil organic C pool composition and C stabilization. *Global Change Biology*, ***18***(7): 2218-2232.

Doetterl S., Six J., Van Oost K. (2012a): Towards constraining the magnitude of global agricultural sediment and soil organic carbon fluxes. *Earth Surface Processes and Landforms*, **37**(6): 642-655.

Van Oost K., Verstraeten, G., Doetterl, S., Notebaert, B., Wiaux, F., Broothaerts, N., Six, J. 2012. Eroding the C cycle, the legacy of human-induced C erosion and burial on soil-atmosphere C exchange. *Proceedings of the National Academy of Sciences of the United States of America*, **109**(47): 19492-7.

Submitted

Doetterl S., Stevens A., Van Wesemael B., Van Oost K. (*submitted*): Soil-profile organic carbon assessment at high vertical resolution using closed-tube sampling and Vis-NIR spectroscopy. *Soil Science Society of America Journal.*

Doetterl S., Cornelis, J-T. Six J., Quine T.A., Van Oost K. (*submitted*): The varying contribution of pedogenic oxides and clay minerals to stabilize carbon along a slope transect. *Journal of Geophysical Research-Biogeosciences*.

Doetterl S., Stevens A., Quine T.A., Van Wesemael B., Van Oost K. (*submitted*): Spatial-explicit regional-scale prediction of soil organic carbon stocks in cropland employing environmental variables ad mixed-model approaches. *Geoderma*.

1 Introduction

1.1 State of the art

1.1.1 Soil organic carbon

Soil organic carbon (SOC) is recognized as an important soil parameter due to its interaction (e.g. Seybold et al. 1997) with soil functions such as soil structure (Bipfubusa et al. 2008; Cantón et al. 2009), soil water retention capacity (Rawls et al. 2003) and the capacity to bind organic and inorganic pollutants (Schwarzenbach et al. 1993, Lair et al. 2007). Soils are major reservoirs of organic carbon (~1200 Pg in the first meter of soil + 300 Pg litter) and are estimated to store more carbon than both the atmosphere (~780 Pg) and vegetation (~550 Pg) combined (Falkowski et al. 2000; Houghton 2007; Lal 2008b; Hiederer and Köchyl 2012) (Figure 1). In agricultural soils the C input is generally highest at the soil surface and decreases with depth. The main input sources for organic carbon in soils are litterfall from plants and detritus from soil microfauna and decomposing plant roots. In addition, in subsoils, several other mechanisms can add to the process spectrum to sequester SOC. Most notable of these are C input by plant roots, bioturbation, input by dissolved organic matter leached from the surface, and the translocation of particulate and mineral bound organic matter (Rumpel and Koegel-Knabner 2011).

Houghton (2007) estimated the annual exchange between atmospheric and terrestrial C pools at ~120 Pg, which represents a significant amount of the total C stock in those compartments. The largest share of these fluxes is related to exchange between vegetation and the atmosphere, through respiration and photosynthesis, and by decomposition of organic matter in soils, which is replaced with fresh litter (Houghton 2007; Lal 2008). Long term climatic changes can influence the balance between uptake and release of organic carbon from soils significantly (Davidson and Janssens 2006; Smith et al. 2008). However, other disturbances can also affect this balance. Since the beginning of agriculture, land use and land cover change driven by human activities have increasingly influenced both sequestration and release of C in soils (Smith 2008). This influence makes soils and their management an important component in combating and constraining the magnitude of global (climate) change. For this reason, the large impact of soil processes

on the global carbon cycle has been recently recognized by climate modelers, politicians and land use planners (IPCC 2007).

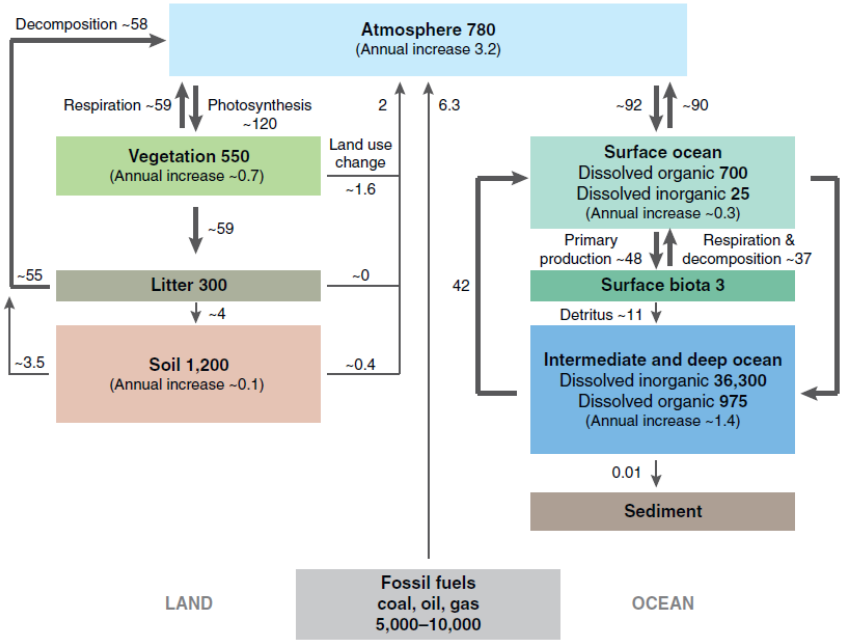

Figure 1: The global carbon cycle in the 1990s. Units are in Pg C or Pg C yr^{-1}.Taken from Houghton (2007).

1.1.2 Mechanisms of SOC sequestration and stabilization

Process-based research has clarified mechanisms and timescales involved in stabilizing SOC at the plot scale and this understanding has been implemented in models of SOC dynamics over the past decades (Coleman & Jenkinson 1999; Parton et al. 1988). Carbon in soils can be stabilized against decomposition by three key mechanisms: (i) inherent biochemical recalcitrance since some SOC fractions are an energetically poor nutrient source for decomposers, (ii) organo-mineral associations by interaction with mineral surfaces, and (iii) physical protection by spatial separation of C from decomposers or inaccessibility of SOC within soil aggregates (Tisdall and Oades 1982; Sollins et al. 1996; Six et al. 2002; von Luetzow et al. 2006 for review). Furthermore, SOC is not a homogeneous pool but consists of fractions with different turnover times ranging from days to millennia (i.e. Trumbore 2009; Schmidt et al. 2011). The gross of the annual, short term

soil-atmosphere C fluxes is related to decomposition of labile, non-protected carbon. The medium to long term stability (i.e. decadal to centennial scales) of protected SOC fractions, however, remains uncertain, despite their distinct differences in terms of chemical and physical properties (Trumbore & Czimczik 2008; Kleber et al. 2011). Salomé et al. (2010) argue, therefore, that SOC stabilization is strongly influenced by soil environmental conditions too. Soil humidity (McHale et al. 2005; Thomsen et al. 2003), aeration (Zhang et al. 2011; Ayra et al. 1999), temperature (Davidson and Janssens 2006) and SOC distribution density in soils (von Luetzow et al. 2006; Holden and Fierer 2005; Rumpel and Koegel-Knabner 2011) were identified as key controls on microbial activity and hence SOC stability. The importance of each of these factors for SOC stability is, however, still a matter of debate. Some authors (Mikutta et al. 2006; Sing et al. 2012) suggest that biochemical recalcitrant carbon, such as fire–derived black carbon (BC) or lipid compounds are stable in soils over centuries to millennia while others argue that environmental factors (Kleber 2011; Dungait 2012), interactions with the mineral phase (Torn 1997) or physical inaccessibility (Six 1998, 2002) rather than biochemical recalcitrance govern SOC stability in soils. Finally, these stabilization mechanisms can also be interactive (i.e. Lehmann et al. 2007; Rabbi et al. 2010; Schmidt et al. 2011). For example, there can be aggregation of organo-mineral associations that already include biochemically recalcitrant SOC (Figure 2).

Without doubt, one of the most important factors in stabilizing carbon in agricultural soils is the soil matrix (i.e. Feng et al. 2011). Clay-sized minerals have been identified as major components in organo-mineral associations given their high specific surface area and hydrolated reactive surfaces (Schnitzer and Kodama 1992; Kaiser and Guggenberger 2003; Totsche et al., 2010 for review). The silicate mineral reactivity depends on their typology (expandable 2:1 versus non expandable 2:1 and 1:1 clay), which partly controls their ability to stabilize SOC through links with variable pH-dependent surface charge and intercalation in the interlayers (Kleber et al. 2005, 2007; Kaiser and Guggenberger 2007). The formation of reactive Fe-, Mn-, Al-oxy-hydroxides throughout the soil weathering process also partly controls the SOC stabilization through complexation/coprecipitation and adsorption processes (Tipping 1981; Torn et al. 1997; Wagai and Mayer 2007, Eusterhues et al. 2008) and in supporting soil aggregation (Pinheiro-Dick and Schwertmann 1996; Duiker

et al. 2003). Therefore, the mobility and reactivity of Fe, Mn and Al (oxy)(hydro)oxides depends on soil pH and redox conditions, and these minerals can act as soil pH buffers over a large range of pH values (Schwertmann et al. 1987; Süsser and Schwertmann 1991) in the order Mn>Fe>Al. Hence, the interdependent relationship between soil reactivity and SOC stabilization might be strongly pH dependent and differ between topographic positions and soil depths.

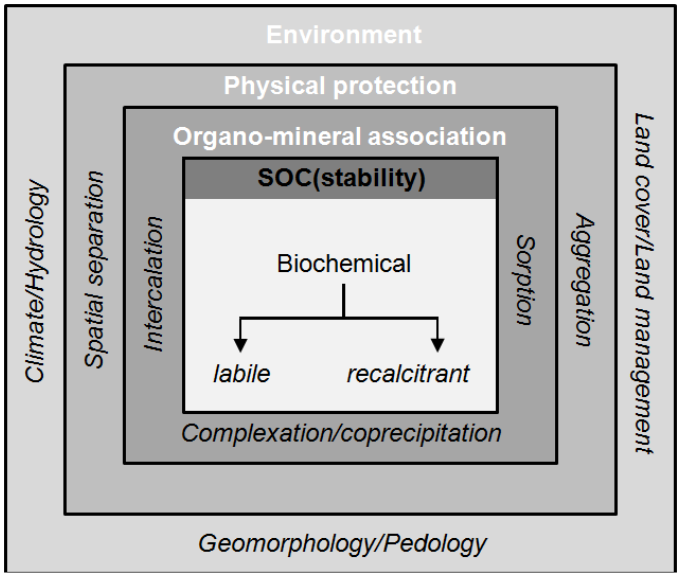

Figure 2: Box model concept of variables affecting SOC stability. To be viewed from center to periphery. Each level represents a different set of controls with decreasing direct influence on carbon stability.

1.1.3 A landscape scale perspective on SOC

At large spatial scales (i.e. watersheds, regions and up to continents) the main controls on SOC stock variability are considered to be climate dependent variables such as soil temperature (Rustad et al. 2001; Davidson and Janssens 2006; Smith et al. 2008) and soil moisture regime (McHale et al. 2005; Thomsen et al. 2003), vegetation and land use (Rees et al. 2005; Guo and Gifford 2002; Li et al. 2012), land management (Paustian et al. 1998, Lal et al. 2007, Van Wesemael 2010) and soil properties such as soil texture (Torn et al. 1997; Guo et al. 2006; Schjønning et al. 1999) (Figure 2). The influence of these different controlling factors on SOC contents differs with soil depth (Jobbágy and Jackson 2000) and is governed by local

processes at very fine scales. The resulting large spatial and temporal heterogeneity hampers the generalization of SOC dynamics at spatially relevant scales (regions, continents, globe) (Trumbore & Czimczik 2008). An integrative understanding of the interactions and feedbacks between the processes that control SOC turnover, which operate at different scales is therefore important. At large scales, current approaches of modeling SOC dynamics are pragmatic and exclude qualitative differences of SOC between different elements of the landscape. In contrast, at the scale of pedon and soil plots, the interaction between soil properties (see i.e. Krull et al. 2004; Koegel-Knabner et al. 2008; Mikutta et al. 2009; Totsche et al. 2010), environmental variables (Kleber et al. 2010; Dungait et al. 2012) and SOC has been well documented. At larger scales, the effect of geomorphic processes (which are largely controlled by topography) on the variability of SOC storage capacity is usually not considered (e.g. Lettens et al. 2005; Goidts et al. 2007, 2009a; Batlle-Aguilar et al. 2011). The representation of the horizontal and vertical patterns of SOC in current assessments is typically informed by data from stable, non-eroding landforms. Nevertheless, topography can have a strong influence on the local micro-climate and -hydrology (Burt and Butcher 1985; Kang et al. 2000, 2003; Schwanghart and Jarmer 2011) and, if soil erosion takes place, it can control the spatial patterns of SOC (Gregorich et al. 1998).

1.1.4 The role of soil redistribution

Under natural conditions, soil systems are considered to be sustainable as the loss of soil material by erosion is approximately balanced by the production of soil as a result of weathering (Montgomery 2007; Verheijen et al. 2009). A conversion from natural to agricultural land use removes the protective natural vegetation and this typically increases soil erosion by one to two orders of magnitude (Montgomery 2007), thereby accelerating physical erosion well over equilibrium levels. Human activities have not only drastically accelerated the rates but also altered patterns of soil erosion and deposition (i.e. Wilkinson & McElroy 2007). In the highly mechanized agriculture of industrial nations, tillage erosion can reach the same magnitude of soil loss as water erosion taking place in the same field (Van Oost et al. 2006). While the highest rates of water erosion occur at the foothill where water accumulates (for situations where Hortonian overland flow dominates), tillage erosion is highest in the steepest uphill convex

shoulder of the hillslope and leads to additional transport of soil downslope (Li et al. 2008). In environments with high soil redistribution rates such as agro-eco systems, soils can then exhibit a large variability in SOC quantity due to the burial of SOC rich topsoil material at colluvial foothill sites and C depletion at eroding slope positions (Gregorich et al. 1998; Quine and Zhang 2002; Van Oost et. al. 2005; Heckrath et al. 2006; DeGryze et al. 2008; Wang et al. 2010; Schwanghart and Jarmer 2011; Vandenbygaart et al. 2012; Nadeu et al. 2012). This interplay between soil redistribution and soil carbon dynamics has been studied quantitatively (e.g. Roosenbloom 2006; Yoo et al. 2005, 2006). However, there is evidence that erosion and deposition processes lead not only to temporally and spatially dynamic patterns of SOC stocks but also alter the quality and turnover of SOC (e.g. Berhe et al. 2008, 2012a, 2012b, Rumpel and Koegel-Knabner 2011). Topsoil removal by erosion causes previously stabilized SOC from the subsoil horizons to be incorporated into the topsoil layer at eroding sites. There, it is mixed with fresh and more labile material that may strongly affect the turnover of this 'former' subsoil SOC (Fontaine et al. 2007). Similarly, sediment deposition at the foothill results in the burial of former topsoil SOC, enriched in labile compounds (Gregorich et al. 1998).

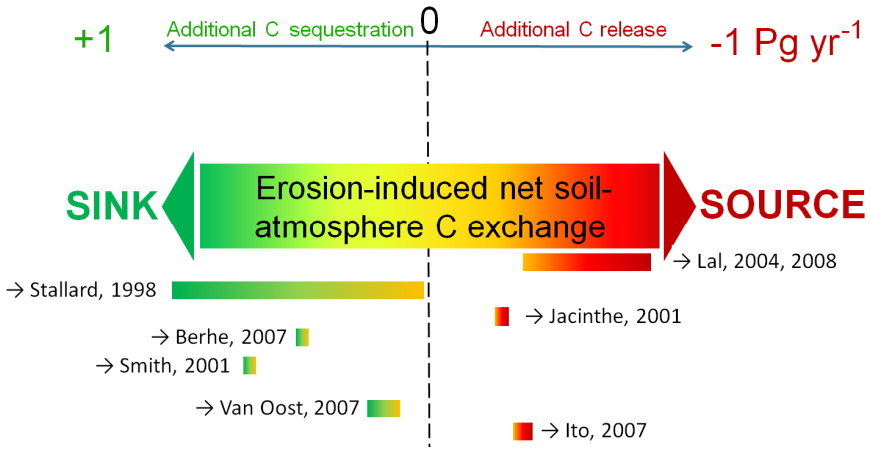

Figure 3: Overview of recent estimates of soil erosion as a sink or source for atmospheric C, relative to soil systems that are unaffected by soil redistribution. Ranges of estimates are taken from articles listed on the right end (sources) or left end (sinks) of each horizontal bar.

Several global assessments of the influence of erosion processes on the SOC cycle suggest a net uptake or sink of carbon, but results are very divergent

(Figure 3). The role of within-basin fluxes in the C cycle remains an area of particular controversy (e.g. Lal & Pimentel 2007) and suggested rates of decomposition and sequestration range between -1 to +1 Pg C yr^{-1}. Although it is clear that there is insufficient understanding of the interactions between erosion and carbon cycling at the process level (e.g. Liu et al. 2003), the wide range of proposed values for the sink or source functions of soils influenced by erosion also reflects uncertainties associated with estimates of the magnitude of agricultural erosion (e.g. Boardman 2006; Quinton et al. 2010), and the fact that different elements of the terrestrial carbon cycle (soils vs. sediment deposits) are analyzed separately or at different time scales (agricultural research: short-term, sedimentological research: long-term), which can lead to contrasting results.

1.2 Problem statement

1.2.1 SOC in dynamic landscapes

Until now, most studies on the role of soils in global carbon cycling only consider (i) the vertical exchange of C between the soil, atmosphere and groundwater and (ii) the cycling between different SOC-pools within the top layer of the soil profile. More recently, the erosion-induced changes in bio-geochemical cycles have received considerable attention (e.g. Kutsch et al. 2010), and there is growing awareness that focusing only on vertical C fluxes is an oversimplified view as soil landscapes are far from static. Recent findings from ecology, soil science, geomorphology and biogeochemistry demonstrate that, concerning SOC, soils have to be considered as dynamic and internally connected systems at the landscape scale (i.e. Berhe et al. 2008, Birkeland 1999, Brady & Weil 2008, Lal 2009) with interactive effects between soil (carbon) redistribution and vegetation (Osterkamp et al 2012).

There is also large uncertainty as to whether the altered soils act as a sink or source for atmospheric C. There is now growing evidence that the current paradigm of vertical soil-atmosphere C exchange is a simplification of reality as erosion and sedimentation influence the stabilization mechanisms and turnover of organic material in soils (e.g. Harden et al. 1999, Berhe et al. 2008). Dynamic landscapes may sequester large amounts of SOC in depositional settings as burial constrains the decomposition process (e.g. Liu et al. 2003). Van Oost et al. (2007) estimated that more than 20 Gt of

"young" SOC was buried in agricultural landscapes in shallow valley deposits during the last 50 years. Furthermore, a significant fraction of the eroded SOC is replaced at eroding positions by C sorption to the newly exposed mineral surfaces, driving an important local net C sink (Harden et al. 1999). Others (Lal & Pimentel 2007) challenge this view either by arguing that eroded SOC is almost completely decomposed and that erosion reduced the SOC sequestration potential of soils, or that the stability of old carbon is largely decreased when brought into contact with more labile SOC (Fontaine 2007).

Recently, conceptual models have been developed that combine geomorphic models with models of carbon dynamics. These models have been applied to eroding micro-catchments and were able to closely reproduce the observed SOC depth profiles for a wide range of erosional and depositional settings (Rosenbloom et al. 2006; Liu et al. 2003; Dlugoß et al. 2011). Without exception, these model runs provided strong support for the assertion that lateral fluxes exert an important control on carbon dynamics at the landscape scale. However, the observational data did not allow for the accurate estimation of the strength of the coupling between soil fluxes and carbon dynamics and did not improve our mechanistic understanding of geomorphic effects on SOC storage in soils.

1.2.2 Scales in SOC research

The transfer of knowledge on SOC dynamics to applications on larger scales has so far been limited. For example, it is well known that SOC stability changes with soil depth, with more stable SOC pools found in deeper layers (Rumpel & Koegel-Knabner 2011). However, SOC research has traditionally focused on mechanisms and controls in topsoils. This focus ignores, that between 30-63% of the organic carbon in the top one meter of soils is stored below 30cm depth (Batjes 1996). Relatively little is known about SOC dynamics in the subsoil (Rumpel and Koegel-Knabner 2011) and as a consequence, predictions of depth-explicit SOC models are associated with high uncertainties, particularly at greater depth. Furthermore, landscape SOC models rely largely on process-understanding and on the spatial distribution of SOC stocks and SOC quality derived from soil profiles in flat, non-eroding landscapes (Quine and Van Oost 2007). The relationship between topography and patterns of SOC storage, on the other hand, has generally been investigated at the scale of individual slopes. As a result, the

importance of this small-scale variability induced by topography-related processes for a larger-scale C storage assessment is unclear. Hence, the implicit assumption in landscape SOC models that SOC dynamics at larger spatial and temporal scales can be assessed by considering the soil system as a 1D soil profile representing an area of similar soil, climate and management (Trumbore & Czimczik 2008; van Wesemael et al. 2010) might be an oversimplification. However, it is a necessary step in order to reduce the complexity of SOC models as the data and methods to add more insight into SOC dynamics at larger scales are currently very limited.

Thus, reliable qualitative and quantitative data validated on larger scales is needed to understand how mankind influences global biogeochemical cycles (Lal, 2007b; Quinton et al. 2010). As a result of this observation, recent SOC research has identified the need to generate large amounts of spatial explicit soil data (Smith et al. 2012). At present, this data simply does not exist yet on a global scale and traditional analysis is too expensive and too time intensive to provide suitable tools to solve this "data crisis" (McBratney et al. 2006). This largely hampers our ability to provide accurate data on the future of SOC dynamics on scales interesting for landscape planners and policy makers. Advances in remote sensing and SOC modeling have led to new ways to estimate SOC stocks at the scale of landscapes and regions, and have improved our ability to map its horizontal and vertical variability in a quantitative manner (Meersmans et al. 2008; Schwanghart and Jarmer 2011, Stevens et al. 2010). However, large uncertainties remain (Goidts et al. 2009b). Quantifying temporal changes in SOC content at larger spatial scales is challenging researchers for several decades now and these changes cannot yet be reliably estimated. As a consequence, the balance between accumulation and depletion of SOC in dynamic landscapes is still surrounded with large uncertainty. Linking the increasing knowledge of SOC dynamics on micro-scales to larger scales for more generalized statements remains difficult and has not yet been done.

1.3 Thesis objectives

The aim of this PhD thesis is to improve our understanding of the effects of soil redistribution on SOC dynamics and to highlight the connectivity of controls on these dynamics at different scales. For this, a multi-scale analysis covering different aspects of the soil C/Soil redistribution continuum has been conducted. The presented work particularly focuses on (i) the identification of (soil) (environmental) controls on carbon dynamics and carbon distribution patterns along geomorphic gradients in landscapes affected by soil redistribution, (ii) the different carbon stabilization mechanisms and (iii) the role of the mineral phase in stabilizing carbon. A broad range of state-of-the-art physical and chemical soil analysis methods, GIS tools and advanced statistics will hereby be applied.

1.3.1 Hypothesis

This thesis postulates that (a) the influence of erosion and deposition along hillslopes is one of the major drivers not only behind patterns of SOC quantity, but also for SOC quality on cropland and (b) that the analysis of local and regional topography is a key aspect for studying SOC dynamics across scales if hydrological, climatic and pedological site parameters are known (Figure 4).

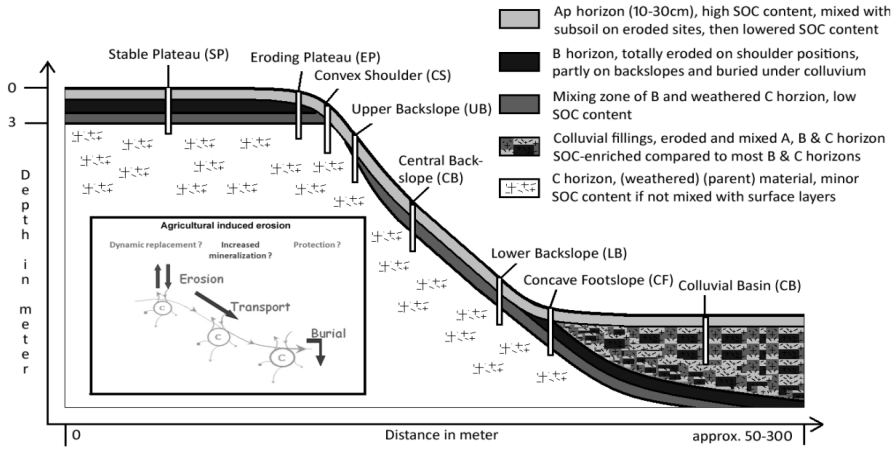

Figure 4: Study concept: Soil erosion modifies soil profiles and introduces large lateral soil fluxes along a geomorphic gradient. These fluxes must leave a "footprint" in the distribution as well as on the quality and quantity of SOC stocks. Under similar climate, land use and pedology, topographical features determine SOC distribution and development.

The main hypothesis of this work can then be formulated as**:**
"In an otherwise homogeneous region, topographic features and topography related soil redistribution patterns can be used to model SOC distribution at various scales in space and time and to identify processes controlling SOC dynamics."

To address this, the main hypothesis can be broken down into the following compartments.

(H1) *The spatial distribution of SOC stocks can be discriminated by simple climatic, topographical and pedological parameters.*
(H2) *The (spatial-explicit) cropland SOC (pool) composition and its recalcitrance are controlled by geomorphic processes.*
(H3) *Soil redistribution affects the soil's capacity to sequester new or stabilize old carbon.*

1.3.2 Research questions

The main research questions addressed in this thesis can be summarized as followed:

1. SOC dynamics are controlled by micro-scale processes - How can we describe and model the vertical and horizontal SOC distribution on a regional scale? What tools are necessary? What controls can be identified and what time scales need to be considered?
2. In current models of SOC dynamics it is not considered that, due to erosion and deposition, SOC stocks and SOC quality are continuously evolving - What influence do soil redistribution processes have on SOC quality? What distinguishes stable from eroding landscapes and what chemo-physico soil properties can be identified as important for the understanding of SOC stabilization at different landscape positions?

1.3.3 Framework and thesis outline

This thesis has been conducted in close cooperation and in exchange with other researchers in the framework of the ARC project "*The hillslope as elementary unit for regional scale modeling of soil organic carbon"* at the Université catholique de Louvain. The general research objectives of the

project are: "**To improve regional soil carbon budgets by integrating soil carbon dynamics and lateral redistribution processes as coupled models".** For this, the project integrates a wide range of research perspectives, from primary research through on-field assessments and laboratory manipulation experiments to geo-statistical modeling, integrating the former experimental findings. The presented thesis focuses on the "**Characterization of the SOC distribution (horizontal and vertical) in croplands from the hillslope to the region**" and "**Experiments on the response of carbon pools across a range of depths (desurfacing/burial)**" using laboratory experiments.

This thesis uses a top to bottom research approach, in which SOC assessments are performed at the regional, landscape and hillslope scale, with an increasing level of detail in terms of SOC dynamics and quality as the scale decreases. The focus and motivation of each results chapter is given in a short outline at the beginning of the respective chapter. The main findings of each chapter and their relevance to the main research questions are summarized in section 8.1. Special emphasis in this work is given to the dependency of the applied methods on the respective scale of investigation and the transfer of knowledge from one scale to another with respect to carbon dynamics and environmental controls. The workflow and design of the study is presented in Figure 5 and can be summarized in the following way:

Before answering the main research questions, an introductory chapter (chapter 2) on the magnitude of global agricultural (SOC) erosion addresses the question if historical and current agricultural erosion has a significant impact on SOC distribution on a global scale. This "setting the stage" chapter is not closely tied to the main research questions but aims to illustrate the significance of research on soil redistribution by constraining the magnitude and spatial pattern of global agricultural soil (C) erosion. The second part of the thesis (chapter 3) is a first regional sampling campaign aiming to identify key environmental controls for cropland SOC stocks in different soil regions (*addressing hypothesis H1*). This campaign reveals the limitations of traditional sampling designs when applied for a depth-explicit regional scale SOC assessment. For this reason, a novel approach (chapter 4) for estimating the depth explicit SOC distribution has been developed which

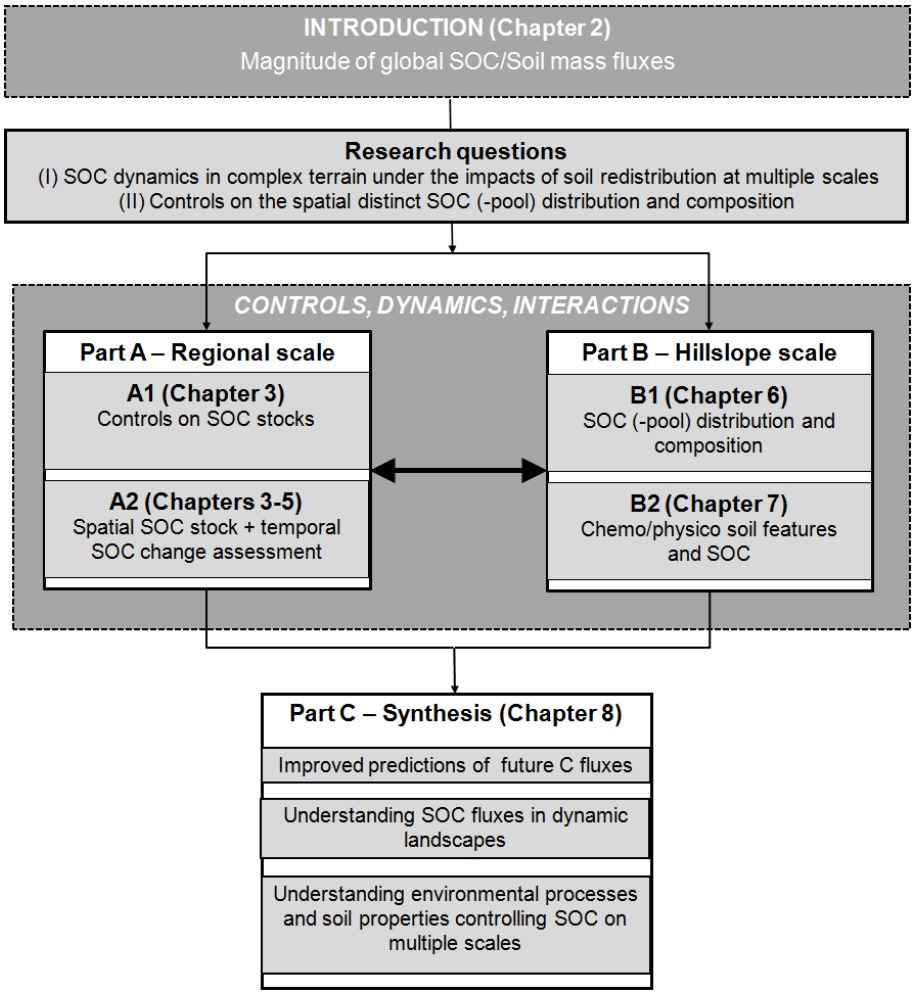

Figure 5: Complete flow chart of the research project.

consists of an improved sample preparation methodology and the application of a rapid spectroscopic soil analysis technique for depth-explicit SOC studies on a regional scale. In the following short chapter (chapter 5), the use of this methodology is exemplified as a tool to detect temporal changes and spatial patterns of cropland SOC stocks in the Belgian loambelt. The third part of the thesis (chapter 6) is a detailed investigation of the effects of soil redistribution on carbon quality at the hillslope scale and an assessment (chapter 7) of chemo-physico soil properties along the hillslope influencing SOC dynamics (*addressing hypothesis H2 and H3*). Finally, a synthesis chapter (chapter 8) attempts to present the main findings of this thesis within the framework of state-of-the-art scientific knowledge, especially focusing

on the issues of scale dependency in SOC research and the larger implications of the findings for future C assessments.

2 Towards constraining the magnitude of global agricultural sediment and soil organic carbon fluxes at the global scale[1]

2.1 Outline

The quantification of agricultural soil erosion and resulting SOC fluxes at a global scale is a difficult task because the temporal and spatial variability of soil erosion is extremely high. Soil erosion processes occur at very fine scales in heterogeneous patches on the landscape and their response to environmental conditions greatly vary between locations. When moving to larger spatial scales, the quantification of landscape heterogeneity is therefore crucial but large information gaps exist. These gaps are due to the fact that spatially comprehensive methods, such as remote sensing, are currently lacking for examining and synthesizing erosion processes over the Earth's surface (Stallard 1998). Often, global estimates are therefore based on the extrapolation of results derived from soil erosion experiments at the plot scale. Using these methods, existing estimates of agricultural soil erosion range between 24 and 120 Pg yr^{-1} and 0.5 – 3.7 Pg SOC yr^{-1} respectively (Table 1). Several factors, however, may introduce substantial uncertainty in these estimates. First, it has already been shown that the experimental data used in these estimates are derived from only a few observations which may be strongly biased towards steep slopes, bare soil conditions, extreme rainfall events and hence high rates of erosion (Cerdan et al. 2010). Second, although global model applications may provide an indication of areas at risk, they have to rely on coarse-scaled input data which are not compatible with the scales at which erosion models were parameterized. The fact that previous assessments based on global models remain unverified, mainly due to the lack of model-testing data at larger spatial scales (i.e. regions or continents), is adding further to this uncertainty. Implicit in the assumption that erosion plot data can be extrapolated to global scales is that the experimental conditions are representative for global

[1] **The content of this chapter has been published as:** Doetterl S., Six J., Van Oost K. (2012): Towards constraining the magnitude of global agricultural sediment and soil organic carbon fluxes. *Earth Surface Processes and Landforms*, **37**(6): 642-655.

agricultural land. Similarly, global estimates based on the application of hillslope scale erosion models assume that small-scale processes do not require re-parameterization when used at the global scale.

Table 1: Comparison of global erosion estimates based on different methods taken from studies in the last two decades.

Source	Type of erosion	Method	Estimated eroded soil or sediment [Pg yr^{-1}]	Estimated eroded C [Pg yr^{-1}]
Myers 1993	Total erosion	Extrapolation of plot data	75.0	-
Pimentel et al. 1995	Erosion on agricultural land	Extrapolation of plot data	73.5	-
Stallard 1998	Total erosion	Model extrapolation of different sediment yield scenarios	23.7 – 64.9	0.45 - 1.23
Hooke 2000	Construction and agricultural practices	Erosion data per capita, extrapolation using population figures	120.0	-
Yang 2003	Total erosion and human increase of soil erosion	Modified RUSLE based simulations (Soil erosion increase by humans 60%)	132.7	-
Lal 2003	Total erosion	Extrapolation of river sediment estimates	201.0	4.0 - 6.0
Berhe et al. 2007	Erosion on agricultural land	Extrapolation of plot data, taken from Pimentel 1995	75.0	1.1 - 3.7
Ito 2007	Water erosion	Modified RUSLE modeling approach	172.2	1.6
Van Oost et al. 2007	Pasture & Cropland erosion	Erosion plot data, modified RUSLE for local extrapolation	33.4 ± 4.4	0.5 ± 0.06
Wilkinson & McElroy 2007	Erosion on agricultural land	Plot erosion data, modeled extrapolation	28.1 - 39.9	-

The main objective of this study is therefore to test these assumptions underlying current assessments and to reduce the uncertainty associated with

global estimates of agricultural soil and organic carbon erosion. To do this, a hybrid approach is applied here: A simplified erosion model driven by coarse global databases is parameterized, calibrated and validated with an empirical database that covers large spatial and temporal scales and is consistent with observations at the hillslope scale. First, the NRI database (USDA 2000) was used to identify the key controls on accelerated erosion at the continental scale. This spatial database presents estimates of soil erosion across the conterminous USA representing a wide range of climatic, soil, topographic, cropping and management conditions. In a second step, a mechanistic model was developed and validated that quantitatively describes the relationships between erosion and the key controlling factors. The results of the NRI were used to parameterize the model and the results confronted with the original NRI estimates. Third, the estimates, based on coarse but global-scale datasets, were evaluated against independent estimates derived from high resolution and high precision datasets for Europe, South Africa and Australia. As such, scaling issues and fine-scale processes operating at hillslopes are explicitly addressed. Finally, the model is applied to estimate global fluxes of sediment and organic carbon on agricultural land and the global significance of accelerated carbon erosion as well as uncertainties in relation to previous estimates are discussed.

2.2 Materials and Methods

2.2.1 NRI

The NRI is a statistical survey of land use and natural resource conditions and trends on U.S. non-Federal lands (USDA 2000; Nusser & Goebel 1997). Data are available for several years since 1982 but here the results of the survey conducted from July 1997 to October 1998 are used as this covers the same period as the land use datasets used in the approach (see further). This extensive database, with 417357 entries for US agricultural land, is currently the most detailed database describing land use, crop type and factors controlling soil erosion for crop- and pastureland that covers a large region (i.e. the conterminous USA). For each observation point, water erosion (sheet, interrill and rill erosion) was computed as average annual rates from NRI data based upon measured long-term climate data, inherent soil and site characteristics, cropping and management practices and calculated using the USLE (USDA 2000; Wischmeier & Smith 1978). The USLE is an empirical

equation that predicts the annual average, long-term water erosion as the product of a rainfall erosivity factor (R), a soil erodibility factor (K), a slope length factor (L), a slope steepness factor (S), a crop cover factor (Cc) and a management factor (P). The estimates of USLE factors are determined for a representative portion of a scientifically selected NRI sample site and in almost all cases these sites represent re-samplings of the 1982 data points following the same sampling protocol. Release of NRI results is guided by NRCS policy and is in accordance with USDA Quality of Information Guidelines (USDA 2000).

In addition to soil erosion estimates, the database also provides estimates for each USLE factor separately based on field observations and information on land cover and use. According to USDA (2000), the *margin of error* is approximately twice the estimated standard error, and can be used to construct a 95 percent confidence interval for the estimate. The lower boundary of the interval is obtained by subtracting the margin of error from the estimate. The upper boundary is obtained by adding the margin of error to the estimate.

In the analysis, the NRI estimates are spatially aggregated to two levels: Counties and HUC4 watersheds (Seaber et al. 1987), resulting in 2755 and 211 observations points with a mean surface area of c. 2900 and 43000 km^2, respectively. A stepwise linear multiple regression analysis (Forthofer et al. 2006) was performed on the NRI database to identify the key factors controlling soil erosion variability at the continental scale. The stepwise linear regression allows integrating one explaining variable after another in a linear regression ranked according to their importance for explaining the remaining variability of soil erosion. The partial correlation coefficients (r-values) indicate hereby how much of the remaining variability can be explained by including the respective variable, while the Model R^2 indicates the explained total variability with the respective model structure. These and all further correlations regarding erosion rates have been performed using a weighted approach, with the weight as the area of cropland or pastureland that each value represents, taken from the NRI and aggregated on the respective level (Counties or HUC 4).

2.2.2 Estimating erosion factors with global databases

In the analysis, high precision and fine resolution NRI data were confronted with estimates derived from coarse, but global scale, databases. Here, the

global databases that are used are described. Land use data was derived from the gridded HYDE 3.1 dataset (Klein-Goldewijk et al. 2010) which represents the fraction of agricultural land (both cropland and agriculturally used grassland, i.e. sum of pastures and rangelands) with a resolution of 5 by 5 arc-minutes for the year 2000. While a direct comparison between the NRI and HYDE databases can be performed for croplands, this is not the case for grasslands. Erosion related estimates in the NRI database only cover pastures and not rangelands; this prohibited a meaningful spatial correlation with HYDE estimates. As will be discussed below, this limited the analysis and estimates for global pastures. Global estimates for the R factor were calculated at a resolution of 5 by 5 arc-minutes from the annual precipitation (Hijmans et al. 2005) using the empirical relationship between annual rainfall and rainfall erosivity presented by Renard & Freimund (1994). The GTOPO elevation model (USGS 1996; Gesch et al. 1999) is used to derive slope estimates at a 5 arc-minute resolution using the methods described in Van Oost et al. (2007). The USLE slope steepness factor was then calculated using the continuous function of Nearing (1997). The global crop type abundance map of Leff et al. (2004) at a resolution of 5 by 5 arc-minutes is used to estimate C factors. The NRI point estimates were used to calculate mean Cc factor values for all major US crop types and a weighted mean Cc factor was then calculated for each grid using crop type abundance. The analysis showed that soil erodibility (K), slope length (L) and management (P) did not contribute much to explaining NRI-based variability in soil erosion at the continental scale (see further), and therefore, were not included in the analysis. For each erosion factor derived from global databases, correction functions are proposed by minimizing the difference between NRI- and global database- derived USLE factors for both cropland and grasslands.

2.2.3 Model implementation

After identifying the key-controls on soil erosion at the continental scale and scaling global databases, erosion rates for cropland on a 5 by 5 arc-minutes grid are calculated using the following formula:

$$E_{WC} = S_r * R_r * Cc_r * E_{NRIref}$$

(1) where E_{WC} is the estimated average soil loss per year on cultivated cropland by water erosion (Mg ha^{-1} yr^{-1}), S_r is the local S factor dived by the NRI derived mean for the US, R_r is the local R factor dived by the NRI derived mean for the US, Cc_r is the local Cc factor dived by the NRI derived mean for the US and E_{NRIref} is the average annual erosion rate for US cultivated cropland for 1997 normalized to a slope of 9% (Mg ha^{-1} yr^{-1}).

This approach ensured that the mean erosion estimate for the US derived from global databases equals the NRI estimate. Using the HYDE cropland area (L_c, km^2), E_{WC} was then converted into an erosion flux (F_{WC}, in Mg yr^{-1}). The same approach was implemented for erosion on agricultural grassland (E_{WAG} and F_{WAG}). For grasslands, C_r was not derived from global databases due to the lack of data but was reduced by 42%, relative to croplands, conform to the findings of Yang et al. (2003) for grassland Cc factors and assuming an equal distribution of sparse and dense grassland on eroding pastures.

Also considered is the effect of rock fragments on erosion processes in stony soils (Poesen et al. 1994). In the global application, the protective effect of rock fragments against splash erosion is taken into account and reduced erosion by 80% for stony soils which is consistent with field observations (Poesen et al. 1994). Based on the average gravel content reported for WISE 1.1 (Batjes 2006) map units dominated by litho- and regosols, stony soils were identified as having gravel content above 12%. Using the WISE 1.1 (Batjes 2006) soil type distribution on a 5 by 5 arc-minutes grid and the WISE 3.1 (Batjes 2008) spatial soil profile database with information on gravel content from more than 10000 soil profiles, a global map reflecting the protection by stones against splash erosion has been created. This analysis was performed by only considering profiles that were identified as agricultural soils. In the estimates for pasture and rangeland erosion, only environments where vegetation is sparse and which are subjected to accelerated erosion when grazed were considered. This approach is consistent with observations that erosion rates on grasslands in humid, temperate regions are very low (Cerdan et al. 2006). This was done by only taking into account areas where the potential vegetation is grassland or steppe as described in the ISLSCP Potential Vegetation Types database (Ramankutty and Foley 1999). The model was then applied to the global

scale at a 5 by 5 arc-minutes resolution. Using the soil carbon content (%), the amount of cropland and pasture/rangeland soil erosion was then converted into carbon erosion. The estimated average percentage of SOC in the toplayer (upper 20 cm) of cropland and pasture/rangeland was taken from the WISE 3.1 database (Batjes 2008), and only those profiles that were identified as agricultural soils were considered.

2.2.4 Uncertainty assessment

In order to constrain the uncertainty associated with the assessment, the following approach was adopted. First, the estimates were evaluated by comparing them to large-scale estimates of water erosion reported in literature for cropland outside the US. These observations are therefore outside the data cloud where the model has been calibrated. Secondly, an analysis was conducted to identify the potential error of key parameters and the total model error using the NRI dataset as a validation set following the methodology described in Van Rompaey & Govers (2002). The error of the model output associated with the input data was assessed by Monte Carlo analysis. The model was run 100 times for each HUC4 watershed with stochastically generated input layers, where for each input-parameter (i.e. R, S, and Cc) a probabilistic distribution was assessed. The error on each parameter was considered to have a normal distribution with a zero mean and a standard deviation of 1.5 times the observed standard deviation for each HUC4 watershed. The latter was extracted from the NRI database. The relative root mean square error (RRMSE) of the model output was then calculated by comparing the 100 model estimates for total erosion with the NRI-derived estimates. In addition, an analysis was performed to assess the model error. Three simplified models were derived from the full model (see equation 1) where one factor was kept constant. For each simplified model, the spatially distributed input was replaced by a single constant value. The latter was considered to be the mean value of the eliminated factor. The results of this analysis were then interpreted in terms of the required model complexity. This analysis was performed using the totals of cropland water erosion estimates. However, the resulting uncertainty estimate is also used on estimates for tillage erosion and pasture water erosion, as the lack of similar data for these types of erosion prohibits a similar separate assessment.

2.3 Results

2.3.1 Identification of key factors controlling erosion in the US

The findings show that slope steepness and rainfall/runoff erosivity are the most important factors controlling erosion rates on cropland at the continental scale (Table 2). About 75% of the water erosion variability can be explained by rainfall and slope alone, while other factors such as slope length, support practice, soil erodibility and crop type contribute little and slope length and management factor are not significant. In contrast to croplands, rainfall erosivity plays a minor role for pastures while up to 64% of the water erosion variability is explained by slope steepness alone. Rainfall erosivity and slope steepness, and to a lesser extent crop type, are thus the primary controls on soil erosion by water at the continental scale. If the variability of these key factors can be captured by global databases, they can be used to provide estimates of soil erosion variability at larger spatial scales.

2.3.2 Characterizing R, S and C with global datasets

After aggregation at the HUC4 watershed level, low resolution and low precision rainfall erosivity, slope steepness and crop factor estimates derived from global databases were compared to high resolution and precision estimates from the NRI database.

Rainfall erosivity factor. For both land use types good spatial correlations between NRI and global database estimates (R^2=0.8) were observed (Figure 6). The rainfall erosivity was underestimated by 2% and 52% for cropland and pastures, respectively, and has been corrected for this systematic bias.

Slope steepness factor. The comparison for cropland indicated a substantial overestimation of cropland slopes in watersheds which are situated in mountainous regions. This can be explained by the global slope estimates being based on a study that focused on lowland agriculture (Van Oost et al. 2009). This also indicates that croplands in mountainous areas are preferentially situated on relatively flat terrain, and this is not captured by global databases. Therefore, the data was re-analyzed and the predictive power of several topographical indices explored to identify these areas.

Table 2: Step-wise linear regressions between NRI soil erosion estimates (A) and USLE factors aggregated at the HUC4 watershed level. R = rainfall erosivity factor, S=Slope percent, K= Soil erodibility factor, Cc= Crop cover factor, L=Slope length, P = support practice factor). Significance level p expressed as: 1% = **; not significant (p>0.1) = ^{ns}.

Model	**Factor**	**US cultivated cropland (N=211)**		**Model**	**Factor**	**US pastures (N=208)**		**US dry pastures (N=120)**	
		Model R^2	Partial correlation (r)			Model R^2	Partial correlation (r)	Model R^2	Partial correlation
A=R	R	0.28	0.53**	A=S	S	0.75	0.87**	0.64	0.80**
A=RS	R	0.75	0.81**	A=SR	S	0.8	0.89**	0.8	0.89**
	S		0.81**		R		0.43**		0.67**
A=RSK	R	0.77	0.82**	A=SRK	S	0.86	0.93**	0.84	0.90**
	S		0.81**		R		0.63**		0.74**
	K		0.24**		K		0.55**		0.42**
A=RSKCc	R	0.78	0.83**	A=SRKCc	S	0.87	0.93**	0.86	0.90**
	S		0.82**		R		0.63**		0.75**
	K		0.28**		K		0.55**		0.41**
	Cc		0.25**		Cc		0.19**		0.37**
A=RSKCcP	R	0.78	0.81**	A=SRKCcP	S	0.87	0.93**	0.86	0.89**
	S		0.79**		R		0.61**		0.71**
	K		0.29**		K		0.53**		0.41**
	Cc		0.25**		Cc		0.18**		0.33**
	P		-0.11^{ns}		P		0.09^{ns}		0.11^{ns}
A=RSKCcPL	R	0.78	0.78**	A=RSKCcPL	S	0.87	0.93**	0.86	0.89**
	S		0.79**		R		0.61**		0.71**
	K		0.28**		K		0.53**		0.41**
	Cc		0.25**		Cc		0.18**		0.33**
	P		-0.11^{ns}		P		0.09^{ns}		0.10^{ns}
	L		-0.02^{ns}		L		-0.02^{ns}		-0.04^{ns}

An optimal fit between NRI and global estimates was found when the range of elevation was included as follows:

$$Slope_C = \begin{cases} \left((3.21 + Slope - 0.08ER) * 1.20 + (-0.002EL + 0.26)\right)^{1.08} * 0.95 & if\ EL > 600\ and\ ER > 100 \\ \left((3.21 + Slope - 0.08ER) * 1.20\right)^{1.08} * 0.95 & if\ EL < 600\ and\ ER > 100 \\ \left((Slope * 0.82)^{1.43} * 0.53 * 1.20 + (-0.002EL + 0.26)\right)^{1.08} * 0.95 & if\ EL > 600\ and\ ER < 100 \\ \left((Slope * 0.82)^{1.43} * 0.53 * 1.20\right)^{1.08} * 0.95 & if\ EL < 600\ and\ ER < 100 \end{cases} \quad (2)$$

Where $Slope_C$ is the corrected NRI adjusted slope (%), ER (m) is the range of elevation and EL (m) is the mean elevation in a 3 by 3 window (based on GTOPO data (USGS 1996)). The minimum slope was set to 0%.

This approach resulted in good predictions of cropland slopes at an aggregation level of HUC4 watersheds (R^2=0.62, Figure 6). A similar trend for pastures towards overestimation was observed. Because of the previously described limited entries for agricultural grasslands in the NRI database, correction for these could therefore only improve systematical errors while a spatial evaluation was not possible.

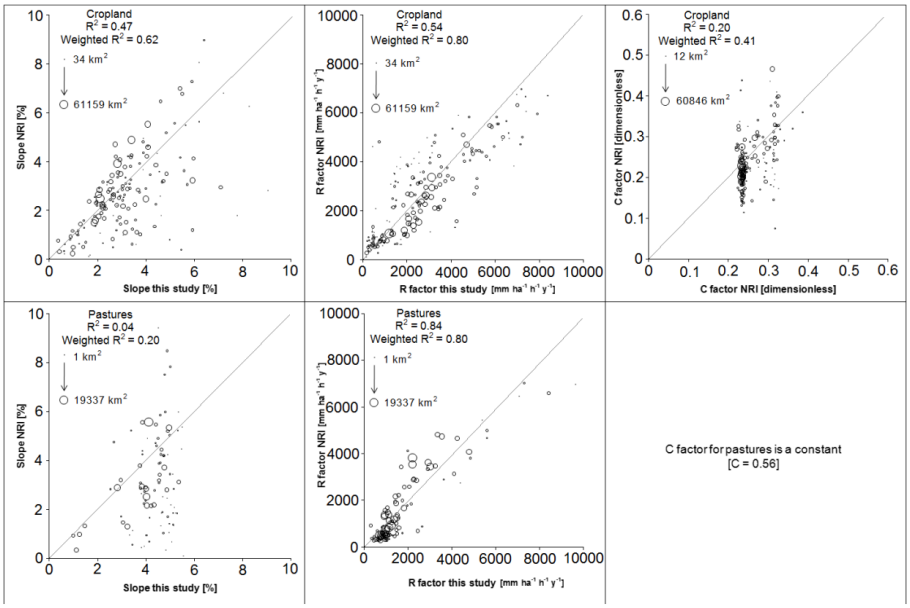

Figure 6: Scatter plots of erosion controlling factors derived from NRI and global databases. Data is aggregated at the HUC4 watershed level.

Crop cover factor. Using the NRI data, mean Cc factor values for all major US crop types were calculated. Spatial estimates based on this information were derived using global crop type abundance maps and compared with NRI estimates. The NRI database showed that US cropland is dominated by maize, wheat and soy; together these crops represent 70% of the total cropland area. The relative contribution of different crop types for the US is well represented by the global database (Table 3). The most important crop types are characterized by a narrow range of Cc factors with mean values that range between 0.22 - 0.24. However, specific crop types have a much higher mean value (e.g. potatoes and sugar beets). Although the global database gave a good prediction of mean Cc factors at the continental scale, the spatial correlation between NRI and global database-derived Cc factors at the HUC4 watershed level was significant, but relatively weak (R^2=0.20, $p<0.001$, Figure 6). It was not possible to relate a global soil dataset to NRI estimates for the K factor (data not shown). Also, those factors that were not contributing significantly to the variation in water erosion at the continental scale, i.e. slope length (L) and management (P) were not included.

Table 3: Cc factor estimates and differences in abundance for major croptypes.

Region	US	US	US	World
Source	USDA (2000); Nusser and Goebel (1997)	USDA (2000); Nusser and Goebel (1997)	Leff et al. (2004)	Leff et al. (2004)
Crop Type	Cc Factor (± 1 StDev)	Fraction (%)	Fraction (%)	Fraction (%)
Wheat	0.22 (± 0.07)	22	22.8	22
Maize	0.22 (± 0.08)	26.4	28.3	13
Rice	0.22 (± 0.08)	1.2	1.3	11
Barley	0.22 (± 0.08)	1.8	2.6	9
Soy	0.24 (± 0.08)	21.3	24.1	5
Potatoes	0.32 (± 0.09)	0.4	0.5	3
Cotton	0.46 (± 0.10)	4.7	6.2	3
Sorghum	0.29 (± 0.08)	3.4	4	3
Sunflower	0.23 (± 0.06)	0.8	1.2	2
Sugar beet	0.31 (± 0.07)	0.4	0.6	1
Other	0.25 (± 0.03)	17.8	8.5	28
Area (10^3km^2)		**1284**	**1471**	**17920**

For these three factors, no spatial estimates were provided but the average value for the US used instead.

2.3.3 Comparison with NRI soil erosion estimates

The estimates were compared, aggregated at the HUC4 watershed level, with NRI derived estimates for cropland and pastureland erosion. For cropland, a reasonably good fit was obtained (Figure 7), although the estimates for larger watersheds were consistently higher than NRI estimates for erosion rates above 10 Mg ha^{-1} yr^{-1} (representing c. 20% of US cropland). This results from the fact that the approach presented here focused on a correct prediction of single factors and did not optimize the output of the multiplicative model, i.e. soil erosion rates. Rather than (re)adjusting individual factors, an adjustment of the erosion estimates for cropland was done as follows:

$$E_{WCf} = 4.7 * Ln(E_{WC}) - 1.79 \quad (3)$$

where E_{WCf} is the final estimate of erosion (Mg ha^{-1} yr^{-1}).

This resulted in an overall model efficiency (R^2) of 0.57 for both water erosion rate and sediment flux (Figure 7).

2.3.4 Uncertainty analysis

Consistent with the identification of key controls on soil erosion, the uncertainty analysis showed that the highest parameter uncertainties were associated with the R and S factors with an rRMSE of the parameter estimates of 52% and 116%, respectively; these are also the parameters with the highest spatial variability. In contrast, the input error for the Cc factor is much lower (rRMSE of 30%). However, the analysis clearly indicated that, when all factors are considered, the effect of uncertainty associated with the model input on model predictions is relatively small. When applying the simplified models where one of the three factors was kept constant, it was observed that the full complexity model was the best model with a total error of 33%. Model structures that do not incorporate slope and rainfall erosivity factors resulted in much higher errors (rRMSE between 43 and 35%). This analysis shows that the model used here is relatively robust because the error on the total erosion flux on US cropland is relatively low (rRMSE of 33%). In a next step the model, which was calibrated with data from the US, is

applied to Europe and confronted the results with independent estimates (Cerdan et al., 2010). The latter study provides estimates for water erosion on different types of land use in Europe with a very high spatial resolution (100 m).

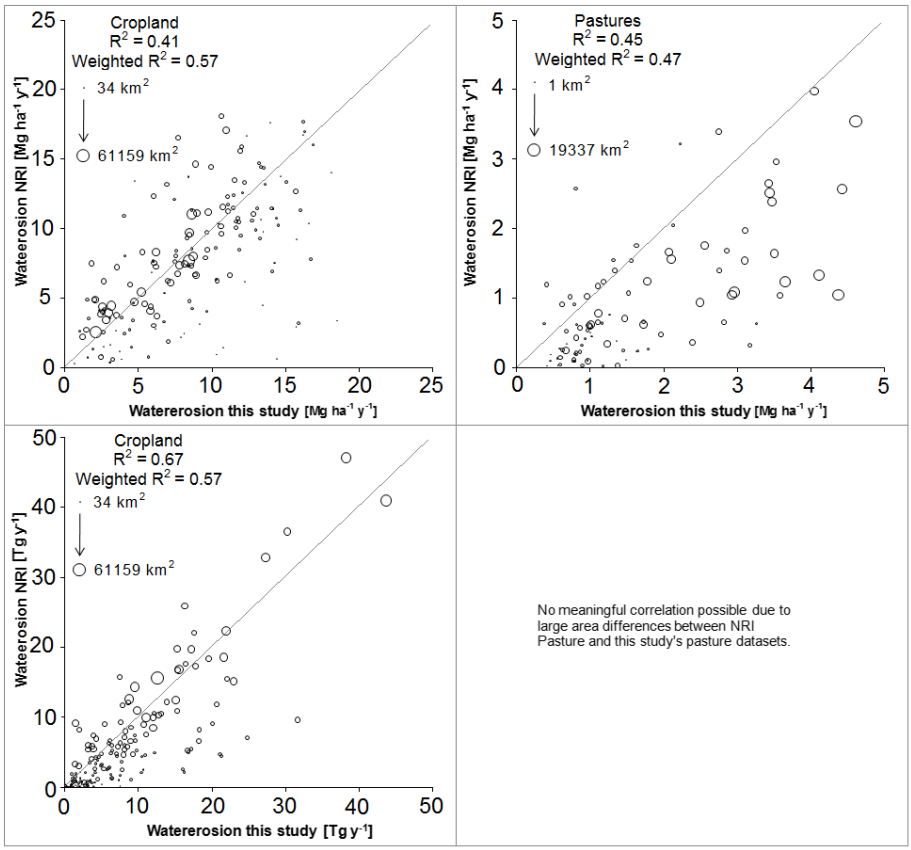

Figure 7: Scatter plots of NRI- and modeled water erosion estimates for US cropland and pastures.

This study is also based on the spatial extrapolation of plot data, but differs from the approach presented here as (i) the spatial databases used have a much higher precision and resolution than the low precision and coarse global databases, (ii) the effect of soil erodibility is explicitly modeled and (iii) the empirical basis is derived from local, and therefore more representative, plot experiments in Europe. Two key observations can be made (Figure 8). First, although there is substantial scatter, there is a significant spatial correlation for both erosion rates ($R^2 = 0.41$, $p<0.01$) and

fluxes (R^2=0.44, p<0.01). This indicates that the approach presented here, which is based on coarse input data and simplified process representation, is able to capture the spatial variability of soil erosion. Secondly, although there is a good spatial fit, the absolute values differ substantially. The Cerdan et al. (2010) estimates are, on average, 58% lower than the estimates (i.e. 9.1 Mg ha^{-1} yr^{-1} vs. 3.9 Mg ha^{-1} yr^{-1}) presented here. This difference is mainly related to the reference soil erosion parameter (i.e. E_{NRIref}, see equation 1), which is 67% lower in the Cerdan et al. study. This clearly shows that, in contrast to the spatial patterns, the uncertainty associated with erosion rates is high (rRMSE = 69%).

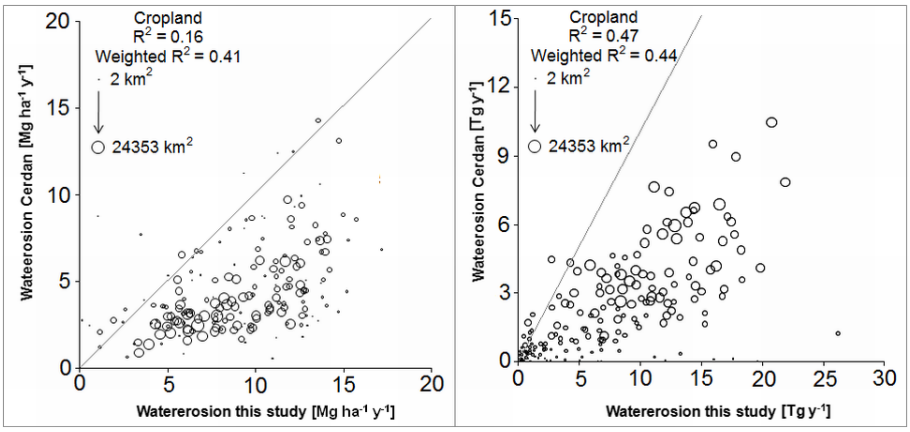

Figure 8: Scatter plots of water erosion estimates taken from the Cerdan et al. (2010) study and modeled estimates for European cropland. Data is aggregated on a regular grid, using the mean HUC4 area estimate for the conterminous USA.

For other regions, e.g. South East Asia, South America or Africa, spatial explicit data concerning soil erosion is still scarce. Based on a RUSLE approach, but using high resolution input data, the Australian National Land and Water Resources Audit (NLWRA, 2001) and Lu et al. (2003) estimated the average annual soil loss due to sheet and rill erosion for cropland in Australia at 3.4 Mg ha^{-1} yr^{-1} and 3.6 Mg ha^{-1} yr^{-1}, respectively. For grassland, the NLWRA reported an erosion rate of 5.6 Mg ha^{-1} yr^{-1}. These independent estimates at the scale of continents are in the same order of magnitude as the estimates presented here, particularly for cropland. The estimates for Australian cropland and grassland are 4.7 Mg ha^{-1} yr^{-1} and 0.9 Mg ha^{-1} yr^{-1}, respectively. For South-Africa, Compton et al. (2010) estimated the rate of sheet water erosion at 6.9 Mg ha^{-1} yr^{-1} for cropland and 1.1 Mg ha^{-1} yr^{-1} for grassland. Their method was based on a quantitative assessment of land

degradation in combination with detailed land cover maps. Again, this is similar to the estimates presented here of 8.4 Mg ha^{-1} yr^{-1} for cropland and 1.6 Mg ha^{-1} yr^{-1} for grassland.

In summary, the results of the Monte Carlo analysis and comparison with independent estimates for Europe, Australia and Africa suggest that the model is able to accurately describe spatial patterns of soil erosion at the continental scale. The error associated with the estimation of the total agricultural sediment flux is much higher. Although a fully analytical error analysis is at present not possible due to data gaps, the analysis suggests that the error is in the order of 30% to 70%.

2.3.5 Global application

When the model is applied to global agricultural land, an accelerated sediment flux (water and tillage erosion) of 20.5 (± 10) Pg yr^{-1} is obtained for the year 2000, with a relative contribution of water erosion of ~85%. This estimate corresponds to a SOC erosion flux of 0.4 (± 0.2) Pg C yr^{-1}. Even though total cropland area is around half of the total considered agricultural grassland area, 15.9 Pg yr^{-1}, representing 78% of total agricultural erosion, are eroded on croplands. The average global erosion rate for cropland and pastures is estimated at 10.5 Mg ha^{-1} yr^{-1} and 1.7 Mg ha^{-1} yr^{-1}, respectively, which results in a global average of 4.2 Mg ha^{-1} yr^{-1} for total agricultural area. High rates of erosion occur in tropical regions where steep slopes and high rainfall amounts coincide, whereas erosion for most other regions varies between 6 – 10 Mg ha^{-1} yr^{-1}. The predicted erosion patterns and rates are presented in Figure 9a & b. Most of the erosion occurs in Asia (43% of total agricultural sediment flux), with high rates especially in South-East Asia (Figure 9a and Table 4). Carbon erosion shows a similar spatial pattern as carbon erosion rates are strongly related to soil erosion rates (R^2=0.95). This implies that variability in soil organic carbon content is less important than variability in erosion rates.

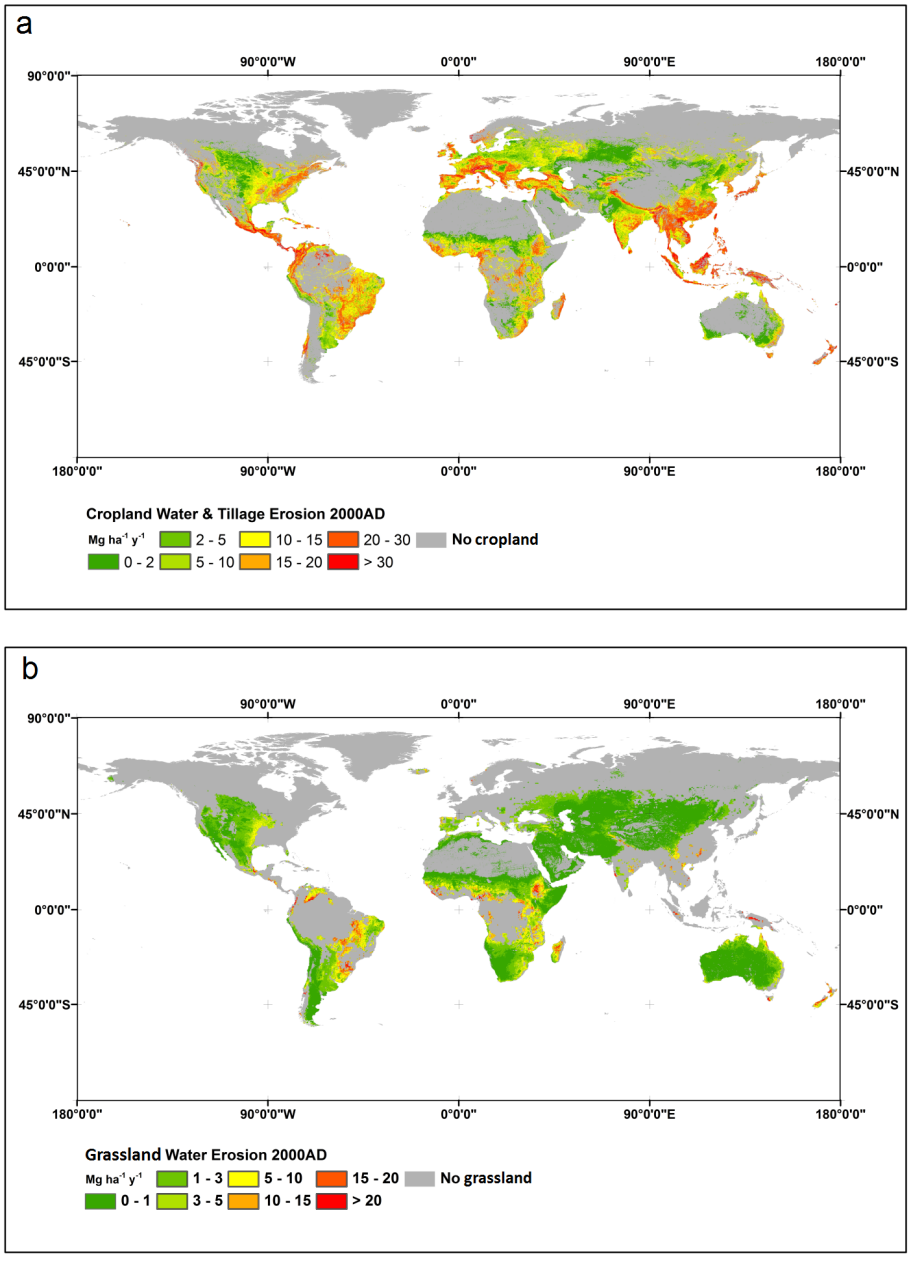

Figure 9: (a) Estimated water and tillage erosion rates for global cropland for the year 2000. (b) Estimated water erosion rates for global pastures for the year 2000. Only pastures in dry environments are considered to erode.

Table 4: Estimates for globally eroded sediment and linked SOC fluxes for cropland (C) and pastures (P) for the year 2000AD. Only Pastures in dry environments are considered to erode.

Region	AREA 2000AD			Sediment Flux			SOC FLUX		
	(10^6 km^2)			(Pg yr^{-1})			(Tg C yr^{-1})		
	C	P	P	C		P	C		p
		Total	Dry	water	tillage		water	tillage	
Central America	0.4	1.0	0.6	0.5	0.2	0.1	9.7	3.6	2.6
Central Asia	0.4	2.8	2.8	0.1	0.1	0.1	1.2	1.0	2.7
China	1.6	4.0	3.0	1.3	0.4	0.2	23.7	7.0	5.4
Europe	2.5	1.4	0.5	1.9	0.6	0.1	39.5	12.0	2.4
India	2.0	0.2	0.1	1.9	0.3	0.0	30.4	3.9	0.5
Middle East	0.6	2.2	2.1	0.4	0.4	0.1	6.8	7.4	1.3
North Africa	0.3	0.7	0.7	0.2	0.1	0.0	2.8	1.1	0.7
North America	2.3	2.5	2.0	1.6	0.2	0.3	31.5	4.5	6.1
North East Asia	0.5	1.7	1.5	0.1	0.1	0.1	3.5	2.5	1.3
Oceania	0.5	4.2	4.1	0.3	0.0	0.5	4.3	0.6	10.5
South America	1.2	4.6	2.9	1.4	0.1	1.4	26.7	2.5	36.2
South East Asia	0.9	0.2	0.0	1.5	0.2	0.1	31.2	3.0	3.0
Sub Saharan Africa	2.0	8.1	7.0	1.8	0.2	1.7	29.9	2.5	38.0
TOTAL	**15.1**	**33.4**	**27.4**	**13.1**	**2.8**	**4.6**	**241.1**	**51.7**	**110.7**

2.4 Discussion

2.4.1 Comparison with other global estimates

A global flux of 13.1 (±6.6) Pg yr^{-1} by water erosion on cropland is obtained. Syvitski et al. (2005) present an assessment of the human impact on global river sediment discharge. They estimate the global human-induced river sediment flux at 2.3 ± 0.6 Pg yr^{-1}. Here, this river flux is discussed in relation to the estimates of accelerated erosion, which reflects mobilization of sediment in uplands. This is done by taking into account the retention and delivery of sediments to the fluvial system. Although controlled by a series of factors including basin area, climate and topography, between 10 to 30% of the material mobilized by accelerated erosion are typically delivered to

the fluvial systems (e.g. De Vente et al. 2007; Walling and Web 1996). When this ratio is applied to the estimates of this approach, a human-induced river flux of 1.8 - 5.4 Pg yr^{-1} is obtained. This is similar to the flux estimated by Syvitski et al. (2005) and suggests that the global estimates presented here are in the right order of magnitude.

Montgomery (2007) presented currently the most comprehensive study on soil erosion rates under conventional and conservation agriculture as well as soil production rates. The extrapolation of plot-data to global agricultural lands is the most commonly used method to estimate global fluxes (e.g. Pimentel 1995; Hooke 2000). Here, the mean value of the plot studies presented in Montgomery (2007) is taken and compared to the estimates of the approach presented here. This shows that the estimate for cropland erosion is approximately five times lower than the mean value of erosion rates derived from plot experiments (i.e. 10.5 Mg ha^{-1} yr^{-1} versus 54.0 Mg ha^{-1} yr^{-1}, assuming a soil bulk density of 1.45 g/cm^3. A comparison of the cumulative distribution (Figure 10) shows that the approach presented here results in an erosion rate below 20 Mg ha^{-1} yr^{-1} for 80% of the cropland area, while this true for less than 50% of the experimental studies.

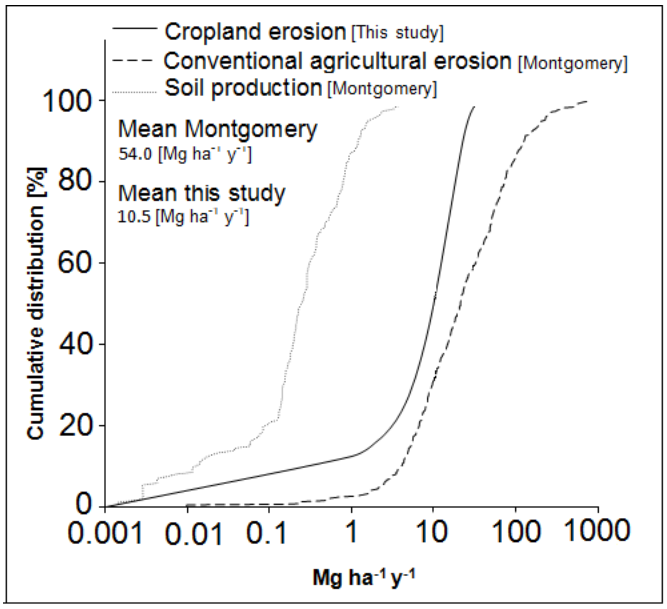

Figure 10: Frequency distributions of soil erosion and soil production derived from point observations (Montgomery 2007) and the estimates of cropland water erosion presented in this approach for the year 2000.

Comparison to global estimates (Table 1) available in literature and which are based on extrapolation of erosion plot data (e.g. Myers 1993 [50 Pg yr^{-1}]; Wilkinson and Mc Elroy 2007 [28.1 Pg yr^{-1}]; Pimentel et al. 1995 [73.5 Pg yr^{-1}]) shows that these estimates are two to five times higher than the estimate presented in this approach here. Similar, using river sediment data and applying a yield enhancement factor (e.g. Stallard 1998 [23.7-64.9 Pg yr^{-1}]), extrapolation using erosion rates per capita (Hooke 2000 [120 Pg yr^{-1}]) or the application of erosion models on a global scale (e.g. Van Oost et al. 2007 [28.3 Pg yr^{-1}]; Yang 2003 [79.6 Pg yr^{-1}]; Ito 2007 [172.2 Pg yr^{-1}]) result in much higher fluxes than the approach presented here. This indicates that empirical studies are biased towards areas which are characterized by high erosion rates and are probably not fully representative for global cropland. Extrapolating without taking into account the spatial variability of controlling factors or applying erosion models with relatively coarse input data will therefore overestimate total erosion and consequently lead to erroneous conclusions when applied to large areas. Although this suggests that existing estimates are likely to be overestimations, rates of accelerated erosion are well above typical rates of soil formation (which is estimated on average at 0.53 Mg ha^{-1} yr^{-1}, assuming a soil bulk density of 1.45 g cm^{-3}; Montgomery 2007).

2.4.2 Soil erosion as a soil modifier

In the previous paragraphs, the magnitude of the erosional disturbance is addressed. Here it is discussed how this lateral transport of sediment and organic carbon is relevant for the cycling of carbon between the terrestrial ecosystem and the atmosphere. On eroded sites, former subsoil mixes with remaining topsoil resulting in SOC depleted topsoils when compared to non-eroded profiles. Partial to complete replacement of eroded C via crop production may results in net uptake of atmospheric CO_2 (Stallard 1998). On depositional sites, former topsoil gets buried under continuously deposited material which may inhibit decomposition of SOC and deep profiles, enriched in SOC develop. The erosion-induced alterations of the net CO_2 fluxes between the soil and the atmosphere thus critically depend on the rate of mixing subsoil material into topsoils and the replacement of SOC at sites of erosion (Quine & Van Oost 2007; Van Oost et al. 2007). The approach described above allows us to quantify this dilution process on a global scale by linking the model with the spatially explicit WISE 3.1 soil profile

database. Assuming constant erosion rates, the SOC profile modifications induced by agricultural erosion for the period 2000AD – 2050AD is estimated. The SOC profiles change in response to erosion and are updated each year. The amount of SOC eroded is proportional to the erosion rate (derived from the model) and the SOC inventory of the topsoil layer (0-20 cm, derived from WISE 3.1). As a result of erosion, a fraction of the subsoil layer is incorporated into the top soil layer. The results indicate that this dilution effect is important for the vast majority of cropland (Figure 11). For example, the average dilution of the topsoil in the EU-25 states equals 22% for the whole period or a loss of 20.59 (± 6.7) g C m^{-2} yr^{-1} (assuming a soil bulk density of 1.45 g cm^{-3}). In relation to other C fluxes this value is comparably low, as the C balance is dominated by gains and losses due to Net Primary Production (NPP), harvest and respiration (Ciais et al. 2010). However, it is in the same order of magnitude as other disturbances of these dynamics and offsets carbon gains from improved management, e.g. fertilizer C input (+ 26 g C m^{-2} yr^{-1}) (Table 5).

Table 5: Cropland C fluxes in the EU-25 compiled by Ciais et al. (2010) in relation to the estimate of C losses presented here due to erosion-induced dilution.

Flux	**C gains (+) and losses (-) g m^{-2} yr^{-1}**
Net Primary production	(+) 490 - 846
Heterotrophic respiration	(-) 299
Harvest	(-) 239 - 275
Fertilizers	(+) 26
River outflux	(-) 9.6
Net biome production	(-) 8.3(± 13) -13(± 33)
Trade net	(+) 6.8
Fires	(-) 3.3(± 1)
Erosion induced dilution (This study)	(-) 22.6(±10)

On a global scale, the highest losses are simulated in the (sub)tropics, where a combination of steep slopes and high rainfall results in high erosion rates, such as Brazil, South-East Asia or Ethiopia. This is consistent with the observations of Ziegler et al. (2009) and Valentin et al. (2008). However, topsoil enrichment is also possible: due to erosion, the organic sublayer of

specific soils (e.g. Histosols) is incorporated into the topsoil layer. The cropland area experiencing gains is small (22%) compared to cropland experiencing SOC losses (78%) (Figure 11). It is important to note that the data present here should be interpreted in terms of a disturbance. It is clear that dynamic processes such as the replacement of eroded carbon by new photosynthate, changes of microbial decomposition rates and erosion-induced changes in soil properties are essential to fully understand SOC dynamics (e.g. Billings et al. 2010; Jacinthe & Lal 2001; Jacinthe et al. 2001). However, this analysis shows that erosion-induced changes in topsoil carbon content are significant at a global scale and that agricultural soils should be considered as dynamic systems that can change rapidly. For example, the substantial dilution has implications for soil carbon monitoring studies that usually do not consider erosion and identify all (topsoil) soil carbon losses as a source for atmospheric CO_2 (e.g. Goidts et al. 2009a).

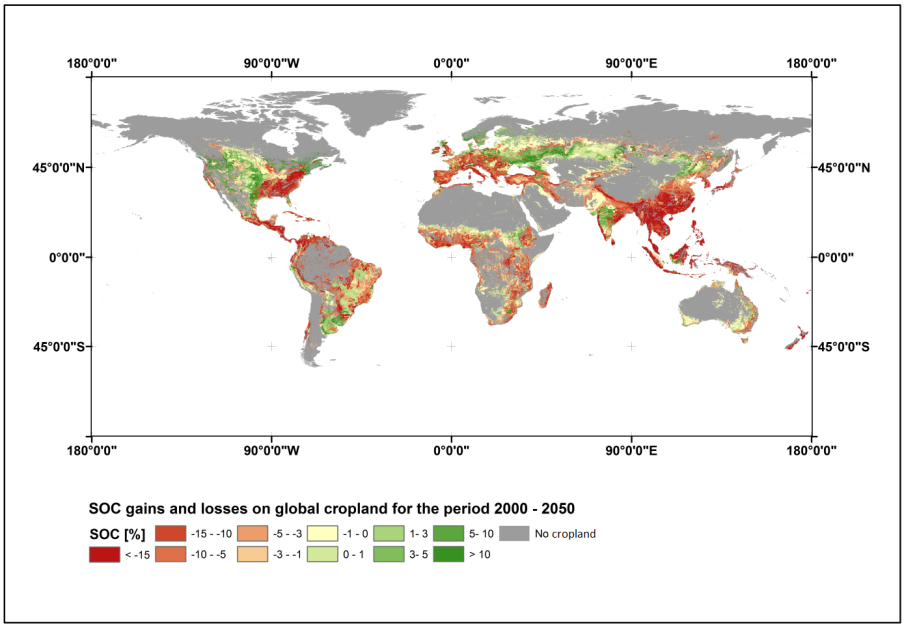

Figure 11: Simulated changes in topsoil SOC contents due to soil erosion for the period 2000–2050. Gains are related due to the inclusion of carbon rich subsoil.

2.4.3 Caveats

The approach taken here aims to simplify and parameterize the key factors that control accelerated erosion and SOC erosion based on quantities that can

be inferred at global scales. As is the case with any global-scale model, it is subject to drawbacks and it does not capture the subtleties that drive small-scale variation. Although the analysis shows that a simplified model and coarse, but global, input data allow for a good prediction of spatial patterns in both the US and Europe, the uncertainty associated with the magnitude of global accelerated erosion is without any doubt high.

US conditions are diverse and can be considered to be representative for a large fraction of global agricultural land. However, US agricultural land may not be fully representative for global agricultural land for various reasons (Table 6). First, US slope factors are on average 35% lower than global values because US cropland is biased towards lowland agriculture in the Mississippi valley. In addition, R factors on eroding dry pastures in the US are about 27% less than the world average, as the US rangelands are typically situated in very dry continental mountain ranges which might not be fully representative for the full range of grassland in other parts of the world (e.g. Australia, Brazil, Central Asia). Although distributions of the major crop types (e.g. wheat, maize) are similar, the more erodible crop types (e.g. potatoes and sugar beets) are more abundant on global cropland (Table 3) than in the US. In particular, the combination of steep slopes and high rainfall erosivity is rare in the US, while the global extrapolation shows that these conditions make up most of the global accelerated erosion (e.g. more than 26% of the global flux occurs in South-East Asia and India, Table 4 & Table 6).

Table 6: Representativeness of US cropland and grasslands.

Factor	World average Cropland (± 1 StDev)	US average Cropland (± 1 StDev)	World average Dry Pastures (± 1 StDev)	US average Dry Pastures (± 1 StDev)
Cc	0.26 (± 0.02)	0.25 (± 0.03)	-	-
R	2970 (± 3521)	2688 (± 1452)	2147 (± 4158)	1568 (± 1155)
S	0.48 (± 0.51)	0.31 (± 0.29)	0.44 (± 0.23)	0.47 (± 0.18)
K	0.92 (± 0.24)	0.97 (± 0.15)	0.82 (± 0.32)	0.88 (± 0.29)

At present, accurate continental- or regional scale assessments of agricultural soil erosion are lacking in these (sub)tropical regions and it is therefore not possible to verify the model predictions. In addition, the management of

agricultural land in the US, which is representative for high-input agriculture, might be different elsewhere (e.g. in terms of landscape structure, cover crops, conservation techniques, etc.).
Second, the approach presented here is based on an empirical model. Although the limitations and drawbacks of the USLE were discussed recently (Parsons et al. 2004), it is based on more than 10000 plot-years of soil erosion data and should be considered as one of the largest data-collecting efforts in environmental sciences. However, the USLE was designed for deriving erosion estimates on much smaller scales (i.e. Catena and hillslopes) than addressed in this study. Especially the connectivity of factors that can lead to erosive events at smaller scales cannot be addressed at the resolution used in this approach here.
Third, other processes, which may dominate accelerated erosion at different spatial scales or under specific conditions are not included in the analysis such as (ephemeral) gully erosion, wind erosion and soil losses associated with harvest (Poesen et al. 1996). Currently, neither the required empirical data nor models are available to present a meaningful assessment of these processes at larger spatial scales.
In summary, the approach used here is admittedly not very complex – the lack of (spatial) data on how erosion varies with soil erodibility or management (e.g. terracing), as well as information on what controls agricultural erosion in mountainous (sub)tropical or low-input agricultural systems, precludes a more detailed formulation. However, the good spatial predictions of agricultural erosion suggest that the coarse model presented here is able to capture the variability of agricultural erosion at the continental scale. It is not possible to accurately assess the uncertainty associated with these estimates of global agricultural erosion due to the lack of model testing data in specific regions. However, comparison with estimates for Europe, South Africa and Australia and the results from the uncertainty assessment indicate that the uncertainty will be in the order of ~ 30-70%.

2.5 Conclusion

A simplified global-scale model is parameterized with NRI data for the US. The good agreement between this approach and empirical estimates for larger regions suggests that the approach may capture the essence of accelerated erosion. As such, the model may be used to predict the

significance of accelerated erosion for the global carbon cycle, soil evolution or sustainability of agricultural practices at continental or global scales. The lack of data on how erosion varies with soil erodibility or management, as well as information on what controls agricultural erosion in mountainous (sub-)tropical or low-input agricultural systems, precludes a more detailed formulation and validation. However, to date this global assessment is the only attempt that is (i) consistent with empirical observations at relevant spatial scales and (ii) is validated at the continental scale. Nevertheless, at present it is not possible to accurately assess the uncertainty associated with these estimates of global agricultural erosion due to the lack of model testing data in regions which differ from US conditions.

A soil/SOC erosion rate on a global scale at 10.5 Mg ha^{-1} yr^{-1} / 193 kg C ha^{-1} yr^{-1} and 1.7 Mg ha^{-1} yr^{-1} / 40.4 kg C ha^{-1} yr^{-1} is estimated for croplands and eroding pastures, respectively. This corresponds to a total flux of 20.5 (±10.3) Pg yr^{-1} of soil and 403.5 (±201.8) Tg yr^{-1} SOC due to agricultural erosion for the year 2000. Although the uncertainty is high, these numbers are significantly lower than former assessments based on extrapolation of local data and show that only a small area of cropland and pastures is subjected to high erosion rates. It is likely that empirical studies are biased towards intensively eroding areas and may therefore overestimate global erosion substantially. The analysis presented here demonstrates that simplified global-scale approaches may well capture the spatial variability of accelerated erosion and that existing estimates are likely to overestimate the erosion of SOC induced by human activities. Nevertheless, there is no doubt that even these lower estimates of agricultural erosion largely exceed rates of soil formation - especially in (sub)tropical regions - and this should be considered as a serious threat to the soil resource.

3 Process understanding for SOC stock predictions at the regional scale[2]

3.1 Outline

Recent advances in remote sensing make it possible to acquire large amounts of spatially explicit information on soil properties including SOC concentration covering large areas at a relatively low cost (Cécillon et al. 2009; Rossel and Chen 2011; Mulder et al. 2011). Using hyperspectral airborne sensors and a set of local field calibration data, large areas of bare land can be measured resulting in maps of soil C contents across various soil types and landforms (e.g. Gomez et al. 2008; Stevens et al. 2010). However, when data is acquired using air or space-borne platforms, the signal represents surface properties alone at lower accuracy (RMSE 5.3 -6.2 g C kg^{-1}) than lab-based reference methods. Such applications cannot provide information on SOC contents below this layer and observations of SOC depth distributions are generally sparse on a regional scale. These limitations lead to high uncertainties (± 30%; Meersmans et al. 2009b) associated with the estimation of regional *three-dimensional* SOC distributions. Recent studies have shown the potential of mapping approaches for subsoil SOC predictions, where sparse SOC depth profiles are complemented by more dense secondary attributes that can be derived from available digital elevation model (DEM) data or soil maps (e.g. McKenzie and Ryan 1999; Meersmanns et al. 2009b; Mishra et al. 2010; Schwanghart and Jarmer 2011; Zhang et al. 2012) to extrapolate topsoil SOC information for SOC predictions at greater depths. In many cases, the mapping of SOC stocks is the main objective and it remains unclear (i) how explanatory variables are linked to environmental processes affecting the SOC distribution, (ii) the specific importance of these variables for the prediction of SOC and (iii) at what spatial scale they actually have to be considered to operate.

In this study, the aim is to bridge this gap between spatial explicit SOC stock assessments and process understanding at larger spatial scales. A pilot-study

[2] ***The content of this chapter has been submitted for publication as:*** Doetterl S., Stevens A., Quine T.A., Van Wesemael B., Van Oost K. (*submitted*): Spatial-explicit regional-scale prediction of soil organic carbon stocks in cropland employing environmental variables ad mixed-model approaches. *Geoderma*.

is presented that aims to identify variables that can be linked to environmental processes that control the 3D SOC distribution in cropland at a regional scale. These variables are then used for the prediction of spatial explicit C stocks and ranked according to their importance for these predictions. First, field samples for a region of 500 km^2 in Luxemburg were collected and used to construct a vertically explicit SOC database. Then this dataset is used in combination with climatic, pedologic, topographic and hydrologic data that is derived from existing DEM and climate data for the region in order to identify the key environmental controls on the spatial and vertical patterns of SOC storage and to build a 3D SOC prediction using linear mixed effect models. Finally, the model is used in combination with continuous topsoil SOC data from airborne hyperspectral remote sensing (HRS) to present a regional SOC stock estimate. For this estimate, the spatial variability as well as caveats and potential pitfalls of the approach presented here are discussed. Furthermore, it will be shown how estimates using this approach differ from stable landscape approaches that usually work with depth extrapolation of SOC contents (e.g. Meersmans et al. 2009b) and the implications of the findings for the application of SOC models at the landscape/regional scale are discussed.

3.2 Material and Methods

3.2.1 Study area

The study area is a ~500 km^2 north-south transect in the Great Duchy of Luxembourg (NW corner: 50°03'N 6°03'E; SE corner: 49°33'N 6°12'E). The climate of Luxembourg is temperate semi-oceanic with ~863 mm annual precipitation and a mean annual temperature of 8.8 °C (Climate data 2012). The northern part of the country belongs to the Ardennes massif with a mean altitude of 450 m and has slightly lower mean temperatures than the southern part with a mean altitude of 244 m. The transect covers the major agricultural soil types of temperate Europe including Cambisols, Arenosols and Luvisols (IUSS Working group 2006). In addition, the soil map of Luxembourg classifies colluvial and alluvial areas as a separate class and these areas have been manually assigned to a soil texture class according to the surrounding texture zone (which provides the input material to these depositional settings) taking into account local topography and flow patterns (Figure 12).

The majority of the cropland in the study area (>75%, EEA 2012) is situated in two texture zones, i.e. a loam (68.5 km^2) and clay (79.1 km^2) zone. All further analyses were performed separately for these two dominant classes. Notably, the two texture zones covered in the study differ in terms of landforms. The northern part of the study area, dominated by loamy soils, is characterized by a hilly topography with steep slopes (Slope: 8.1±4.8 %) and most of the cropland is located on either plateaus or slopes. The southern part, dominated by clay-rich soils has a much lower relief intensity (Slope: 5.9±3.6 %) and is less undulating with cropland ranging from plateau over slopes to positions in the valley bottom (Table 7).

Table 7: Cropland area, mean slope of the research area and number of sampled profiles. Abbreviations for positions defined in Figure 12.

Slope position	**Loam**			**Clay**		
	Area covered (ha)	Slope (%)	Profiles (N)	Area covered (ha)	Slope (%)	Profiles (N)
Plateaus(FP; SP)	178	6.3±3.3	22	330	4.8±2.6	22
Slopes (CS; UB; CB ;LB)	101	10.8±4.6	41	82	9.6±2.8	21
Footslope & Basin (CF;B)	18	11.7±5.2	10	46	7.0±4.0	19

3.2.2 Field sampling

In the loamy and clay-rich texture zones within the study area, 100 soil cores were sampled from cropland up to 1 m depth (Figure 12). The profiles (further called LUX profiles) were sampled at 15 slope transects along geomorphic gradients: profiles on flat or less sloping plateaus at the hilltop, slope positions with differing steepness, curvature and positions on the footslope and in the valley bottom. The cores were sampled undisturbed using a closed tube sampling system (Ø 4.5cm) (Eijkelkamp, The Netherlands). The cores were stored in sealed PVC-tubes at -18 °C until preparation for analysis. In order to increase the number of available soil profiles, data from 35 soil profiles was added to the database (further called SDP profiles), provided by the pedologic soil survey service of Luxembourg.

This data originates from soil surveys conducted in the 1960's and (BDSOL LU 1969) were used to create the pedologic map of Luxembourg.

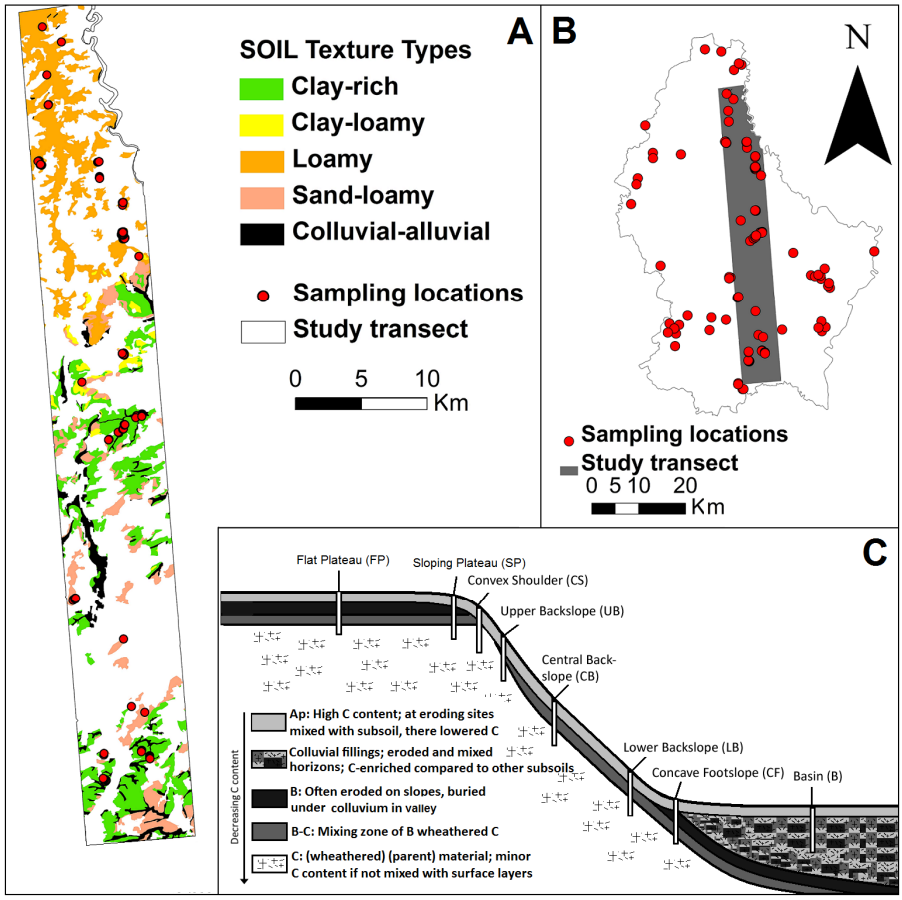

Figure 12: Soil texture zones distributed on Luxembourg cropland (A), the location of study transect and study sites (B) and a conceptual view on the sampling design as well as typical horizontation as found in hillslope studies on cropland (C).

3.2.3 Soil analysis

Soil bulk density (BD) was analyzed according to Blake & Hartge (1986) and stone content (as percent mass) was assessed by dry sieving at 2 mm. The fine SOC content of the LUX profiles was measured by depth intervals of 10 cm to a depth of 1m for each profile using a VarioMax CN dry combustion Analyzer (Elementar GmbH, Germany) and analyzed in

duplicate. Samples containing inorganic C were pre-treated before the combustion by adding 3 % HCl to remove inorganic C (Elementar GmbH 2009). Carbon in the SDP dataset has been estimated with dichromate wet combustion (Walkley and Black 1934), including a constant factor of 1.33 correcting for the incomplete combustion using this method. As bulk density information is not provided for SDP profiles, the mean BD values of the major soil zones for each respective soil layer was used for these profiles from the LUX dataset. The soil C stocks derived from the soil profiles were aggregated for the following soil layers for which all further analyses were performed separately: (i) the total SOC stock (0-100cm), (ii) the plowed topsoil (0-20cm) (iii) the shallow subsoil (20-40cm) as a mixing zone between top- and subsoil dynamics and (iv) the deeper subsoil (40-100cm) as a layer unaffected by plowing activity. The SOC stocks (kg/m^2) of the specific soil layer were calculated as:

$$SOC_{stock} = \frac{(Cconc * (1 - Stcor) * BD * Svol)}{1000} \quad (4)$$

Where C_{conc} ($gC\ kg\ soil^{-1}$) is the mean SOC concentration of the fine soil mass (<2mm),St_{cor} a correction factor for the stone content (>2 mm) (dimensionless), BD the mean bulk density ($kg\ m^{-3}$) and S_{vol} (m^3) the soil volume of the respective soil layer.

Additionally, for five fields in the clay zone and two fields in the loam zone, ^{137}Cs inventories along a geomorphic transect covering the slope positions described above (Figure 12) have been analyzed. The basic methodology is described by Quine and Van Oost (2007) but the sampling scheme was modified by drastically reducing the number of samples per field: Four reference profiles per field at stable plateau positions and one profile per geomorphic position were sampled for each analyzed field. This low density sampling scheme has been chosen in order to estimate the regional soil redistribution intensity (SRI). It cannot be used to derive slope scale patterns of erosion and deposition rates in the research area as the individual core data are too varied to derive mean erosion rates based on arithmetic means of core ^{137}Cs activity rates. In total, 72 cores up to a depth of 75cm were analyzed with an average analysis time of 37h per sample and a detector efficiency of 1.35. The measured mean ^{137}Cs activity is rather low at 4.9±0.5

mBq g^{-1}. As a qualitative statement on the SRI in the different fields, the relative difference (%) of the mean coefficient of variation (CV) at undisturbed reference sites at stable plateaus to the CV of the eroding and depositing field sites is used. When $CV_{field} < 1.5 \times CV_{ref}$, we suggest limited SRI. Where $CV_{field} > 1.5 \times CV_{ref}$ and $CV_{field} < 2 \times CV_{ref}$, we suggest moderate SRI. When $CV_{field} > 2 \times CV_{ref}$, we suggest high SRI. The CV for field or reference site X is then calculated as:

$$CV_{(X)} = \frac{SD(x)}{Av(x)} \quad (5)$$

with SD as the Standard Deviation and Av as the arithmetic mean.

The SRI for field X is then calculated as:

$$SRI_{(X)} = \frac{CV(field)}{CV(ref)} \quad (6)$$

3.2.4 Environmental covariates

A broad range of spatial data covering hydrologic, topographic, climatic and pedologic parameters was collected and their content was linked to the soil profile database as potentially explaining variables for the 3D SOC stock distribution (Table 8). The pedologic parameters included in the modeling are soil texture and the measured mean topsoil SOC (0-20cm) concentration. Meersmans et al. (2008, 2009a) showed that soil texture plays a crucial role in subsoil SOC predictions. As soil texture measurements were not available for all sampled cores, the dataset was split according to the two texture classes as derived from the soil map of Luxembourg (Clay and Loam). Meersmans et al. (2009b) also demonstrated that in landscapes with low relief intensities, topsoil SOC concentration can be used to predict SOC with depth through an exponential function, which depends on soil type and drainage. Hydrologic parameters included in the modeling were flow accumulation, upstream flow area and the topographic convergence index (TCI) (Beven and Kirkby 1979), also referred to as the wetness index. The topographic characteristics of a profile are addressed by including slope, profile, plan and general curvature and the topographic position index (TPI)

Table 8: Overview of the considered environmental covariates and their peculiarity.

Covariate and typology (T) = Topographic; (H) = Hydrologic; (P) = Pedologic;(C) = Climatic; (TH) = Interaction topographic/hydrologic	Low (or neg.) value	High (or pos.) value	Clay		Loam	
			Range	Mean (±SD)	Range	Mean (±SD)
(T) Slope (%)	Flat landform	Steep landform	0 - 13	5.8±3.5	0 - 19.8	9±4.1
(T) Profile curvature	Convex curvature	Concave curvature	-1.6 - 0.6	-0.1±0.3	-1 - 0.7	-0.1±0.2
(T) Plan curvature	Concave curvature	Convex curvature	-0.5 - 0.6	0±0.2	-0.9 - 1	0±0.2
(T) Total curvature	Concave curvature	Convex curvature	-0.6 - 2.1	0.1±0.4	-1 - 1.2	0.1±0.4
(H) TCI	Low wetness	High wetness	2.1 - 8.2	5.1±1.4	2.1 - 8.9	4.6±1.3
(H) Flow accumulation	Low flow accumulation	High flow accumulation	0 - 248	18±38	0 - 685	26±85
(C) Precipitation seasonality (CV; % of Mean)	Low seasonality	High seasonality	9 - 12	10±1	11 - 13	12.9±0.4
(C) Temperature seasonality (SD*100)	Low seasonality	High seasonality	581 - 599	589±6	566 - 585	576±3
(C) Annual mean temperature (°C)	Low mean temperature	High mean temperature	8.6 - 9.4	9±0	7.6 - 9.2	8±0.2
(C) Annual precipitation (mm/yr)	Low precipitation	High precipitation	742 - 899	804±32	712 - 996	890.9±39.9
(P) SOC Topsoil %	Low topsoil C %	High topsoil C %	0.7 - 3.7	1.87±0.6	0.8 - 3.4	1.93±0.6
(TH) Upstream flow area	Short upstream area	Long upstream area	10 - 6571	188±471	1340623	115±188
(TH) TPI	Lowland position	Upland position	-0.5 - 0.8	0.1±0.2	-0.4 - 0.4	0±0.1

(Jenness 2006), a relative measure of a cell's elevation in comparison to its neighborhood. Note that some of these variables such as the upstream flow area, TCI and TPI are composite parameters as they include both geomorphic and hydrological information. Finally, the following climatic covariates were considered: Mean annual temperature and precipitation as well as annual range and seasonality of these variables. Temperature seasonality (T_{seas}) is hereby calculated as 100 times the standard deviation (SD) of the mean annual temperature. The precipitation seasonality (P_{seas}) is calculated as the coefficient of variation of the annual precipitation (Hijmans et al. 2005). A 5x5 m DEM was built on a triangulated irregular network (TIN) surface elevation model based on 10 m contour line data using linear interpolation in ArcGIS 9.3 3D-Analyst (ESRI Enterprise, Redlands, CA). All hydrologic and topographic variables were derived from this DEM. The derivates of the elevation model were created using ArcGIS 9.3 Spatial Analyst (ESRI Enterprise, Redlands, CA) and the ArcGIS 9.x extension Topography toolbox 9.2 (ArcScripts 2010). The climatic variables were taken from the worldclim 1km^2 resolution dataset of bioclimatic variables (Hijmans et al. 2005) resampled to the DEM resolution. The soil texture classification was taken from the digitalized soil map of Luxembourg (LSP 1969). As environmental co-variates may act and vary at very different scales (e.g. McKenzie and Ryan 1999; Mayor and Bautista 2012, Zuo et al. 2012), for each pixel the mean and SD of pixels that are in a neighborhood of 25 m^2, 2500 m^2, 10.000 m^2, 40.000 m^2 and 1 km^2 of the input location were computed, resulting in a total of 45 potential explanatory variables.

3.2.5 Model building, implementation and statistics

Slope position classifications (Jenness 2006; Weiss 2001) have been performed using the ArcGIS 9.x extension Topography toolbox 9.2 (ArcScripts 2010) and calibrated using the on-field observed topographic position of each soil profile. All statistical analyses were done in SAS 9.3 (SAS Institute Inc., Cary, NC) and R 2.11.1 (R Development Core Team 2010). To eliminate variables that are cross-correlated and show poor explanatory power for the SOC stock of a depth layer, a preliminary stepwise linear regression model was run. Then, randomly selecting 90% of the data for calibration and retaining 10% for validation, a linear mixed effect model (LMM) was fitted for each texture zone and each soil layer using the "nlme" package (v. 3.1-104) for R 2.11.1 (R Development Core

Team 2010). LMM's have been shown to work well in similar studies (e.g. Stewart et al. 2007, Haskard et al. 2010; Suuster et al. 2012), can estimate both random and fixed effects and allow modeling spatially autocorrelated observations and errors using semivariograms. The latter is crucial as the sampling design, which uses a catena approach, is by its nature clustered. Random effects were obtained through restricted maximum likelihood and fixed effects using maximum likelihood. The model errors of the mixed effect models are assessed using the standard error, while the relative root mean square error (rRMSE) was used to assess the error associated with predictions of the validation data. The quality of the model fit was assessed using the Aikake information criterion (AIC) (Akaike 1973) and its amended version corrected for small sample sizes (AICc) (Anderson et al. 1998). The Akaike information criterion (AIC) is an estimate of the relative distance between the fitted model and the unknown true equation (or process) that produced the observed data (Burnham and Anderson 2001, Stewart et al. 2007). AIC and AICc were calculated as:

(7) $$AIC = -2 \log L[(\theta_i \mid Y)] + 2K$$

(8) $$AIC_c = AIC + \frac{d2K*(K+1)}{n-K-1}$$

with $L[(\theta_i \mid Y)]$ as the maximized likelihood, a function of the unknown parameters θ_i, given the data Y and the model, K as the number of parameters and n as the number of samples.

This criterion was used to rank the models in order to select the "best" model and, hence, the model with the highest degree of information (smallest AIC(c) values) to explain SOC stocks. Furthermore the importance of each variable for the prediction of SOC stocks in different depth layers is assessed by computing the difference in AICc (expressed as δAICc) between the full model with all significant variables and a model with only the variable under study. For the computation of AIC and AICc as well as the importance ranking the "AICcmodavg" (v.1.25) and "caret" (v.5.15-023) packages for R 2.11.1 (R Development Core Team 2010) were used. Roughly, differences in AICc of 1-5 can be interpreted that the models contain similar information and prediction strength, 5-20 indicate significantly lower prediction ability but still a good fit of the one parameter model and differences above 20

indicate very poor model fit and minor improvements using this variable. Throughout the article, differences between the means of classes have been performed using multi-group ANOVA Bonferroni corrections and Tamhane's T2 and all statistical analysis has been performed on a significance level of $p<0.05$.

3.2.6 Regional SOC stock assessment using HRS topsoil SOC data

Using the regression models presented in the results section, the mean regional SOC stocks for the two texture zones in different soil layers are estimated. To provide a full spatial coverage of all explanatory variables in the different models, the measured topsoil SOC concentration is replaced with high resolution estimates of topsoil SOC concentrations obtained by remote sensing (Stevens et al. 2010). In this study, the topsoil SOC concentration for a large number of cropland fields in the transect shown in Figure 12 (c. 7.6km^2 = 5% of total cropland in the area) has been measured and predicted using airborne HRS and visualized on a 2.5x2.5m raster grid. The data further covers all possible cropped landforms in the research area and no spatial bias was identified. The prediction accuracy of the method has been evaluated at ~3-4 g C kg^{-1}. The estimates provided by Stevens et al. (2010) represent the SOC concentration in the 0-5cm soil layer under seedbed conditions. In the approach presented here, topsoil SOC concentration represents the layer 0-20 cm. Therefore, before including the HRS data into the models for a regional extrapolation and in order to make them representative for the depth interval 0-20 cm, a systematic bias towards higher SOC values in the HRS derived 0-5 cm data compared to the measured 0-20cm SOC concentration was corrected for. The HRS 0-5cm is on average 33.0 % higher than the measured 0-20cm SOC concentration in the clay zone and 31.2 % higher in the loam zone. Hence, for the clay zone HRS 0-5 cm SOC data is scaled by a factor of 0.66 and for the loam zone by a factor of 0.69.

3.3 Results

3.3.1 Description of the soil profile data

The lower boundary of the plow layer in the research area varies between 10-30 cm, with thicker Ap layers on plateau and colluvial positions than on steep slopes. The bulk density increases gradually from topsoil (Loam:

1.4±0.3 g/cm^3; Clay: 1.4±0.1 g/cm^3) to subsoil (Loam: 1.6±0.3 g/cm^3; Clay 1.8±0.1 g/cm^3) in both texture zones. The ^{137}Cs data shows that lateral soil redistribution acts at a moderate but also very variable rate with a mean SRI value of 165 % (Table 9). Hence, the soil cores that were used to calibrate the model are influenced by lateral soil fluxes in both texture zones. The mean observed total SOC stock for the clay profiles is 9.3±3.3 kg/m^2. (**Figure 13**).

Table 9: ^{137}Cs derived CV and SRI results for fields in the two different texture zones showing high rates of lateral soil fluxes transporting soil through the landscape.

	Field	CV_{ref}	CV_{Field}	SRI (%)	Soil redistribution
Clay	11	0.43	0.33	76	Limited
	14	0.19	0.75	395	High
	17	0.28	0.42	151	Moderate
	20	0.2	0.44	224	High
Loam	50	0.15	0.18	120	Limited
	7	0.31	0.47	150	Moderate
	13	0.13	0.2	153	Moderate
TOTAL		**0.24**	**0.4**	**165**	**Moderate**

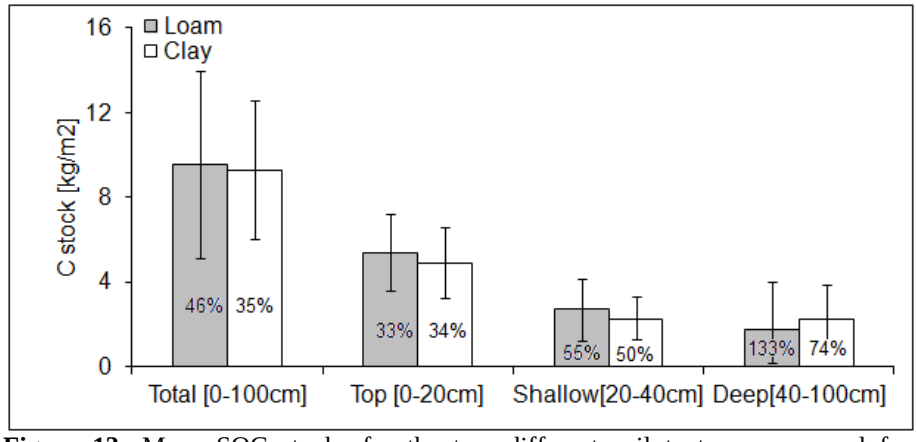

Figure 13: Mean SOC stocks for the two different soil texture zones and for different depths as derived from the profile data. Vertical bars represent the standard deviation from the mean in absolute numbers, numbers in percentage the relative standard deviation from the mean.

The total SOC stock is slightly higher in the loam zone (9.6±4.4 kg/m^2). The variability of SOC stocks of the topsoil and the shallow subsoil along the slope in both texture zones are similar (34-55% deviation of the mean stock). In contrast to the topsoil and shallow subsoil, the variability is much higher in the deeper subsoil (74-133% deviation of the mean stock)
Differences in the regional mean SOC stock for the different slope positions in the two texture zones are not significant (data not shown) which suggests a high regional variability in SOC stocks.

3.3.2 LMM Model fit

The results from the pre-selection process using stepwise-linear regressions and the LMM model fit show that from the 45 potential explanatory variables, only a small set of variables (≤6) remained significant ($p<0.05$) when modeling the SOC stocks at various depths (Table 12).

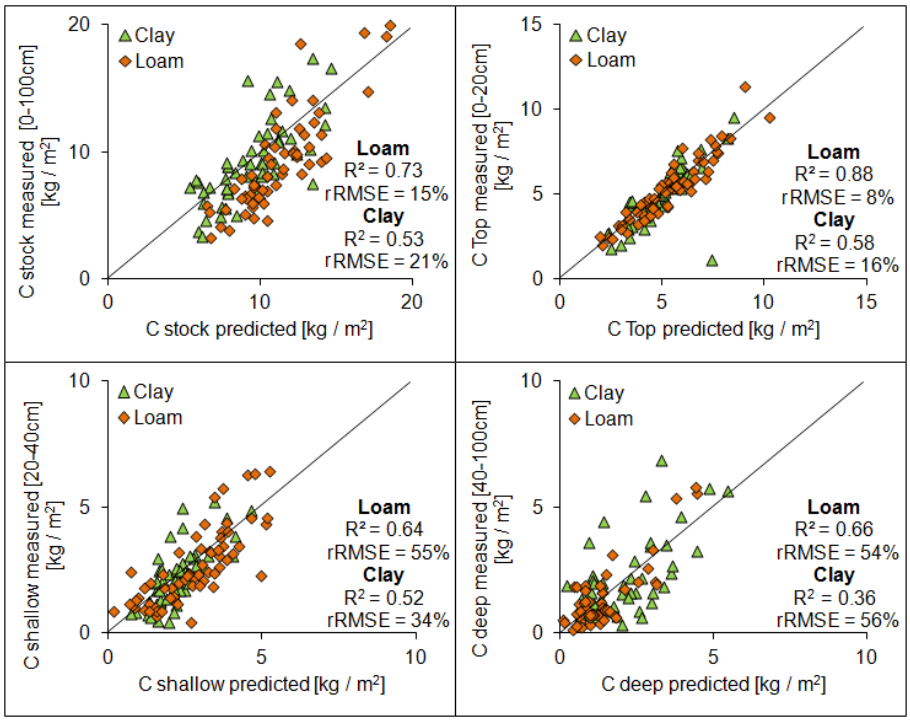

Figure 14: Calibration points of predicted versus observed SOC stocks for the different depths and texture zones. The rRMSE values refer to results using the validation data.

The results show that the Gaussian semivariogram model adequately modeled the spatial autocorrelation of the errors. The only random effect included is the origin (LUX or SDP) of the data. The resulting models (Table 10 and Figure 14) show good spatial fit and the relative standard errors (rSE) of the model means are between 4-24%. However, the uncertainty associated with the estimates increases with depth, reaching rRMSE values of 56%, and is higher in the clay than in the loam zone. The sum of topsoil, shallow subsoil and deeper subsoil SOC stock is close to the total SOC stock (4% underestimation), suggesting that the chosen explanatory variables result in estimates that can be used for a depth explicit SOC stock analysis.

Table 10: LMM performance parameters and SOC predictions for different depth layers.

			Model parameters				
	Soil				Mean SOC		
Texture	Section	N	AIC	AICc	[kg/m^2]	SE	rSE (%)
Clay	Stock(0-100cm)	54	241	246	9.6	0.8	8
	Top (0-20cm)	54	167	170	4.9	0.3	6
	Shallow(20-40cm)	54	141	146	2.3	0.3	13
	Deep(40-100cm)	51	161	165	2.0	0.5	24
Loam	Stock(0-100cm)	65	315	319	10.1	1.1	11
	Top (0-20cm)	65	147	152	5.4	0.2	4
	Shallow(20-40cm)	65	186	189	2.9	0.3	11
	Deep(40-100cm)	53	137	142	1.4	0.2	17

3.3.3 Explanatory variables

Table 11 shows the explanatory variables for the SOC stocks of different depth layers in the two investigated texture zones, ranked according to their importance and explanatory strength for the respective SOC stock prediction. The analysis reveals that the explaining variables differ with depth and soil type. As expected, the topsoil SOC concentration proves to be the most important variable for the overall SOC stock and for the topsoil SOC stock (0-20 cm). But its importance decreases in the subsoil significantly. It is no longer a significant variable for the deep subsoil in the clay zone and is the least important significant variable for the deep subsoil in the loam texture zone.

Table 11: Ranked explanatory variables for the SOC stocks of different depth layers in the two different texture zones. All variables are significant at $p<0.05$. Abbreviations: M=Mean; SD=Standard deviation; Nbh = Neighborhood.

Profile Section	Importance ranking	Texture Zone Loam					Texture Zone Clay				
		Variable	Type	Coeff.	Nbh. (m^2)	δ AICc	Variable	Type	Coeff.	Nbh. (m^2)	δ AICc
Stock(0-100cm)	Variable 1	**(Pe) C Topsoil %**	M	3.96	Point data	7	**(Pe) C Topsoil %**	M	2.69	Point data	16
	Variable 2	**(Cl) Prec. seasonality**	M	-2.29	$10*10^5$	38	**(Hy) TCI**	M	1.71	$10*10^3$	25
	Variable 3	**(To) Profile curvature**	M	15.12	$25*10^2$	42	**(TH) Upstream Flow area**	SD	0.003	$10*10^3$	27
	Variable 4	**(TH) TPI**	SD	10.65	$10*10^3$	43	**(Hy) TCI**	SD	-1.57	25	29
	Variable 5						**(Cl) Annual mean temp.**	M	-7.03	$10*10^5$	30
	Intercept			31.86					61.43		
Top (0-20cm)	Variable 1	**(Pe) C Topsoil %**	M	2.78	Point data	24	**(Pe) C Topsoil %**	M	1.86	Point data	2
	Variable 2	**(To) Profile curvature**	M	7.19	$25*10^2$	88	**(Cl) Prec. seasonality**	M	0.55	$10*10^5$	40
	Variable 3	**(Hy) TCI**	SD	0.61	25	89					
	Variable 4	**(To) Slope**	M	0.17	25	90					
	Variable 5	**(TH) Upstream Flow area**	SD	0.02	$25*10^2$	90					
	Intercept	**(To) Profile curvature**	M	6.84	$40*10^3$	99			-4.36		
Shallow(20-40cm)	Variable 1	**(Pe) C Topsoil %**	M	2.02	Point data	15	**(T) Profile curvature**	SD	-2.23	25	14
	Variable 2	**(TH) TPI**	M	-0.32	$10*10^3$	37	**(To) General Curvature**	M	-16.18	$40*10^3$	17
	Variable 3	**(Cl) Annual mean temp.**	M	1.53	$10*10^5$	43	**(Pe) C Topsoil %**	M	0.67	Point data	17
	Variable 4	**(TH) TPI**	SD	3.88	25	45	**(To) Plan curvature**	M	1.59	25	21
	Variable 5						**(To) Profile curvature**	M	-6.74	25	23
	Intercept			-13.52					1.68		
Deep(40-100cm)	Variable 1	**(To) Profile curvature**	M	1.40	25	4	**(Cl) Annual mean temp.**	M	-5.87	$10*10^5$	8
	Variable 2	**(To) Plan curvature**	SD	3.24	25	8	**(Hy) TCI**	M	0.76	$10*10^3$	17
	Variable 3	**(Cl) Temp. seasonality**	M	-0.20	$10*10^5$	9	**(Cl) Temp. seasonality**	M	0.13	$10*10^5$	23
	Variable 4	**(Cl) Prec. seasonality**	M	-0.95	$10*10^5$	10					
	Variable 5	**(Pe) C Topsoil %**	M	0.89	point data	10					
	Intercept			127.09					-26.36		

Topographic variables, especially curvature and compound indexes such as the TPI play an important role for subsoil SOC prediction, especially in the hillier, steeper loamy texture zone. Hydrologic and climatic variables play an important role for the deep subsoil SOC prediction in the less hilly clay zone and for the deep subsoil SOC prediction in the loam zone.

Not only the mean values, but also the variability of TPI, TCI and the seasonality of climatic predictors such as temperature and precipitation were found to be important predictors of the SOC stock. Generally, hydrologic variables are included mostly on a medium or local neighborhood size of 2.500-10.000 m^2. Topographic variables are mostly included on a local neighborhood size (25-2500m^2). A similar assessment for the neighborhood size of climatic and pedologic variables could not be performed, as the initial pixel size for the climatic variables is 1 km^2 and pedologic variables are derived from profile data. The coefficients of the included explanatory variables presented in Table 11 reveal that in the flatter clay rich zone, the highest SOC stocks can be expected where the topsoil SOC concentration and wetness conditions are high and the annual temperature and variability in (local) wetness and upstream area are low. In the hillier loam zone, SOC stocks are positively influenced by topsoil SOC content, profile concavity, landscape variability in topographic positions (TPI) and negatively related to precipitation seasonality.

3.3.4 Regional SOC stocks

The application of the models presented here and the scaled topsoil HRS SOC data results in a first regional estimate for mean SOC stocks of the first meter of cropland soils in the two texture zones (Figure 15). The mean SOC stock in the loam zone is higher (11.3±2.4 kg/m^2) than in the clay zone (9.4±3.1 kg/m^2). The variability of the total SOC stock in the loam zone is hereby lower than in the clay zone: Only 26.2 % of SOC stocks in the loam zone are estimated higher or lower than the mean SOC stock ± SD. In the clay zone, 38.7 % of all values are outside this range and SOC stocks are generally more spread across a broader range of values. For the area covered with HRS topsoil SOC data (Loam: 3 km^2; Clay: 4.6 km^2), this results in a total SOC stock of the first meter of the soil profile of 33.9 Gg in the loam zone and a total SOC stock of 42.8 Gg in the clay zone. Topsoil and shallow subsoil SOC are near normal distribution. In contrast, there are pronounced

differences in the deeper subsoil, which in return have a significant impact on the total SOC stock.

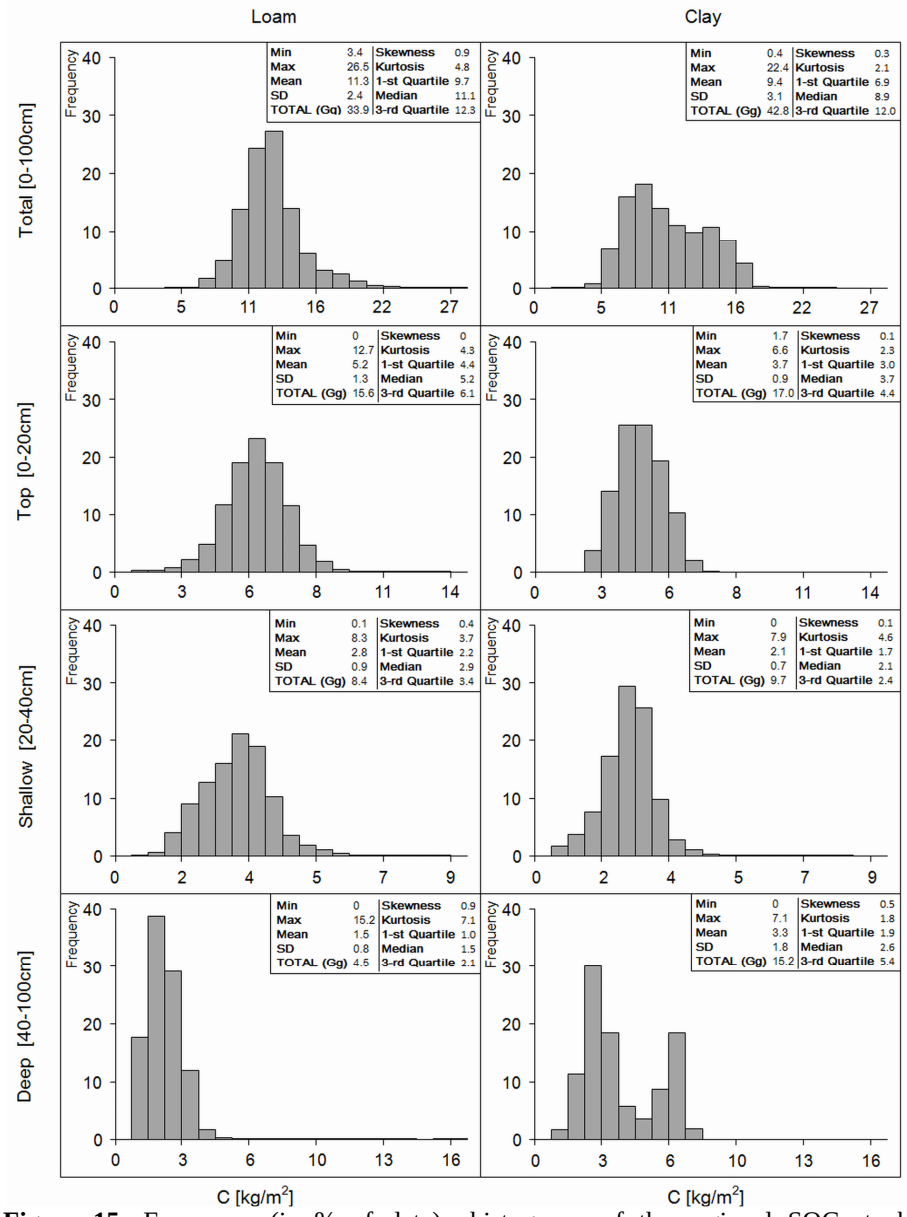

Figure 15: Frequency (in % of data) histograms of the regional SOC stock estimates for different depth layers using the model structure presented here and HRS topsoil SOC data for the cropland covered by HRS. The data shows pronounced differences in SOC distribution for the deeper subsoil between the two regions.

SOC stocks decrease strongly with depth in the loam zone (deeper subsoil: 1.5±0.8 kg/m^2) and are biased towards lower values, while there are extensive areas with SOC enriched subsoils in the clay zone (3.3±1.8 kg/m^2) and the SOC stocks there have a bimodal distribution pattern.

3.4 Discussion

3.4.1 Control mechanisms of SOC distribution

The explanatory variables presented in Table 11 show that topographical, hydrological and climatic factors are closely related to SOC stocks, especially for deeper soil layers and can result in meaningful predictions of depth and spatially explicit SOC stocks (Figure 14). In order to use those variables to identify environmental processes affecting SOC stocks, it is crucial to understand cross-links and interactions between groups of variables, such as topographical and hydrological variables. In the following section the results are interpreted taking these interactions into account and an overview on the most important processes on a regional scale is given, referring to established knowledge about the effects of those processes on SOC dynamics.

Landscape characteristics and topography. SOC profiles along local slopes show a characteristic subsoil SOC distribution pattern, as has been identified in several independent hillslope studies under (i) different climate conditions and (ii) rates of erosion (Gregorich et al. 1998; Berhe et al. 2008, 2012; Vandenbygaart et al. 2012) (Figure 16). SOC stocks standardized for the local plateau SOC stock show low SOC contents on the slopes and high SOC contents in foothill and valley bottoms. Concave landscape positions and those with low TPI values, generally found in valley bottoms and at the foothill, typically have higher SOC stocks in both soil regions, while SOC stocks on the convex slopes are generally low which supports the supposed connection between the processes outlined above (Table 11). Both texture zones follow these general patterns of SOC stocks but differences between the two zones are observable on a regional scale (Table 7 and Figure 15). In the extrapolated regional estimate, ~ 20% of the deeper subsoil in the clay zone have high SOC stock values, clearly differing from the majority of the deeper subsoils of the clay zone, where SOC values are lower and similar to the loam zone estimates. More SOC is stored in the depositional deeper

subsoils of the clay zone compared to the loam zone and there is a higher degree of SOC depletion in the deeper subsoil at eroding sites in the loam zone (Figure 15 and Figure 16) compared to eroding sites in the clay zone. This is to a large extent driven by soil redistribution processes and local topographical landscape characteristics: As shown by the ^{137}Cs data (Table 9), lateral soil fluxes act at a high rate in the research area, presumably having a strong effect on SOC dynamics in the study area: SOC is transferred from high to low decomposition environments at depositional sites at the foothill and valleys by burial of SOC rich topsoil with deposited slope sediments. In the loam zone, a large part of the cropland is situated on highly eroding slopes and hardly any cropland is situated in depositional areas in the steeper loam zone (Table 7 + 8). The clay zone, on the other hand, is generally flatter but it covers a large number of soils in depositional areas where SOC rich topsoil gets buried in deeper subsoil. This means that the loam zone will include a large area of eroded soils with SOC depleted subsoils, while in the clay zone a considerable amount of soils is placed in a depositional environment where SOC enriched buried topsoil are present.

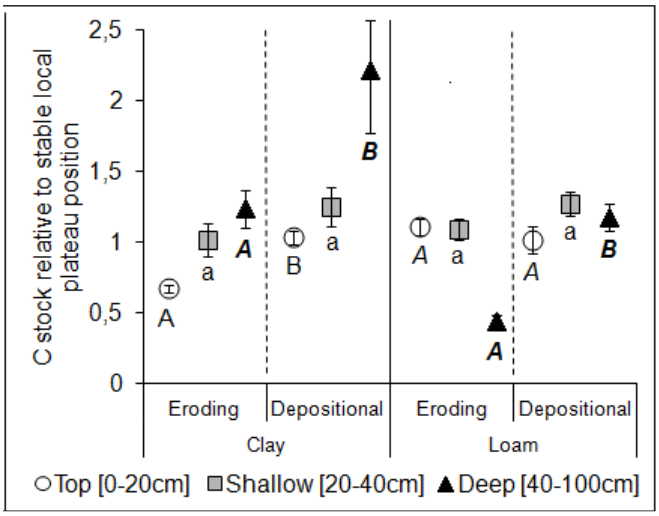

Figure 16: Relative SOC stock differences of slope (eroding) and foothill/valley bottom (depositional) positions to the local stable plateau profile showing the variable impact of soil redistribution on SOC deposition (clay zones, deep soils) and strong erosion/depletion on steep slopes (loam zones, deep soil). Same letter above nods indicate no significant difference in SOC stocks between eroding and depositional soil layers. ($p < 0.05$, tested separately for both texture zones and soil layers).

Hydrology and pedology. Additionally, hydrological factors play a role for SOC dynamics at these positions: In depositional areas high soil wetness promotes the conservation of buried SOC rich topsoil layers in valley bottoms. There, over parts of the year, the convergence of water can lead to a high, stagnant water level and hence lead to an anaerobic soil environment, which causes low oxygen availability in subsoils and hence presumably lowers the rates of microbial SOC decomposition at these sites (Wang et al. 2000; Freeman et al. 2001; Eckschmitt et al. 2008; Rumpel and Koegel-Knabner 2011). In addition, the accumulation of water in valley profiles is well known to provoke redoximorphic processes, leading to the formation of organo-metallic complexes, as oxy-(hydro)oxides can be associated with water-soluble SOC (Eusterhues et al. 2011). Secondly, the higher availability of water (Noorbakhsh et al. 2008; Xu et al. 2005) and nutrients eroded upslope together with soil material (Quine and Zhang 2002) and deposited at foothill positions has been shown to promote biomass production at these sites compared to slope positions (Moulin et al. 1994, Quinton et al. 2010). Those postulated controls on SOC stocks are in accordance with the regression models for the clay zone (Table 11), where wetness (TCI Mean) is positively correlated to SOC stocks in the deeper subsoil and the total SOC stock. The importance of these hydrology related controls differs hereby between the two texture zones related to local topography (Table 7): The steeper and more sloping loam zone has a very strong local geomorphic (curvature) control on the SOC stock of the deeper subsoil layers, with large scale climatic variables (temperature and precipitation seasonality) only being of secondary importance (Table 11). On the contrary, the deeper layers of the flatter clay zone are exclusively controlled by large scale climatic (temperature) and hydrologic (wetness) controls.

Similarly, topography has to be considered when addressing the differing effect of soil wetness *variability* on SOC stocks of the two zones: in the clay zone soil wetness variability shows negative correlation to SOC stocks. A high variability in wetness there indicates a more sloping local topography and hence includes depleted eroded subsoils in the predictions. This effect seems to be more important than the potential impact of higher wetness in the valley bottoms on SOC decomposition rates and is consistent with the inclusion of upstream area variability as a factor having a lowering effect on SOC stocks in the clay zone (Table 11). In the loam zone, no strong link between soil wetness variability and SOC stocks could be identified. Only a

very minor positive correlation to topsoil SOC content was observed. This can be explained by the hillier landscape structure and the coarser soil texture, which generally allows water to be transported more quickly into the valley system and out of the cropland (e.g. Arya et al. 1999, Brady and Weil 2008). Wetness effects are therefore superseded by topographic variables in the loam zone but are dominant controls in the clay zone.

Bio-climatic variables. Climatic variables have shown to be important for soil C stocks in a large variety of bioclimatic settings (Davidson and Janssens 2006; Crayne et al. 2010). Also in the research area investigated here, bioclimatic variables have shown to improve C stock predictions when included into the models, but are, however, in most cases of secondary importance (Table 11). The interpretation of these effects is difficult as we have no experimental proof of the bioclimatic conditions in our study area on soil carbon. Temperature and precipitation patterns might affect biomass production, microbial activity, soil aeration and the erosional regime of the two zones (e.g. Arya et al. 1999; Schjønning et al. 1999; Zhang et al. 2011). Stronger seasonality of precipitation can indicate periods where aeration is improved and promote biomass yield or conversely cause water stress on plants or increase C decomposition due to enhanced microbial activity (e.g. Jabro et al. 2010; Smith et al. 2003, Noorbakhsh et al. 2008). Higher mean annual temperature and temperature seasonality allow for higher heat transfer and enhanced C decomposition by microorganisms in deeper soil layers (Davidson and Janssens 2006), or conversely increase C inputs at greater soil depths (e.g. Melillo et al. 2002). We relate the differing response between the clay and the loam zone to changes in these variables to differing topography and soil texture. For example, in the flatter clay zone the precipitation seasonality is weakly positively correlated to higher topsoil C stocks indicating a net positive effect of the various implications of higher precipitation on C stocks there i.e. by improved soil aeration. In contrast, in the sloping loam zone higher precipitation seasonality will cause water limitations for plants, leading to reduce the biomass C input into soils (Noorbakhsh et al. 2008) and promote erosion (Yan et al. 2010) as cropland in the loam zone is biased towards steep slopes (Table 7) compared to the clay zone. Interestingly, a weak positive link of soil carbon with higher temperatures can be observed in the loam zones, suggesting that the positive

effect of higher temperatures on biomass production and hence C input supersedes potential negative feedbacks with C decomposition in this zone.

Importance. The variability of SOC stocks, especially in the subsoil, is higher in undulating landscapes due to the processes and factors described above. This differences in the SOC distribution pattern caused by soil redistribution and in-situ differences of the soil environmental conditions have important consequences for SOC modeling: Generally, the quantitative differences in SOC stocks of the first meter along a slope catena are rather small (10-20% more SOC in landscapes with soil redistribution vs. stable landscapes (Van Oost et al. 2012)). However, changes in SOC quality (e.g. Berhe et al. 2012) and controls on SOC stocks between top- and subsoils (Salomé et al. 2010; Rumpel and Koegel-Knabner 2011) can differ significantly. Hence, the transport of SOC from areas of high to low decomposition potential and vice versa (e.g. Gregorich, et al. 1998; Stallard 1998; Quinton et al. 2010), plus the advection of SOC depleted subsoil at eroding sites (e.g. Harden et al. 1999; Van Oost et al. 2007; Quinton et al. 2010) are crucial aspects that need to be considered for landscape scale applications of SOC models. At the moment, these aspects are only very limitedly taken into account in current assessments and SOC models (Parton et al. 1987; Coleman et al. 1997; Falloon and Smith 2002; Van Oost et al. 2005b; Ogle et al. 2007; González-Molina et al. 2008).
Depending on the actual landscape structure and the part of the cropland which is in an eroding or depositional environment and because of the low control of topsoil SOC concentration on SOC stocks at greater depth, the traditional approach of using topsoil SOC content and extrapolation to greater depth can over- or underestimate the actual SOC stocks. In this study here, SOC depth extrapolation derived from stable landscape distributions, would overestimate the loam stocks and underestimate the clay stocks.

3.4.2 Extrapolation and caveats for a regional application

Several studies have identified the conversion factors between wet combustion and total combustion derived SOC values as a source of uncertainty and to differ for different soil texture classes (Brown et al. 2006, Goidts et al. 2009b). No direct comparison between dichromate wet combustion and total combustion derived SOC values has been done for the SDP datasets so that this issue remains a source of uncertainty in this

assessment here. However, this factor has been proven to be fairly constant for a wide range of loamy soils under cropland in Belgium and for soils with varying carbon contents (Lettens et al. 2005; Sleutel et al. 2007; Meersmans et al. 2009) and SOC values in the SDP dataset have been shown to be in a similar range as the SOC values in the Lux dataset (SDP: 0.04 – 3.67% SOC; LUX: 0.02 – 3.64 % SOC). Furthermore, no significant differences in the model structure were observed when building the model with one dataset only (data not shown), and no bias in the predictions using both the SDP and LUX dataset was observed (Figure 14). The fact that the origin of the dataset is identified as a random effect in the model is related to the horizon orientated sampling design of the SDP dataset while the LUX sampling design is denser and strictly depth-orientated and is not related to bias in SOC predictions.

The results from the model extrapolation using HRS topsoil SOC data (Figure 15) show significant differences when compared to the model results gained from the profile data (Table 10): The sum of topsoil, shallow subsoil and deeper subsoil SOC stock is close to the total SOC stock in the clay zone (3% underestimate) but underestimates the total SOC stock in the loam zone by 18%. The average total SOC stocks from the HRS extrapolation are 2% lower than the modeled profile estimates in the clay zone and 12% higher in the loam zone, respectively. The depth layered HRS extrapolated SOC stocks in both zones are between 4-32% lower than the modeled profile data in the topsoil and shallow subsoil, while the HRS extrapolated deeper subsoil SOC stock is estimated 7% in the loam zone and 65% higher in the clay zone. Tracking the source for these discrepancies is difficult and most likely a set of various factors: First, the number of sampled profiles per slope position is not related to the actual distribution of those slope positions in the research area and differences in mean SOC stock estimates just reflect this discrepancy to a certain extent. Second, only a small set of profiles is available for both zones and the rRMSE errors of the different models increase with increasing soil depth (Figure 14). This indicates that even though the utilization of a diversified set of environmental variables can reproduce meaningful results for the whole range of SOC stocks investigated here in different soil layers (Figure 14), the sampled dataset might not be fully representative for the full spectrum of environmental conditions in the landscape for certain depth layers. Third, in those layers with the strongest deviations between the HRS extrapolation and the models predicting the

profile SOC stocks, namely the topsoil and deeper subsoil in the clay zone, the included climatic variables, proven to be strong controls on the SOC stock, were only available at a coarse resolution of 1km^2. Changing micro-climatic conditions along the slope (Kang et al 2000, 2003) and within the different landscapes might require including climatic variables at a finer resolution, for which the data is not available in the study area. Fourth, the sampling campaign is biased towards integrated local hill slope studies. This bias might hamper the effort to elucidate the explanatory strength related to large scale factors, such as climatic variables, which play a role on the regional scale investigated here. Finally, replacing the measured topsoil SOC concentration with airborne HRS derived estimates adds additional errors related to the prediction accuracy of the method. For these reasons, the introduction of a more fully representative dataset may require the applied coefficients to be re-adjusted and weaker explanatory variables might at the end be insignificant.

3.5 Conclusion

The model could successfully be calibrated and applied to predict SOC stocks in different soil layers for cropland at a regional scale using a mix of measured soil data, spatially-explicit environmental variables and HRS derived topsoil SOC data. The model predicts meaningful patterns of SOC distribution for the two major soil texture zones in Luxembourg and a high spatial variability of SOC stocks.

Topographical and hydrological variables could be identified as the strongest controls over the local SOC stocks, while climatic variables control differences between larger regions and in flat terrain. Results of soil redistribution rates and patterns derived from ^{137}Cs isotope distributions give evidence for a highly dynamic environment concerning lateral soil fluxes.

Top- and subsoils are controlled by differing sets of variables. The topsoil SOC concentration, often used for SOC depth extrapolation, loses its importance with greater soil depth and shows little explanatory strength for SOC in the deeper subsoil, illustrating the disconnection between topsoil and subsoil SOC dynamics. The results suggest the modification of current SOC modeling and mapping approaches towards using a more complex model structure such as spatially explicit models that include lateral flows between modeled cells.

In summary, the findings indicate that a regional study, as in the example given here, can help to understand and identify sets of different environmental factors needed for SOC predictions and can result in reasonable estimates at this important scale. The interpretation of these variables is strongly dependent on the investigated region and can change with landscape characteristics.

4 Assessment of SOC dynamics using closed-tube sampling and Vis-NIR spectroscopy at the landscape scale[3]

4.1 Outline

The discrepancy between the growing demand for high-resolution and spatial explicit soil data on larger scales and the availability of this data is one of the big challenges in contemporary soil science (Grunwald et al. 2011). Current digital soil maps are often coarse-scaled and do not provide quantitative information on soil properties (Sanchez et al. 2009). One of the most active and, in the light of global climate change, important debates on soil properties is the spatial and vertical distribution of soil organic carbon (SOC).

SOC contents follow roughly an exponential decrease when soil depth increases, but the parameters of the exponential function are affected by numerous interacting environmental variables (Jobbágy and Jackson 2000). Because of their costly and time intensive nature, existing sampling strategies and standard analytical methods typically provide data restricted to the upper 30 cm of the soil or at best with a coarse vertical resolution (i.e. between 10 to 30 cm), and SOC analyses are often based on composite samples. The current methodologies cannot provide enough data for correctly monitoring and modeling the soil system and are therefore not able to solve the "soil data crisis" (McBratney et al. 2006).

Visible and Near-Infrared (Vis-NIR) diffuse reflectance spectroscopy has been suggested as a cost and time saving alternative to established analysis methods (O'Rourke and Holden 2011). The usefulness of Vis-NIR spectroscopy for rapid acquisition of soil data has been shown in several studies. For example, Kuang and Mouazen (2011) applied Vis-NIR spectroscopy at the field scale to predict SOC and discuss the necessary calibration models for applying Vis-NIR on larger scales. Wetterlind and Stenberg (2008) applied near infrared spectroscopy as a tool to reduce the

[3] ***The content of this chapter is submitted for publication as:*** Doetterl S., Stevens A., Van Wesemael B., Van Oost K. (*submitted*): Soil-profile organic carbon assessment at high vertical resolution using closed-tube sampling and Vis-NIR spectroscopy. *Soil Science Society of America Journal.*

number of samples, and hence the costs, for farm scale SOC assessments. Ben-Dor et al. (2008) and Kusumo et al. (2010) presented innovative designs for on-site spectroscopic SOC assessments of the soil profile. Vis-NIR Spectroscopy has also been used for mapping surface SOC content using on-the-go multi-sensor platforms (Bricklemeyer and Brown, 2010; Knadel et al., 2011). However, these studies suffer from lower accuracy compared to reference methods due to the high variability in soil conditions (soil moisture, surface roughness) or long preparation times of the samples on field before scanning. Solving these problems is the focus of recent advances (Deng et al. 2012).

Here, an approach based on Vis-NIR spectroscopy is presented that that aims to provide the same accuracy as standard analysis methods. An adapted percussion drilling technique is used that reduces the time spent on field and allows the preparation and description of the soil cores in the laboratory while the spectroscopic measurements produce SOC observations at a high vertical resolution along prepared soil cores.

4.2 Material and Methods

4.2.1 Study area

The study area is located in the intensively used cropland of the central Belgium Loambelt (Figure 17) and has been chosen because of the high density of cropland, the variability in topography as well as its coverage with data from existing soil profiles sampled from 1955-1958. The study area is characterized by a rolling topography with plateaus, slopes (up to 20%) and generally well drained, dry valley bottoms. The climate of the region is a temperate oceanic climate with mild winters and cool summers. (Köppen climate Cfb, 821 mm yr^{-1}; 9.7°C) (IRM 2011). The geological substrate is a several meters thick Pleistocene aeolian deposit of calcareous loess, in which Luvisols have developed. The majority of the cropland in the research area (~93%) is situated on loamy soil texture facies and only to very minor extent on other soil texture facies. Loess deposits are typically thicker on south facing slopes than on north facing slopes and are overlaying tertiary sands (Wouters & Vandenberghe 1994). In some locations (data not shown), these sandy layers are already outcropping at the surface, as soil erosion has truncated several meters of the original soils and loess deposits. First traces of agriculture date back to the Late Bronze/Iron age and both sites have been

under continuous agricultural land use since at least 1770 (Rommens et al. 2005; Lannoo 2009).

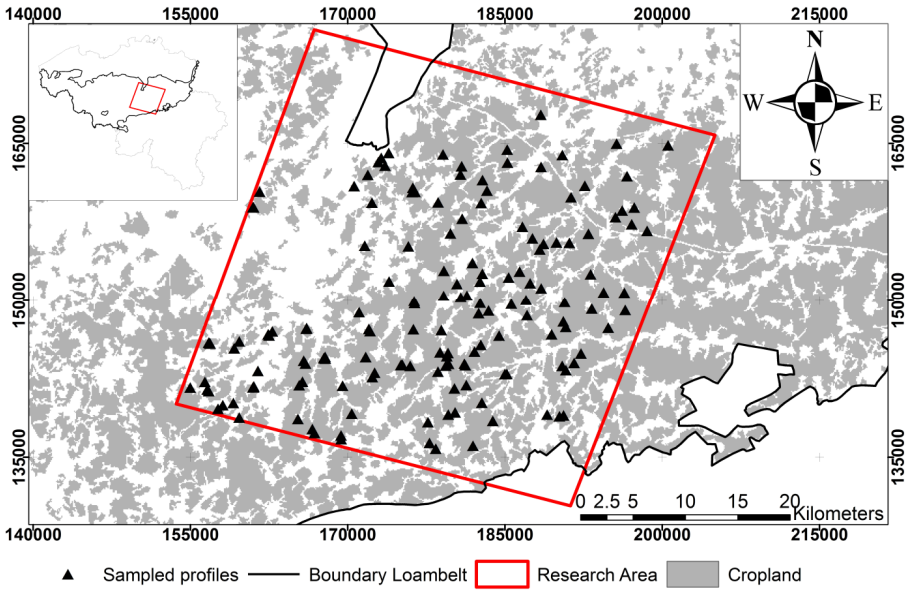

Figure 17: The study area in relation to its position in the Belgium Loambelt, its cropland coverage and the position of sampled soil profiles.

At present, the main crops in the region are cereals (46%), sugarbeet (20%), silage maize (10%) and potato (7%) (Van Wesemael et al. 2010) with typical C inputs to the soil by plants estimated at 1.93 Mg C ha^{-1} $yr^{-1}$and by manure at 1.1 Mg C ha^{-1} yr^{-1}. No detailed information about the long-term (i.e. several centuries) crop rotation or C input is available.

4.2.2 Sampling design and sample preparation

Besides testing the proposed methodology, the aim of the sampling campaign was to resample historical soil profiles across the cropland of the region and to analyse changes of SOC with time (see chapter 5). One hundred fourty-seven soil profiles were sampled, chosen randomly from those cropland soil profiles in the historical soil database where the spatial reference could be verified (Figure 17). The sampling was conducted up to one meter depth using a closed tube sampling system (Ø 4.5cm) (Eijkelkamp, The Netherlands) for undisturbed sampling. The cores were stored in a sealed PVC-tube frozen at -18°C until preparation for analyses. Preparation steps included (Figure 18):

(1) PVC tubes in which the frozen cores are stored were sliced up lengthwise and a ~ 4 cm broad and 1 m long part of the plastic tube was removed.

(2) The cores were dried at 60°C for 3 days. The dried soil cores are generally hardened by this treatment and the surface stays intact, as the loamy material in these profiles is cohesive. However, soil cores which contain sandy layers were handled with special care to not loose structure. Minor cracks can occur in all soil cores due to shrinkage of clay minerals during drying.

(3) The convex surface from the soil profiles stored in the plastic tubes was first flattened and smoothed using a 4 cm broad metal brush attached to a common power drill and then remaining dust removed from the prepared surface with a high-pressure air torch.

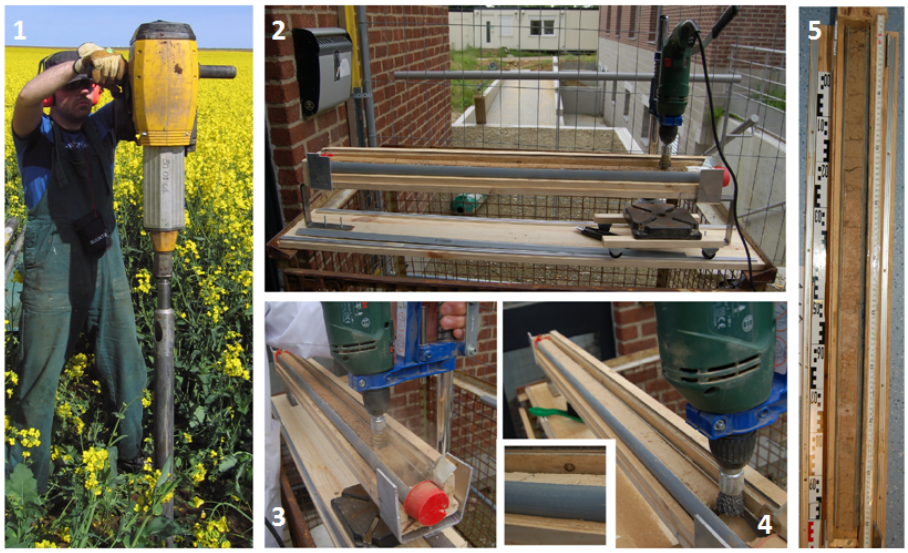

Figure 18: Illustration of the work steps for acquiring undisturbed samples for continuous spectroradiometric measurements; 1: Soil sampling with closed sampling systems; 2-4: Polishing and flattening of the soil surface of the sampled cores after the core has been dried; 5: Visual description of soil features and artifacts of the sample preparation.

These steps allowed preparing a dry, flat and clean soil surface for acquiring the soil spectra. All soil description can be done on intact cores under laboratory conditions. The prepared soil cores were then described noting (i) redoximorphic features, (ii) texture discrepancies (sand, presence of gravel),

and (iii) artifacts of the sample (plant or plastic pieces) and the preparation technique (cracks or rough surface).

4.2.3 Spectral measurements

Soil radiance was measured in a dark room laboratory using an ASD Fieldspec-Pro spectroradiometer (ASD inc., Boulder, USA), in the Vis-NIR range (350–2500 nm), with a Full Width Half Maximum of 3 nm in the Vis and 10 nm in the NIR. A contact probe device (ASD inc., Boulder, USA), with its own light source (100 W halogen reflectorized lamp) and measuring a spot size of 10 mm, was used to acquire the soil spectra (Weiser et al. 2007). Reflectance factors were computed by dividing the soil radiance by the radiance of a white reference panel (ASD inc., Boulder, USA) measured every 15 minutes. The scanning has been performed directly on the prepared surface of each soil core. The soil cores were scanned continuously along the complete core at 3cm depth intervals. This process resulted in a total of 4800 soil reflectance spectra. Ten soil profiles (~5% of the analyzed soil spectra) were randomly chosen for re-scanning at the end of the experiment to assess the repeatability of the method.

4.2.4 Spectroscopic predictions

D*ata pretreatment.* The spectral matrix was smoothed using the Savitzky-Golay algorithm (Savitzky and Golay 1964) with a window size of 21 nm and a polynomial degree equal to 3. The spectral matrix was subsequently transformed by Standard Normal Variate (SNV) (Barnes et al. 1989) to reduce spectra variability (light scattering) induced by possible variations in sample surface characteristics (rugosity, packing, etc). A total of 88 spectra were excluded from further analysis as they showed obvious artifacts (i.e. larger desiccation cracks) or they contained more than 5% gravel.

Calibration sampling. The database was divided into a training set (547 samples) for developing the spectroscopic models, a validation set (100 samples) for assessing their performance and a prediction set with the remaining samples. All the samples at the top of each soil profile were assigned to the training set (147 samples). The remaining training samples were selected using the Kennard-Stone algorithm (Kennard and Stone, 1969). The validation samples were selected by random sampling.

SOC analyses. Samples selected for the training and validation set as well as samples for which spectroscopic predictions could not be obtained due to

artifacts were analyzed for SOC content using a VarioMax CN dry total combustion Analyzer (Elementar GmbH, Germany). Samples containing inorganic C were treated using 6M HCL containing 3% by weight $FeCl_2$ $4H_20$ in order to measure inorganic C following Sherrod et al. (2002) and to derive SOC values from the measured total C by subtraction of the inorganic C.

Model building. Spectral data were calibrated against SOC analyses using Partial Least Square Regression (PLSR, Wold et al. 2001), Random Forest (RF, Breiman 2001), radial-basis Support Vector Machine Regression (SVMR, Smola and Schölkopf 2004) and Model Trees (MT; Quinlan 1993). These multivariate models have been shown to deliver good predictions for soil spectroscopic data (Minasny and McBratney 2008; Viscarra-Rossel and Behrens 2010). The models were developed with the *caret* package (Kuhn et al. 2012) of the R statistical software (R Development Core Team, 2010). All the models were run on a grid of model parameters with default values defined by the *caret* package. Models were cross-validated using 10 random partitions having a probability of selection of 3/4 (ie. leave-one-group-out cross-validation). Following Breiman et al. (1984), the best set of parameters for each model was selected as the ones producing a model having the smallest Root Mean Square Error (RMSE) of cross-validation within one standard error of the minimum RMSE of cross-validation.

Prediction accuracy and repeatability. The accuracy of the predictions was assessed with the RMSE in the validation set and the Ratio of Performance to Deviation (RPD, the ratio between the standard deviation and the RMSE). A model yielding an RPD value above 2 is considered to produce accurate predictions (Chang et al. 2001). The best model approach amongst the different model runs was selected as the one minimizing the RMSE. The repeatability of the spectroscopic models was assessed by computing the Standard Error of Laboratory (SEL) with:

$$SEL = \sqrt{\frac{\sum_{i=0}^{n} {\varepsilon_i}^2}{2n}} \quad (9)$$

where ε_i is the difference between duplicate measurements of sample *i*. The optimal model was then used to predict the content of samples with unknown SOC values.

4.3 Results

4.3.1 Model performance and repeatability analysis

The lowest RMSE of validation was achieved by the MT algorithm (1.22 g C kg^{-1}), followed by SVMR (1.45 g C kg^{-1}), PLSR (1.46 g C kg^{-1}) and finally RF (1.55 g C kg^{-1}). These values are close to the analytical error of the dry combustion technique (~1 g C kg^{-1}). The RPD values of these models oscillated between 2.43 and 3.1, indicating very accurate models. The predicted-observed graph of the MT model shows that the model fit for the training set is particularly good at low SOC values (< 10 g C kg^{-1}) while the residuals tends to increase at higher values (Figure 19 - Training).

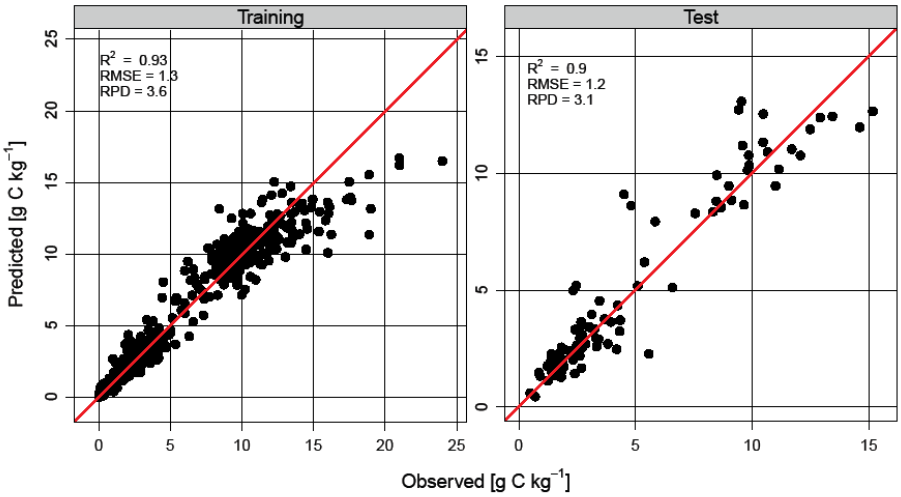

Figure 19: Predicted versus observed SOC content (g C kg^{-1}) as produced by the best spectroscopic model.

No SOC values above 15 g C kg^{-1} were present in the validation set (Figure 19 - Test), so that the RMSE of validation might be slightly underestimated. The repeatability analysis yielded a SEL value of only 0.4 g C kg^{-1} suggesting that the method is highly repeatable.

4.3.2 SOC distribution with depth

The spectroscopic predictions show clear differences in the depth distribution of SOC content across a range of soil textures and pedologically different soil samples. SOC contents in the topsoil range from 6 to 38 g C kg^{-1} declining to ~1g C kg^{-1} at one meter soil depth (Figure 22). The general depth distribution of SOC on cropland is characterized by insignificant

changes of SOC concentrations within the plow layer and an exponential decrease below this layer.

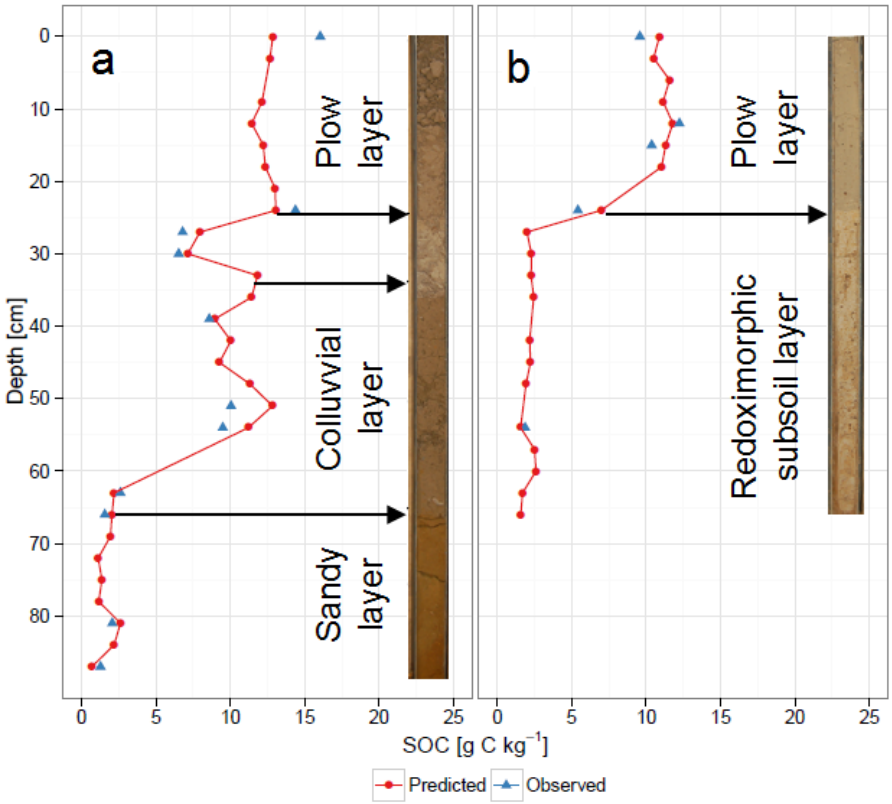

Figure 20: Two soil cores with variable features illustrating the precision and accuracy of the method. Figure 20a represents a complex profile covering C depleted (25-34cm; 65-87cm) and SOC enriched (0-25cm; 34-65cm) layers and rapid changes between loamy (0-65cm) and sandy soil textures (65-87cm). Figure 20b represents a profile with sharp boundaries between the Ap layer (0-24cm) and a redoximorphic loamy subsoil layer (24-66cm).

The spectroscopic predictions could successfully represent rapid changes in the SOC distribution along the different soil profiles (Figure 20). Boundaries of the topsoil were clearly identifiable and allow interpreting changes in the SOC depth distribution at a high vertical resolution. Furthermore, the approach can show differences in carbon depth profiles under variable soil texture substrates, especially at greater depths. Finally, the method is well suited not only to predict sharp, but also gradual changes, in the SOC depth distribution (Figure 20).

4.4 Discussion

4.4.1 Methodological improvements and limitations

It could be demonstrated that the proposed method can provide data at a similar accuracy as reference laboratory analysis. In addition, the presented approach solves some of the methodological problems of comparable spectroscopic soil analysis approaches, such as disturbance by variable soil roughness (Denis et al. 2009), disturbance by variable soil moisture (Knadel et al. 2011) and loss of the undisturbed soil matrix (Ben-Dor et al. 2008). However, the assessment method presented here has its limitations: First, the closed tube sampling system is sensitive to the gravel content in soils. Higher gravel content (>5% gravel) or soils with larger gravels (>5cm) will lead to erroneous estimations of the depth distribution of SOC as it hinders the spectral analysis and can lead to problems during the sampling by blocking the core. Therefore, it is recommend to use the proposed technique in fine-textured soils only. Furthermore, due to the use of a percussion drilling system, soil compaction of ~7±8% occurs during the sampling which disturbs the soil matrix, especially in the generally less dense topsoil. A correction factor for this compaction needs to be included if the study aims at depth explicit assessments.

4.4.2 Time and cost comparison

O'Rourke and Holden (2011) demonstrated the cost of SOC analyses by Vis-NIR reflectance spectroscopy is significantly lower than the cost of reference SOC analysis methods (wet combustion or dry total combustion). Here, a similar example has been calculated applied on the sampled dataset (Table 12). The running costs for the analysis of 1m soil cores have been compared from sampling to the final SOC values using dry total combustion and spectroscopy. Two scenarios were considered: data points are required either at low resolution (10 cm depth intervals) or high resolution (3 cm depth interval). The following calculations have been made under the assumption that all soil cores were sampled up to one meter depth. All soil cores were sampled up to one meter depth. The sampling of 150 soil cores with heavy drilling equipment required two persons to work for 208 man-hours. The time saved by sampling with closed PVC tubes (~5 min per core) compared to using a traditional open percussion gouge, which includes on-site sampling of 10cm depth intervals from the cores (~15 min per core), is substantial (Table 12). Preparation of the soil cores in the laboratory for the

spectral measurements, including all pre-treatments, required 80 man-hours (~30 min per core). Performing the spectral analysis was finished in 56 man-hours (~20 min per core). Additional time is saved in the laboratory by reducing sample preparation time due to soil crushing and sieving, which is not necessary in the approach presented here and takes ~20 min per sample for the low-resolution scenario and ~10 min per sample for the high-resolution scenario (since less soil material has to be processed).

Table 12: Running costs and time expenses for a traditional sampling campaign and a campaign using the proposed approach. Note the varying depth intervals between the low and high depth resolution scenario. $^{+}$ = Time is doubled as two operators are needed for field work.

		Traditional low-res	**Traditional high-res**	**This approach high-res**
Criteria	Depth resolution [cm]	10	3	3
	Depth intervals per core [1meter]	10	33	33
	Number of soil profiles	150	150	150
	Required samples for dry combustion	1500	4950	800
Time per core (min)	Sampling (2 operators)	30^{+}	30^{+}	10^{+}
	Preparation	200	330	30
	Scanning	0	0	20
	Total (man-hour)	**3.8**	**6**	**1**
	Total (man-hour, per sample)	**0.38**	**0.18**	**0.03**
Running costs per core ($)	Operator costs	921	1443	240
	Analysis (10$ per sample)	100	330	65
	Total	**1021**	**1773**	**305**
	Total (per sample)	**102.1**	**53.7**	**9.2**

In total, using the spectroscopic approach represents a reduction of the time spent for sampling and preparation of about 75% compared to a traditional low-resolution analysis approach and 85% compared to high resolution approach respectively (Table 12) with the additional advantage that soil cores stay intact. The use of spectral analysis also largely reduced the

analysis costs of the samples, due to lower labor costs and a lower amount of samples to be analyzed by dry combustion. Instead of 1500 and nearly 5000 soil samples analyzed with the dry total combustion technique in the low and high resolution scenario (~10$ per sample), only ~ 800 samples were analyzed to derive SOC values for calibrating and validating the spectroscopic models. The approach presented here represents only 9% of the costs for the same campaign using a traditional low resolution sampling design and 36% using a high resolution sampling design respectively. Furthermore, time and cost efficiency may improve if further research is conducted in the same geographical area, as the calibrated spectroscopic model can be used in future campaigns without further re-analysis, provided that the same measuring protocol is followed, as demonstrated by the repeatability analysis. Hence, this justifies the initially high capital costs for purchasing a spectrometer, here estimated at ~50.000$.

4.5 Conclusion

The method presented in this article is a rapid, low cost alternative for sampling and analyzing SOC depth gradients. It is a repeatable methodology and can provide high resolution depth explicit SOC datasets necessary for the verification of current models and assessments on a regional scale. The method can provide data at a similar accuracy as reference laboratory analysis, at least for fine-textured soils, and solves some of the methodological problems of comparable spectroscopic soil analysis approaches, leaving the soil cores intact for later analytical purposes. The technique can therefore provide a suitable tool for digital soil mapping and SOC assessments at larger scales. The cost benefit during the analysis

5 Re-sampling historical soil profiles – Caveats and opportunities

5.1 Outline

In the former chapter, a novel approach for estimating the depth explicit SOC distribution has been illustrated as a tool for SOC studies on a regional scale at high resolution and accuracy. As the conducted sampling campaign represents a re-sampling of historical soil profiles, an assessment of the temporal SOC dynamics could be performed using historical soil profile data and soil data from the modern campaign. The focus of the following short chapter is on (i) discussing the potential controls on temporal SOC changes related to management, pedology and geomorphology, (ii) uncertainties related to the methodology and the historical soil database and how to overcome those in future studies, (iii) as well as a comparison to existing estimates on temporal SOC changes in the region.

5.2 Material and methods

Information about the study area and the details of the applied analysis methodologies can be found in chapter 4 (section 4.2).

5.2.1 Sampling design and historical soil data

An extensive depth-explicit database with historical soil profile data is available for the study area. This dataset, called Aardewerk (AW) has been used to create the soil map of Belgium and includes both site characteristics and depth explicit information on soil properties (Van Orshoven et al. 1988, 1993). The original AW sampling campaigns took place from 1947-1968. For the study area 623 profiles on cropland are available sampled from 1955-1958. This dataset was checked for its spatial integrity by comparing the noted original coordinates on topographic maps of the soil survey conductors to the GPS coordinates entered in the dataset's digitalized format and excluded 132 soil profiles with uncertain spatial reference. From the remaining 491 historical profiles 147 soil profiles (~24% of the total cropland profiles) were re-sampled, chosen randomly across cropland in the study area (Figure 17). The acquired data covers a full geomorphic gradient from stable, flat plateaus over slopes of differing steepness and concavity to

valley basins. The acquired data covers a full geomorphic gradient from flat plateaus over slopes of differing steepness and concavity to valley basins.
Carbon in the AW dataset has been estimated with dichromate wet combustion (Walkley and Black 1934), a method with the necessity to correct SOC estimates for incomplete combustion. This has been done by multiplying the SOC estimates with a constant factor of 1.33 as identified in former studies on cropland in the same region (i.e. Sleutel et al. 2007; Meersmans et al. 2009a).

5.2.2 Analyzed parameters

The temporal changes in the SOC depth distribution are set in relation to the topographic position of the profile, the plowing depth, soil texture and the erosional/depositional regime at each soil profile. Topographic parameters are based on field observations of the slope and the position of the profile in the landscape (classified on field as stable plateau, sloping plateau, convex shoulder, backslope, concave footslope and valley basin (Figure 4)). The depth of the 1955/1958 plow layers (Ap horizon) are given in the AW database and in the re-sampling campaign derived using the spectroscopic SOC estimates, where the plow layer boundary to the subsoil is defined by the observed sharp decrease of SOC (> -30% decrease). To estimate changes in SOC stocks, the soil bulk density (BD) of the investigated profiles is multiplied with the SOC concentration and the respective soil volume (see equation 4; Chapter 3). BD estimates are taken from the European Soil Database (EC 2011) and are fixed for all profiles to 1.4 g/cm^3 for the Ap horizon and 1.6 g/cm^3 for subsoils. Soil texture for each profile is given in the AW database and assumed not to have changed significantly in the last five decades. As no high resolution DEM is available for the total research area, the soil redistribution rate cannot be assessed for the complete dataset. However, the erosive and depositional tendency of each outlined geomorphic class for the northern part of the research area has been assessed using the WATEM/SEDEM model (v.1) (Van Oost et al. 2000), applied on a smoothed 5m resolution raster DEM derived from high precision airborne LIDAR data (AGIV 2003) and using a vector parcel map as a field boundary mask. As topography and pedology in the southern part of the research area are similar, a qualitative indication in how far soil redistribution place a role for temporal SOC dynamics in the different geomorphic classes can be given

using a nominal scale ranging from a high erosional to high depositional regime.

5.3 Results

5.3.1 Soil texture and soil redistribution patterns

The soil texture is dominated by a medium to coarse silt matrix (51±11%) with no significant differences with depth or slope position between the topographic classes. The pattern of soil redistribution is related to the outlined topographic classes (Figure 21). In the northern part of the study area, the highest erosional soil losses were observed for profiles at the convex slope shoulder and the highest depositional gains in profiles in the valley basin. The concave footslope class showed as well profiles of soil gain and of soil losses indicating that other parameters (such as slope length or flow accumulation) need to be considered too in order to characterize the type of soil fluxes (gains or losses) of profiles in this class. The general tendency in this class is nevertheless a gain of soil material, indicating a depositional character of the majority of concave footslope profiles. The smallest changes were detected for the stable plateau profiles, where soil redistribution is a minor factor. Soil redistribution estimates at the sloping plateau and backslope rank between the stable plateau and the convex shoulder positions and partly overlap with estimates of profiles in those classes.

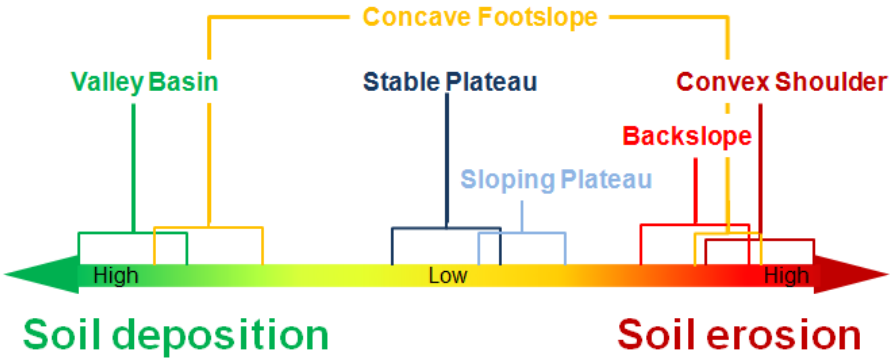

Figure 21: Nominal ranking of the defined topographic classes in terms of the dominating regime of soil redistribution. Profiles in the concave footslopes can be both in an eroding or depositing regime, depending on local site characteristics.

5.3.2 Spatio-temporal SOC patterns

The variability of the SOC depth distribution between profiles in different topographic groups is generally high (Figure 22). The outlined classes do not result in significant spatial differences with the AW SOC data. However, in the modern re-sampling campaign, the description of the topographic position of the profile is a meaningful measure to identify different spatial patterns of SOC depth distribution along the geomorphic gradient:

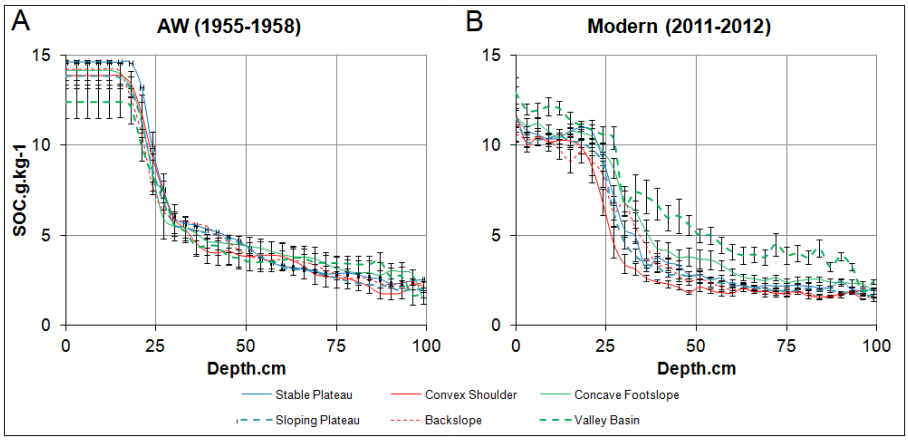

Figure 22: Mean SOC depth distribution in the AW database (Figure 22A) and the re-sampling campaign (Figure 22B) for each topographic class at the time of re-sampling. Vertical bars represent the standard error of the estimates.

The depth distribution of the SOC content varied greatly amongst eroding or depositional profiles with eroding profiles being generally SOC depleted below (>35cm) the plow layer compared to plateau profiles and depositional profiles being SOC enriched respectively. Profiles in the valley basin are generally SOC enriched compared to profiles at other slope positions. Profiles in concave footslope positions store more SOC than comparable plateau or slope profiles, while profiles at the convex shoulder position are SOC depleted. Stable and sloping plateaus, as well as backslope positions show no significant differences regarding the SOC depth distribution. The overall balance of temporal changes for cropland SOC stocks is negative with a loss of ~20% SOC between 1955/58 and 2011/12 which corresponds to an average loss of 2.0 kg C per m^3 from 10.1±7.9 kg C per m^3 in 1955/58 to 8.0±7.8 kg C per m^3 in 2011/2012 and this is in the same order as former assessments on cropland ΔSOC in the region concentrating on topsoils only

and without focus on topography related patterns (Lettens et al. 2005; Goidts et al. 2007; Meersmans et al. 2009a).

5.3.3 Changes in plowing depth

The depth of the plow layer has significantly increased between the historical sampling and the modern re-sampling campaign. This increase is related to improved mechanization and tractor power which allows deeper plowing. In most of the profiles this increase ranges between 1 and 8cm (Table 13) and is in the same range as found by Meersmans et al. (2009a) for cropland in neighboring regions. However, even so this increase varies largely between profiles, a certain tendency related to the topographic situation of the profile can be observed. Generally, the strongest increase has been observed in the concave footslope (+8±3.4cm) while the increase was smallest at the convex slope shoulder (+1±6.7cm).

Table 13: Mean slope steepness and depth of the plow layer in AW and the modern re-sampling campaign as well as soil texture distribution of the data.

Position (N)	**Slope.%**	**AP_AW.cm**	**AP_2012.cm**	**Apdif.cm**
Stable Plateau (42)	1.3±0.8	26±3.0	29±4.2	3±5.1
Sloping Plateau(40)	3.4±1.2	24±3.5	29±3.8	4±5.2
Convex Shoulder(13)	6.2±2.3	25±3.8	26±3.7	1±6.7
Backslope(21)	5.8±1.6	23±3.8	28±7.3	5±7.7
Concave Footslope(20)	3.5±1.8	24±3.1	32±3.9	8±3.4
Valley basin(11)	0.8±0.7	26±4.4	32±4.3	6±5.2
Soil texture class	**0-2µm**	**2-20µm**	**20-50µm**	**50-2000µm**
Total Transect (%)	16±6	23±6	51±11	9±13

5.4 Discussion

5.4.1 Representativeness of historical soil data

The slope steepness distribution of the original AW profiles is well captured by the re-sampling campaign and follows the general slope distribution of the cropland in the region (Figure 23). A majority of the sampled profiles (~56%) is situated on stable and sloping plateaus, while ~ 29% of the profiles are situated on steeper convex slope shoulders and backslopes and ~15% on concave footslopes and in valleys (Table 13). This distribution

represents roughly the topographic distribution of the cropland in the research area. However, already in the AW, a minor bias towards less steep cropland is recognizable (3.2±2.1% slope steepness) compared to the total cropland area (3.6±2.5 % slope steepness). The source of this bias is unclear, but most likely related to the easier accessibility of flat terrain for depth-explicit sampling and hence a tendency of the study conductors to sample those areas instead of steeper slopes. Therefore, for future studies, in order to use the AW for selecting profiles to conduct a topography dependent analysis, a correction towards selecting more profiles at steeper slopes is suggested.

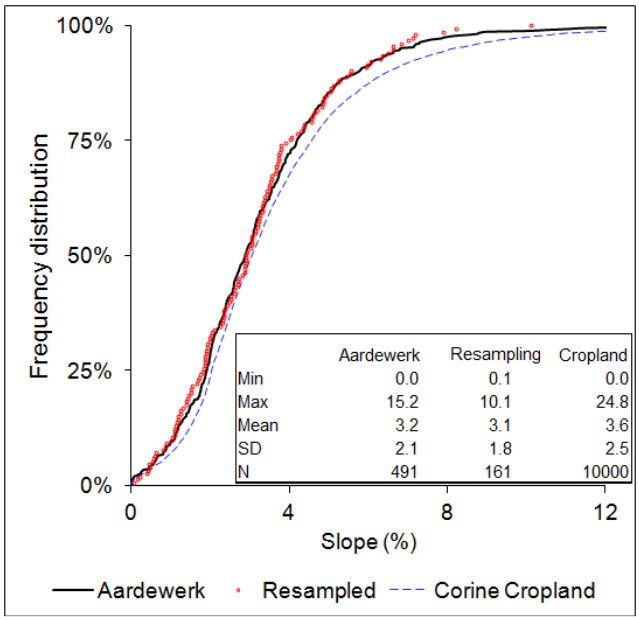

Figure 23: Frequency distribution of slope steepness of the original and re-sampled Aardewerk profiles and the Corine (100m res) – derived cropland in the research area.

5.4.2 Spatio temporal SOC changes – Controls and uncertainties

Topography and methods. Even so patterns of SOC gains and losses between 1955/58 and 2011/2012 appear to be highly related to topographic gradients (Figure 22) along the geomorphic transect, the reasons and magnitude remain unverified. Unlike in the modern re-sampling campaign, no spatial SOC pattern could be identified in the AW database related to modern topography (Figure 22). This is due to the uncertainty (~ 60m) of the

position of the original sampling point because of data transformation between different geoids (Van de Vreken 2011) and uncertainty related to the GPS re-localization of the original sampling point (c. 15m) (Goidts et al. 2009b). Considering that the average cropland in the Loambelt has rather short slopes and hence a rapidly changing topography (i.e. Figure 25), each outlined topographic class includes now a random number of soil profiles situated in a different topographic class which prohibits the identification of topography related SOC patterns in the AW. Consequently, at this magnitude, the spatial uncertainty hinders largely a point to point comparison of the two SOC datasets. For future research an adopted sampling scheme is required: Instead of point to point comparisons of ΔSOC, a comparison of changes in different topographic classes seems promising: Using modern day soil profile data, the landscape can be classified in meaningful topographic or otherwise distinguishable units. Then, those AW profiles that can be clearly identified to belong to a single class (position of the point within a certain distance from the class boundary) should be selected. The class related SOC averages can then be compared between AW and the modern data in order to identify temporal changes.

C input and land consolidation. Another issue are changes in the fieldscale topography. A significant change in land management has taken place in the region in the period 1950-1970 (Van Wesemael et al. 2010). In this phase of land consolidation, land parcels have been massively re-arranged to form larger land holdings. This led to a removal of field boundaries and, in some cases, even to a change of the local topography. For example, some positions described as convex shoulder positions nowadays, have been field boundaries in the past with colluvial deposition and represent old agricultural terraces between formerly separate fields. Parallel to this phase of land consolidation, the composition of crops grown in the region has seen significant changes, too. While the pre-1960 agricultural was dominated by a various small parceled crop mix, with a dominating crop rotation of sugar beet-winter wheat-winter barley, modern agriculture includes large extents of forage maize and areas grown with vegetables decreased (Peeters 2010). While input by manure was kept relatively constant in the study area and the nominal crop yield has increased, the removal of residues led to lower C input in soils (Van Wesemael et al. 2010) and also lower leaching of DOC into subsoils (Kalbitz et al. 2000; Rumpel and Koegel-Knabner 2011).

However, no information on SOC quality is available and this relationship could not be tested here.

Plowing depths. Concerning the increase in plowing depths between the two campaigns (Table 13), part of the SOC losses observed for the 0-20cm Ap layer can be related to dilution with SOC depleted subsoil. This is supported by the observation of an increase of SOC in the deeper (modern) plow layer at 20-35cm soil depths (Figure 24A) which is positively correlated to the increase in plowing depth. However, no reversed trend in the upper layer of the Ap (0-20cm) has been observed, suggesting that other factors such as changes in C input or management supersede this relationship.

Soil redistribution and soil texture. As described above (Figure 21), the most severe SOC depletion is observed in soil profiles at convex shoulder positions. Also in subsoils, losses are bigger than at other eroding or stable positions. This finding points strongly at a lower SOC equilibrium state as the result of intensified erosion. In addition, an effect of soil texture influencing Δ SOC in the deeper Ap (25-35cm) and subsoil (35-50cm) layers (Figure 24B) could be identified. There, the higher the amount of clay and fine silt in soils, the lower the observed SOC losses. This confirms former assessments of the importance of soil texture to stabilize SOC (Hassink 1997; Feng et al. 2011) but also shows that soils dominated by clay and fine silt can sequester carbon more rapidly than other soils and outbalance the loss introduced by the erosional removal of topsoils.

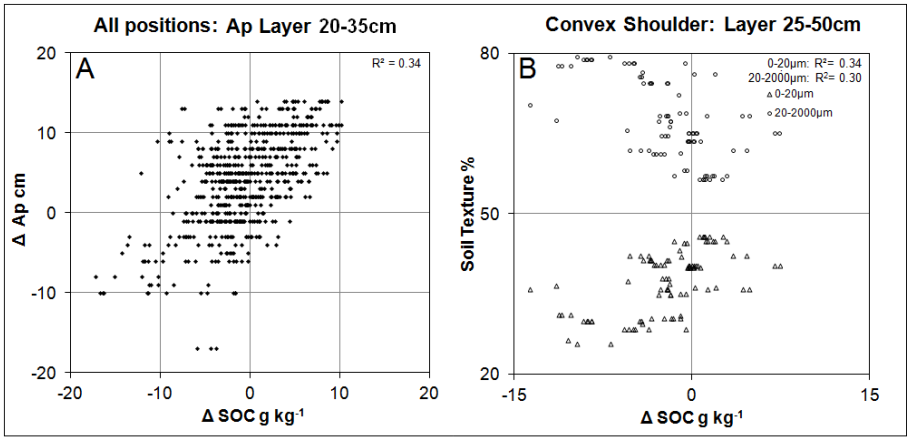

Figure 24: Relationship of the Δ SOC with Δ Ap depth (Figure 24A) for all profiles in the Ap transition layer between 20-35cm soil depth and of the Δ SOC with soil texture (Figure 24B) for the layer 25-50cm soil depth in profiles at the convex slope shoulder ($p<0.05$).

The reversed trend is visible for coarser soil textures, indicating that a shift from finer to coarser soil texture fractions, as anticipated in this region after the removal of the loess parent material, will largely reduce these soils' potential to sequester SOC as underlying coarser textured tertiary sands are introduced into the upper part of the soil column.

5.5 Conclusion

The application of the method was exemplified on a regional sampling campaign of historical cropland soil profiles along a geomorphic gradient, with the aim of analyzing the spatial-dependent temporal changes in SOC depth distribution in relation to land management, geomorphology and pedology. These changes resulted in a net loss of ~20% SOC in the upper one meter of cropland soils in the study area between 1955/58 and 2011/12. This estimate is in the same range as former assessments using a non-topography related analysis approach on ΔSOC on cropland soils in the region. SOC losses can be largely related to changes in land management and dominating crop types. But also the local geomorphologic situation and soil redistribution regime play a role in controlling whether a soil profile accumulates or looses SOC. The presented data indicates a spatial diverse pattern of SOC losses related to topography. Soils with finer soil texture can hereby outbalance losses of SOC better than soils with coarser texture. However, an exact quantification of the influence of each of the outlined factors on ΔSOC is not possible with the given data and due to methodological uncertainties related to the sampling position, an adapted sampling approach is required in future research.

6 SOC dynamics at the hillslope scale[4]

6.1 Outline

The uncertainty about the role of geomorphic processes exists largely because of (i) the lack of spatially comprehensive methods that allow for an integrated assessment of erosion-induced changes in C dynamics from source to sink (Aufdenkampe et al. 2011) and (ii) the focus on short-term studies (i.e. single event to several years, Trumbore 2009) whereby the effect of erosion has to be isolated against the much larger background C fluxes of respiration and photosynthesis (Smith et al. 2003). The objective of this chapter is therefore to improve our mechanistic understanding of C dynamics in eroding landscapes by studying coupled erosion/deposition systems that have been under the impact of human-induced erosion for several centuries. Here, a study is presented where data derived from soil organic matter fractionation and incubation experiments is combined with an assessment of long-term lateral fluxes of sediment and SOC. The difference in SOC pool composition and potential respiration along a geomorphic gradient can yield information about the mechanisms of SOC sequestration (Six et al. 2002; Del Galdo et al. 2003). First, the geomorphic controls on the horizontal and vertical distribution of SOC stocks and pool composition are quantified for the system. Then, the response of SOC pools to vertical redistribution is quantified by linking information on pool composition with soil respiration experiments.

6.2 Material and Methods

6.2.1 Site description

A general description of the research area is given in chapter 4.2.1. Here, the focus lies on the specification of the two study sites. The two sites on cropland were selected in central Belgium: Site 1 (50°45'41.50''N; 4°44'07.36"E) with south/southeast facing slope and site 2

[4] ***The content of this chapter has been published as:*** Doetterl S., Six J., Van Wesemael B. Van Oost K., (2012b): Carbon cycling in eroding landscapes: geomorphic controls on soil organic C pool composition and C stabilization. *Global Change Biology*, ***18***(7): 2218-2232.

(50°48'47.66"N;4°35'44.65"E) with north/northeast facing slope. Site 1 is characterized by a smooth topography with a long slope, whereas site 2 has a much steeper and shorter slope (Figure 25). Both sites are well drained and show no evidence of long lasting hydromorphic conditions. The geological substrate is a several meters thick Pleistocene aoelian deposit of calcareous loess, in which Luvisols have developed.

6.2.2 Field sampling

A total of 11 soil profiles was sampled (2 replicates per position) along geomorphic gradients on each site (Figure 25) covering non-eroding, stable profiles on the plateau, eroding profiles on convex and linear slopes and depositional profiles in the concave footslopes and valley bottoms. The term "stable" for certain flat plateau positions should hereby be interpreted as in contrast to other slope positions that are clearly affected by water erosion. At the non-eroding plateaus, slope steepness and topographic position in the landscape will prohibit any significant soil losses by water erosion. However, some of the original soil material at these positions might have been lost by other types of erosion, i.e. wind erosion, so that they cannot be addressed as fully non-eroded.

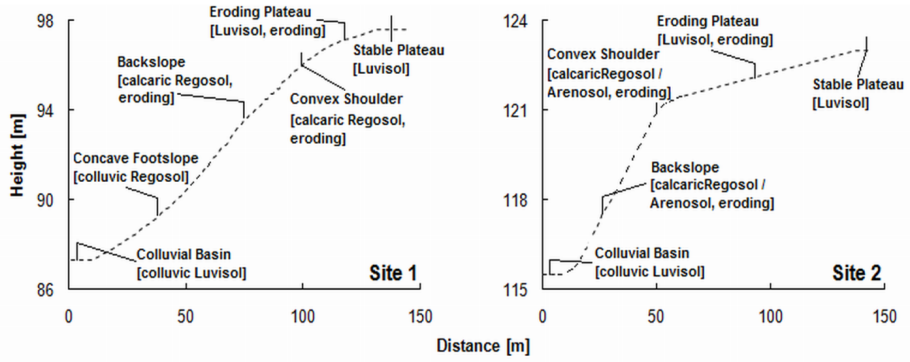

Figure 25: Topographical transects and sampling point locations for both study sites. The soil profiles are classified according to IUSS Working Group WRB (2006).

Soil cores were sampled undisturbed by using a closed sampler (Ø 4.5cm) (Eijkelkamp, The Netherlands) and then stored in a sealed pvc tube. The cores were stored frozen at -18°C until preparation for actual use. An additional core was taken with an open 1m percussion gouge (Ø 8.5cm) (Eijkelkamp, The Netherlands) at the same positions for standard soil

analysis (see further). The material from this core has been oven-dried at 40°C without delay and former freezing.

6.2.3 Soil analysis

The SOC content was measured for depth intervals of 10 cm to a depth of 1m at each slope position using a VarioMax CN dry combustion Analyzer (Elementar GmbH, Germany). Samples containing inorganic C were treated using acid fumigation prior to CN analysis in order to remove inorganic C following Harris et al. (2001). Standard chemical and physical soil analysis were performed on samples of the open percussion gouge. Soil texture was analyzed using an LS 13 320 laser diffraction particle size analyzer (Beckman Coulter, USA) and correction factors for the underestimation of clay in silty soils were applied according to Beuselinck et al. (1998). Bulk density was analyzed according to Blake & Hartge (1986) and soil profile descriptions were done using the WRB classification (IUSS Working Group WRB 2006).

6.2.4 SOC fractionation

The vertical and horizontal distribution of SOC fractions were quantified for both study sites. The soil cores were cut into slices using the following depth intervals: 0-15 cm, 35-50 cm, 55-70 cm; 75-90 cm (last interval only for colluvial basins). These depth intervals have been chosen to maximize the differences in SOC stocks and quality. The depth interval 15-35 cm was not included in the analysis as this layer contained both top- and subsoil material. The samples were gently broken into smaller pieces by hand, sieved through an 8 mm sieve and air-dried to get a homogenous substrate with the inherent aggregate structure remaining largely undisturbed (Six et al. 1998). A subsample of 80g of this homogenized soil was then used in the SOC fractionation analysis. The method used here is based on the conceptual SOC fraction model proposed by Six et al. (1998, 2002) (Figure 26). The scheme consists of a series of chemical and physical fractionation techniques applied to isolate functional SOC fractions, differentiated by stabilization mechanisms (chemical, biochemical and physical) which can also be associated with different turnover times and SOC stability (for an overview see e.g. Christensen 2001; Six et al. 2002; von Luetzow et al. 2006, 2007). In a first step, SOC is fractionated into macroaggregate (>250µm), microaggregate (250µm-53µm), and bulk silt & clay (<53µm) fractions by

slaking to define water-stable aggregates and no dispersion agent has been used. Then, these fractions get further processed to derive more subcompartments (see Figure 26 and Six et al. 2002). The original scheme was modified by (i) not separating the sample into a light and a heavy SOC fraction using density flotation, as the light fraction is typically very small at cropland sites (e.g. Don et al. 2009; John et al. 2005) and by (ii) splitting bulk and aggregated silt and clay fractions into the silt (53-2µm) and clay (<2µm) subfractions using a Sorvall RC 3C Plus Centrifuge (Thermo Scientific, USA). To further isolate highly recalcitrant SOC, silt and clay SOC sources from different parent SOC fractions were subjected to acid hydrolysis (6M HCl). The isolated remaining non-hydrolyzable SOC is considered to be an indicator for the passive SOC fraction stabilized by strong chemical complexation and inherent biochemical recalcitrance. Recovery rates of sample soil mass and the SOC mass were controlled during the fractionation procedure. Recovery rates above 97% were obtained for the soil mass of all fractions except for the clay SOC fractions after hydrolysis. For this fraction, up to 50% of the mass was lost for 15 samples. However, this fraction only represents ca. 11% of the total soil mass. Recovery rates of 94% were obtained for the SOC mass. The isolated fractions were prepared for the removal of inorganic C using acid fumigation following the methods proposed by Harris et al. (2001) and analyzed for total SOC and stable C isotope ratios using a PDZ Europa ANCA-GSL elemental analyzer interfaced to a PDZ Europa 20-20 isotope ratio mass spectrometer (Sercon Ltd., UK).

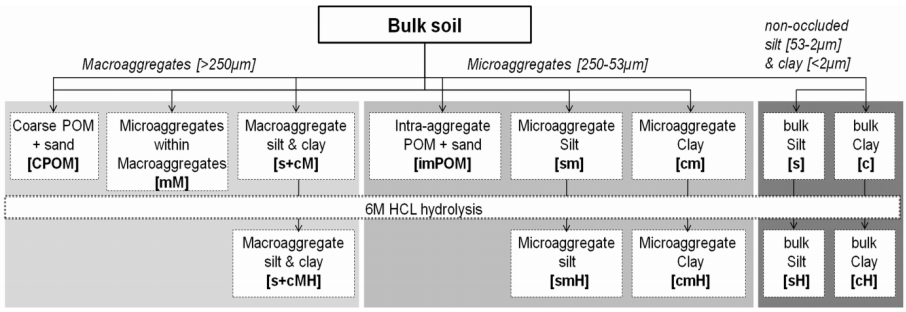

Figure 26: Fractionation scheme used in the isolation of functional SOC fractions according to Six et al. (1998, 2002).

Isotope ratios were expressed as $\delta^{13}C$ in per mille (‰) and relative to PDB standard. The available sample size decreased with each analysis step and

some of the resulting fractions only represented a very small part of the initial total SOC and soil mass. In these cases, all parent material was used in the following analysis step and the source group has been recalculated using results from previous fractionation steps where possible (e.g. m = sm + cm + imPOM, fractions described in Figure 26).

6.2.5 Soil incubation

Three replicate samples of 70g of the soil material that was prepared for the fractionation were incubated, originating from 6 different slope positions along the geomorphic gradient of site 1 (Figure 25) and three different depth intervals (Topsoil: 0-15 cm; Subsoil A: 35-50 cm; Subsoil B: 55-70 cm). Respiration was monitored during a period of 50 days while keeping moisture (at 55 % of the soil water holding capacity) and temperature (25 °C) constant. Thus, optimal conditions for microbial activity were established and induced the (natural) potential maximum heterotrophic CO_2 soil respiration (Paul et al. 2001). Each sample has been put in a 1 quart (≈946ml) sealed mason jar with no further additives except replacement of evaporated water during the experiment. To avoid CO_2 saturation effects influencing microbial decomposition processes, the incubation jars were flushed with fresh air after each measurement. Samples of the gas mixture within the incubation jars have been taken periodically throughout the experiment and analyzed for CO_2 concentration using a Shimadzu GC-2014 gas chromatograph (Shimadzu Scientific Instruments, Japan) and corrected for the according atmospheric reference and standards values. In the analysis here, only the mean respiration rates over the last 20 days of the incubation period, when heterotrophic soil respiration had stabilized, were considered.

6.2.6 Implementation and statistical analyses

The soil profiles taken along the geomorphic gradient were grouped into 3 classes according to their geomorphic setting: (i) non- (or slowly-) eroding profiles on plateau positions, (ii) eroding profiles on convex slope shoulders and backslopes and (iii) depositional profiles in concave and footslope positions. Statistical tests for differences between the means of the geomorphic classes have been performed for the whole dataset and for top and subsoil samples separately using Bonferroni corrections and Tamhane's T2 with SAS Enterprise 4.2 (SAS Institute Inc., USA). In addition, linear

regression analysis was performed to link SOC quality and respiration data to soil depth and quantitative estimates of sediment and SOC redistribution rates. Here, the **C**umulative **S**oil **R**edistribution (CSR, in cm) since the start of agriculture for each geomorphic position was estimated. The depth of the upper boundary of the calcareous, unweathered loess layer was used to estimate cumulative soil erosion and deposition using the methodology proposed by Rommens et al. (2005). Furthermore, quantitative estimates of soil erosion (negative values) and deposition (positive values) are derived by taking the soil profiles at non-eroding plateau positions as references. The latter are assumed to be unaffected by soil redistribution and differences in the depth to the calcareous loess, relative to reference profiles, can therefore be related to soil redistribution. For site 2, at steep slope positions, erosion has already heavily eroded the whole developed soil and loess layers. A minimal conservative estimate of the soil loss has been obtained by using the lower boundary of the loess layer and the transition to the underlying tertiary sands at the non-eroding plateau.

Three sandy subsoil samples (9% of total data) from eroded positions at site 2 with sand content >75 % were excluded from the analysis, as these layers (i) are characterized by different SOC stabilization mechanisms (Schneckenberger and Kuzyakov 2007; Baer et al. 2010) and (ii) are characterized by very low SOC contents, which makes it difficult to accurately identify SOC pools. This resulted in 32 observations for SOC fractions and 18 for potential soil respiration.

6.3 Results

6.3.1 Soil and total SOC patterns

On average, since the start of agriculture, 0.6m of the soil have been removed from the non-eroding plateau profiles and 3m from the eroding slope profiles, while depositional profiles have accumulated 2.4m of sediments (Table 14). Consistent with these soil redistribution rates, relatively undisturbed Luvisols with a clearly developed clay-rich B(t) horizon were found on the non-eroding plateaus. In contrast, the B(t) horizon was completely eroded on the slopes in most cases. For some profiles on the slope, the unweathered loess substrate was found close to the surface and was partly mixed into the plow layer.

Table 14: Study site description. Cumulative soil redistribution (CSR, cm), slope (%) and soil texture (% soil volume) values measured at different slope positions ranging from stable to eroding and depositional settings for site 1 and 2 (*=only one observation available).

	Geomorphic setting	Slope Position	CSR (cm)	Slope (%)	Layer	Clay (<2µm)	Silt (2-53µm)	Sand (53-2000µm)
Site 1	Stable	Stable	±0	3	Topsoil	11.2*	71.1*	17.7*
		Plateau			Subsoil	12.8±5.5	74.1±1	13.1±6.5
		Eroding	-85	7	Topsoil	7.8*	69*	23.2*
		Plateau			Subsoil	11.2±4.8	70.9±3	17.9±7.7
	Eroding	Convex	-200	10	Topsoil	3.2*	58*	38.8*
		Shoulder			Subsoil	6.3±1.3	68.5±2.1	25.2±3.4
		Backslope	-170	12	Topsoil	19.1*	67.7*	13.2*
					Subsoil	8.9±4.8	56.2±1.3	34.9±3.4
	Deposition	Concave	60	10	Topsoil	8.5*	68*	23.5*
		Footslope			Subsoil	13.5±12.1	61.6±1	24.9±13.1
		Colluvial	350	4	Topsoil	3.5*	58.9*	37.6*
		Basin			Subsoil	18.5±3.1	65.4±1.6	16.1±1.5
Site 2	Stable	Stable	±0	1	Topsoil	13.3*	71.8*	14.9*
		Plateau			Subsoil	15.8±3.9	72.3±3.2	11.9±0.7
		Eroding	-160	10	Topsoil	15.8*	70.7*	13.5*
		Plateau			Subsoil	10.8±2.3	70.8±2.2	18.4±0.1
	Eroding	Convex	-410	13	Topsoil	14.6*	72.7*	12.7*
		Shoulder			Subsoil	9.7±11	35.7±41.5	54.6±52.5
		Backslope	-400	8	Topsoil	9.3*	50*	40.7*
					Subsoil	6.4±1.6	7.2±5	86.4±3.5
	Deposition	Colluvial	300	2	Topsoil	3.7*	56.9*	39.4*
		Basin			Subsoil	6±1.9	58.3±1.5	35.7±3.2

Although the redistribution patterns are similar, site 2 differs from site 1 in the almost complete removal of the original loess substrate at the most severely eroded positions (convex shoulder and backslope). Here, the underlying tertiary sands are mixed into the plow layer. The depositional positions of both sites are characterized by thick layers of colluvium and are classified as colluvic Luvisols (IUSS Working Group WRB, 2006; Figure

25). By combining the CSR and the spatial extent of the geomorphic classes (Table 14), it is estimated that ~ 95 % of the sediments eroded on the hillslopes are stored in the thick colluvium of the valley floor of site 1. This also implies that only 5 % of the sediments are exported from the hillslope. In contrast, site 2 has only retained ~ 25 % of the eroded sediments in the depositional profiles while ~75 % has been exported. Texture differences between the profiles along the slope are small (Table 14) and the soils are silt (61 ± 18 %) dominated.

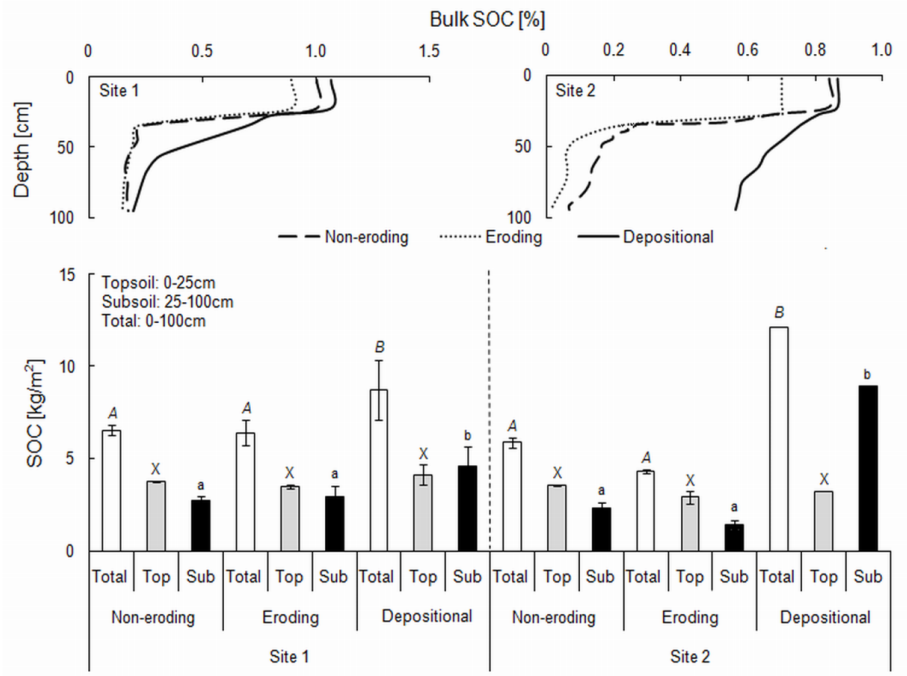

Figure 27: SOC depth distribution and stocks as a function of the geomorphic position. Significant differences between geomorphic positions for three depths (i.e., topsoil, subsoil, and total depth) are presented where the same letter indicates no significant difference between geomorphic positions ($p < 0.1$, tested for site 1 and 2 separately).

Consistent patterns of SOC concentrations at both sites were found with topsoil SOC contents ranging between 0.7 – 1.2 % (Figure 27). Topsoil SOC concentrations were higher for depositional and non-eroding profiles than for eroding profiles. The largest differences, however, were observed in the subsoil. The subsoils of non-eroding profiles have a slightly higher SOC content than eroding profiles while depositional profiles are enriched in SOC

at depth. The depositional profiles store 1.6 (site 1) and 6.2 times (site 2) more SOC in the subsoil (25-100 cm) than eroding profiles (Figure 27).

6.3.2 Patterns of potential soil respiration

Significant effects of soil depth and geomorphic position on the rate of soil respiration were observed during the incubation experiments (Figure 28). The measured CO_2 respiration was negatively correlated with depth while positive correlations with SOC concentration were found (Table 15). The respiration for topsoil samples is much higher than for subsoils (Figure 30A). Soil respiration per unit soil (g) for topsoil samples were lowest at non-eroding profiles (0.19 ± 0.01 µgC h^{-1} gSoil $^{-1}$), while eroding and depositional profiles respire at significantly higher rates (0.25 ± 0.04 µgC h^{-1} $gSoil^{-1}$). For subsoils, the highest respiration rates were found for the depositional profiles (0.06 ± 0.02 µgC $h^{-1}gSoil^{-1}$), and this was significantly higher than the respiration of the non-eroding and eroding profiles (0.04 ± 0.1 µgC h^{-1} $gSoil^{-1}$).

Table 15: Significant correlations. Correlation coefficients of linear regressions between SOC concentration, soil depth or CSR and SOC parameters (**= p<0.05).

Layer	Variable 1	Variable 2	r
Top- and Subsoil [0 - 100 cm]	SOC concentration	Respiration µgC h^{-1} $gSoil^{-1}$	0.97**
		Respiration µgC h^{-1} $gSOC^{-1}$	0.75**
	Soil depth	Respiration µgC h^{-1} $gSoil^{-1}$	-0.91**
		Respiration µgC h^{-1} $gSOC^{-1}$	-0.75**
		Fast Pool C (% of total SOC)	-0.64**
		Passive pool C (% of total SOC)	0.61**
Subsoil [35 - 100 cm]	CSR	δ^{13}C Microaggregate C (ratio)	0.59**
		δ^{13}C Bulk silt C (ratio)	0.51**
		Microaggregate C (% of total SOC)	0.49**
		Bulk silt + clay C (% of total SOC)	-0.61**
		Microaggregate clay/silt C (ratio)	-0.69**
		Bulk clay/silt (ratio)	-0.53**

The topsoil samples also respired at a higher rate than subsoils per unit C (g). For both top- and subsoil, samples from eroding profiles respired significantly more SOC than depositional or non-eroding profiles. Lowest

respiration rates were measured in depositional (topsoil: 23.1 ± 1.0 µgC h^{-1} $gSOC^{-1}$; subsoil: 12.9 ± 1.5 µgC h^{-1} $gSOC^{-1}$) and non-eroding profiles (topsoil: 19.8 ± 1.4 µgC h^{-1} $gSOC^{-1}$; subsoil: 14.5 ± 2.0 µgC h^{-1} $gSOC^{-1}$) and were significantly lower than the respiration rates of eroding profiles (topsoil: 26.6 ± 2.3 µgC h^{-1} $gSOC^{-1}$; subsoil: 16.6 ± 2.6 µgC h^{-1} $gSOC^{-1}$) (Figure 28B).

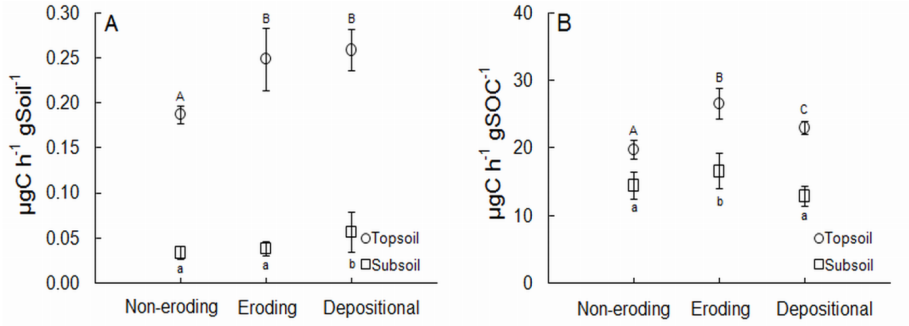

Figure 28: Observed respiration rates for top- and subsoil as a function of the geomorphic position (non-eroding, eroding and depositional). The respiration per unit soil (A) and per unit of C (B) is given. Same letter indicates no significant differences between different geomorphic positions for the two depth classes ($p < 0.1$, tested for Figure 28A & B separately).

6.3.3 SOC fractions and stability

The measured SOC fractions show large differences in terms of C/N ratios and $\delta^{13}C$ compared to their (SOC) source material (Figure 29): The non-hydrolyzable fractions (s+cMaH, smH, cmH, sH and cH) are characterized by depleted $\delta^{13}C$ values and high C/N ratios which may indicate that they are largely derived from stable plant compounds like lignin and waxes (Tiunov 2007; Schmidt and Gleixner 2005) or pyrogenic C (Bird et al. 2012). A significant positive correlation between CSR and the $\delta^{13}C$ signal of microaggregate and bulk silt associated SOC was observed in subsoils (Table 15). These large differences in C/N ratios and $\delta^{13}C$ between the fractions strongly suggest that the fractionation scheme used in this study results in fractions which are different in terms of SOC origin and stabilization mechanisms (Six et al. 2001, 2002).

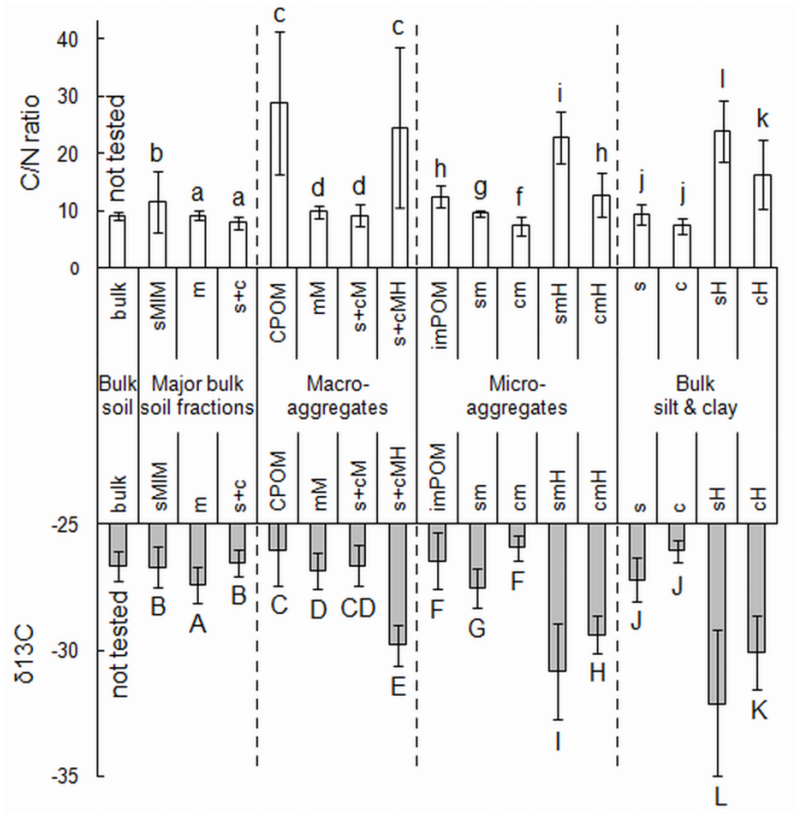

Figure 29: Elemental and isotopic characterization of the measured SOC fractions. The key for the abbreviations is presented in Figure 26. Depth averaged values for C/N ratios and d13C for the measured SOC fractions indicate a clear distinction between non-hydrolyzable SOC fractions sources and other compartments. Same letter above bars indicate no significant differences between SOC fractions ($p < 0.1$, tested separated for both parameters and the different groups separated by the dashed lines).

Based on these findings, the measured fractions were grouped into three functional SOC pools for further analysis (Figure 30): (i) the fast pool is defined as the hydrolyzable SOC in macroaggregates ((CPOM + mM + s+cM) – s+cMH); (ii) the intermediate pool is the hydrolyzable SOC of the microaggregate ((imPOM+sm+cm)-(smH+cmH)) and silt & clay associated SOC ((s+c) – (sh+cH)) and (iii) the passive SOC pool is defined as the non-hydrolyzable SOC of all the isolated silt and clay fractions (s+cMH, smH, cmH, sH and cH). The non-hydrolyzable SOC pool may contain some low density organic matter as no density separation has been performed. However, the incubation data shows that in topsoils, where the abundance of low density SOC is naturally highest, the soil potential respiration is

negatively correlated to the abundance of non-hydrolyzable C (R^2 = 0.41, $p<0.1$, data not shown). This indicates that this effect can be neglected and will further not be considered in more detail.

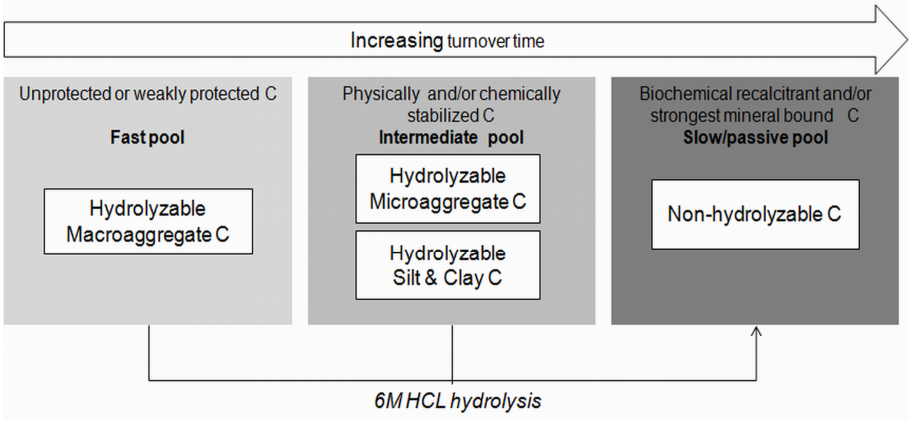

Figure 30: Definition of the fast, intermediate and passive pools in relation to the measured functional SOC fractions. Note that non-hydrolyzable C from POM and mM fractions has not been isolated and is therefore not considered.

6.3.4 Spatial and vertical patterns of SOC fractions and pools

The amount of C associated with the fast pool is strongly related to depth: the fast pool represents 26 (±11) % of the SOC in the top soil and 12 (±4) % in the subsoil (Figure 31). Substantially more SOC is associated with the passive pool in subsoils, i.e. 30 (±6) % for topsoil vs. 55 (±13) % for subsoil. While there is a significant negative correlation between soil depth and the abundance of the fast pool and a positive correlation to the passive pool, no relation was observed for the intermediate pool (Table 15). The pool composition of the topsoil was similar along the hillslope and no significant differences in the abundance of the fast, intermediate and passive pools between the geomorphic positions were found (Figure 31). The depositional profiles contained ~ 20% more SOC in the fast pool relative to non-eroding or eroding profiles, but this was not significantly different from the other positions. In contrast, geomorphic position strongly influenced the abundance of the intermediate and passive pool in the subsoil: significantly more SOC is associated with the intermediate pool in the depositional profiles (45 ± 5%) than in non-eroding (29 ± 3%) or eroding profiles (23 ± 6%). This intermediate pool mainly reflects the contribution of hydrolyzable microaggregate and silt & clay SOC. A significant positive correlation was

found between the geomorphic setting (CSR) and the fraction of SOC in microaggregates with proportionally more SOC stored in microaggregates in the subsoil of the colluvial basin (Convex Shoulder 35 ± 2%; Colluvial basin (49 ± 2%) (Figure 32A and Table 15).

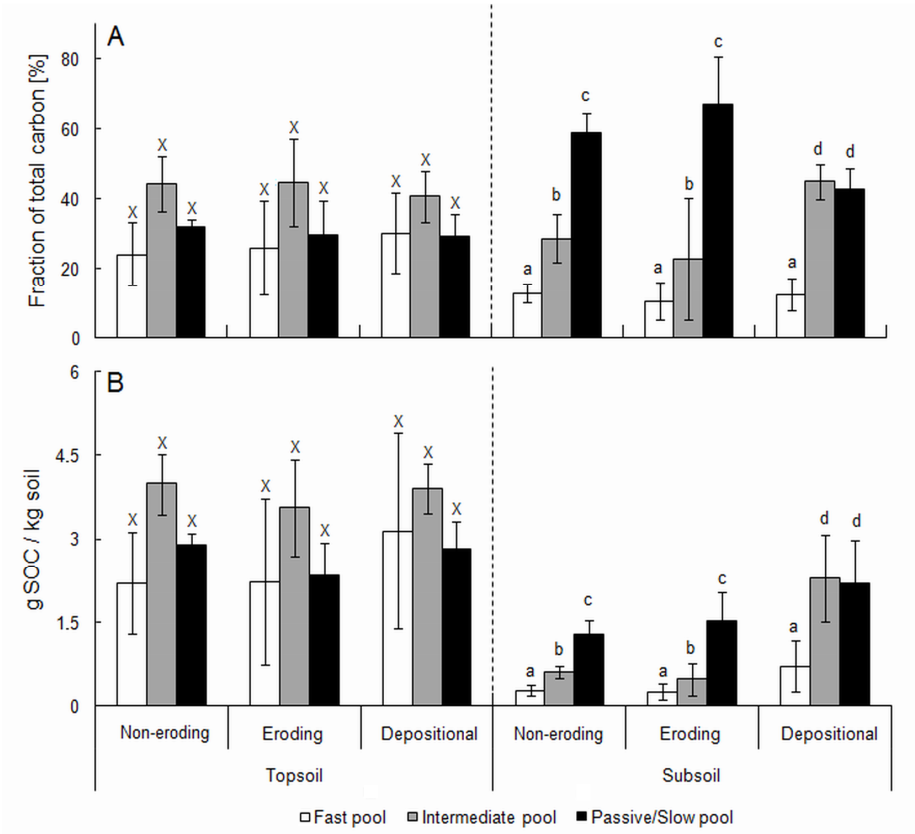

Figure 31: Distribution of SOC pools along the geomorphic gradient as a fraction of the total C in % (a) and absolute amount in g SOC per kg soil (b). Same letter indicates no significant differences between the pools and the geomorphic positions ($p < 0.1$, tested for Figure 31a & b and the top- and subsoil separately).

In contrast, the eroded profiles are significantly enriched in bulk silt & clay SOC fractions relative to the non-eroding and depositional profiles, resulting in a negative correlation between CSR and the fraction of SOC in the silt and clay fractions (Convex Shoulder 53 ± 9%; Colluvial basin (36 ± 1%) (Figure 32B and Table 15). Within the microaggregate fraction, a significant shift between eroding and depositional profiles in the ratio of clay/silt associated SOC was observed with more carbon stored associated with silt sized particles (Figure 32C and Table 15). An identical shift was

present for the non-aggregated clay and silt SOC sources with significantly more silt associated SOC in depositional profiles, while eroding profiles store more SOC in clay associated fractions (Figure 32D and Table 15). The contribution of the passive pool in subsoils was also significantly higher for non-eroding (59 ± 6 %) and eroding profiles (67 ± 14 %) than for depositional profiles (43 ± 6 %), while the abundance of the fast pool at depth was very similar along the geomorphic gradient (12 ± 4 %; Figure 31).

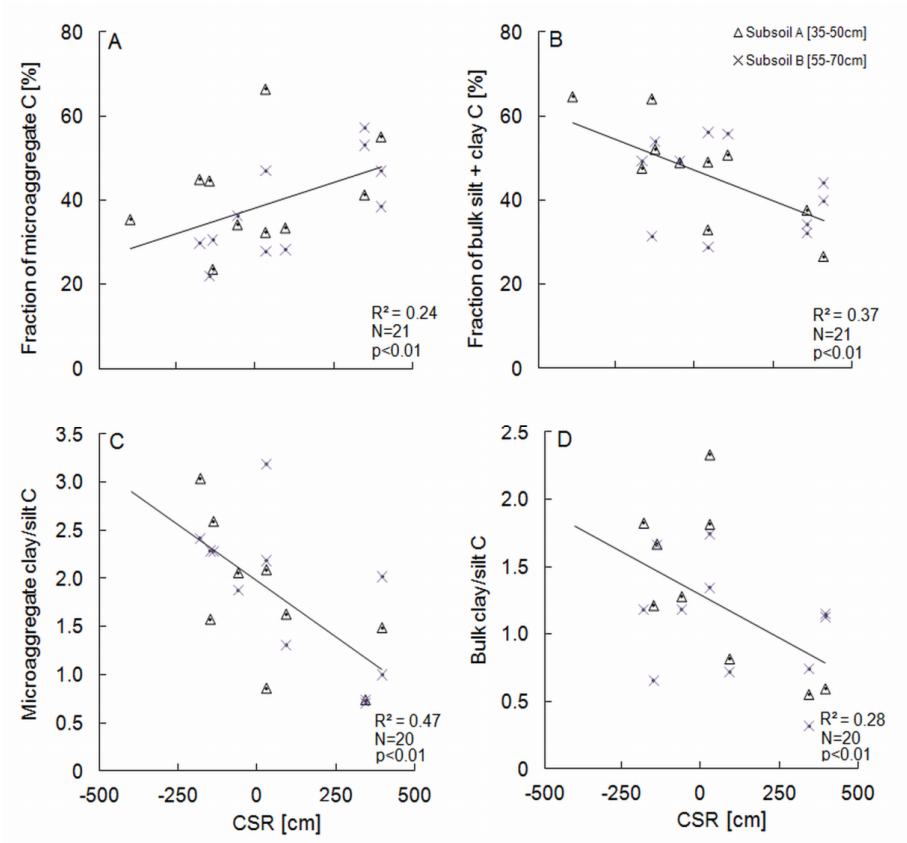

Figure 32: The changing contribution of different SOC fractions along the slope's subsoil. The fraction of microaggregate SOC (Figure 32A) and the contribution of silt associated SOC within this fraction (Figure 32c) and in the bulk silt and clay SOC (Figure 32D) is highest at depositional positions (high CSR values) while the non-aggregated SOC (Figure 32B) and clay associated SOC is highest at eroding sites (low CSR values). No such correlation was found for the slope's topsoil (data not shown).

In summary, the largest differences along the geomorphic gradient were observed for the intermediate and passive pools. An enrichment of

aggregated SOC in buried soils compared to non-eroding or eroding sites was observed. More SOC is stabilized in microaggregate and silt associated SOC fractions in depositional profiles and eroding profiles have more SOC stabilized in clay fractions.

6.4 Discussion

6.4.1 SOC replacement at eroding positions

Erosion processes have removed between 2 and 4 m of soil from the eroding hillslope since the start of agriculture, and much of this soil material is now stored in the depositional profiles at the hill foot. The carbon has been replaced, removed and transported during centuries of disturbance by tillage and other practices. The erosion of the hillslope has resulted in a removal of sediment and SOC from the topsoil of the eroding profiles and the advection of subsoil material to the surface. As a result, SOC depleted material from the former subsoil is mixed into the surface layers. Although erosion has largely disturbed these profiles, there are no significant differences between the SOC stocks of the eroding and stable profiles. The current carbon stock of the former subsoil of the eroding profile thus exceeds the original carbon through the exposure of deeper soil and the fixation of new photosynthate in the more biologically active upper layers of the profile. This is consistent with the concept of dynamic replacement (Harden et al. 1999) and this represents a net sink for atmospheric CO_2 (Berhe et al. 2008). Furthermore, the absence of differences in pool composition of the topsoil along the geomorphic gradient (Figure 31) strongly suggests that the biological processes controlling C turnover operate at a faster pace than the erosion-induced disturbance, leading to a fast replacement of the eroded SOC. This efficient replacement of eroded SOC over long timescales (i.e. centuries) contrasts with the much lower, and only partial replacement of 20% to 40% of the eroded SOC, found by Van Oost et al. (2007) in similar environments, but over much shorter timescales (i.e. 5 decades). This is probably related to the significant increase in soil erosion rates in the study area since the mechanization of agriculture in the 1950s (Van Oost et al. 2005a).

6.4.2 SOC deposition

Significant differences can be observed in the retention and depth distribution between the two study sites (Figure 27). These differences can

be related to the differing slope lengths and slope steepness between the two sites. At the less steep and longer slope of site 1, erosion and deposition is a slower process than at site 2, where the eroding slope is steeper and shorter (Figure 25). In consequence, until C is deposited and buried in zones where decomposition is slowed down takes more time at site 1 than at site 2 and hence less SOC is retained. The higher SOC concentrations in depositional profiles are usually related to the preferential detachment and downslope transport of the more labile, and lighter, SOC fractions which are typically enriched in SOC, relative to the bulk soil (e.g. Gregorich et al. 1998; Kuhn et al. 2007, 2009). However, no enrichment of the labile SOC fraction in the depositional profiles was observed. A possible explanation is that the labile fraction is mineralized before it reaches the depositional profiles. An alternative explanation is that sediment and carbon erosion here are unselective processes as indicated by the small differences in soil texture along the hillslopes (Table 14), the missing correlation between soil texture and SOC (fractions) (R^2<0.3 or not significant, data not shown) and as shown in other studies in the region (e.g. Steegen et al. 2001). Recent evidence from experimental studies on similar types of soil indicates that the latter is more likely (Wang et al. 2010).

6.4.3 SOC burial efficiencies

The SOC profiles (Figure 27) show that the depositional profiles are enriched in SOC at depth and that they store significantly more SOC than non-eroding or eroding profiles and this confirms earlier studies (e.g. Berhe et al. 2008; Hoffmann et al. 2009; Zadoroava et al. 2011). However, the depositional profiles only represent 15% to 30% of the surface area of the entire hillslope and the preservation of buried topsoil material is only partial as the SOC concentrations decline with depth. By assuming that the SOC concentration of the topsoil has remained constant during the period of agriculture, it is estimated that between 26 % (site 1) and 71 % (site 2) of the buried SOC has been preserved, while the remainder has been mineralized. This wide range of observed partial preservation of buried SOC for two similar sites suggests that geomorphic and land use related parameters (e.g. slope length/gradient, sediment delivery ratio, land use history) are important controls but the data presented here does not allow to identify their relative importance.

6.4.4 SOC budget in eroding vs. non-eroding landscapes

Finally, considering the spatial extent of the various geomorphic units along the hillslopes (Figure 25 & Figure 27), the data show that eroding hillslopes store more SOC than their non-eroding counterparts: A landscape budget accounting for the SOC stocks to a soil depth of 100cm results in 10 % (site 1) and 6 % (site 2) more SOC than when only stable profiles in non-eroding conditions are considered. This erosion-induced sink is due to the combination of two processes: (i) the replacement of eroded SOC, i.e. the fixation of atmospheric carbon, in eroding profiles and (ii) the partial preservation of SOC in depositional profiles. It was not possible to quantify the fate of the SOC that is exported from the hillslope systems and that is stored in deeper (>100cm soil depth) colluvial soils, and this could ultimately change the magnitude and sign of the erosion-induced SOC exchange.

6.4.5 Controls on topsoil SOC respiration

The topsoil respiration data show that erosion-induced soil disturbance, affecting both eroding and depositional profiles, increases potential soil respiration relative to non-eroding profiles (Figure 28A). The potential respiration rates were on average 25% higher than those of non-eroding profiles. However, the data do not indicate whether this increase is related to physical disturbance (disintegration of aggregate structure and weakening protection (e.g. Kleber 2010; Six et al. 2000, 2002), biochemical alteration of the material (e.g. Conen et al. 2008) or to a combination of both. The observed differences in respiration rates between top- and subsoils are to a large extent related to the higher abundance of the fast C pool in topsoils (Figure 33A). The composition of the fast pool is only controlled by macroaggregate SOC which contains labile material derived from plant litter and crop residues (Jastrow 1996; Angers and Giroux 1996; Golchin et al. 1996).

6.4.6 Controls on subsoil SOC respiration

In contrast, there was no clear relationship between the fast pool and soil respiration for subsoils. More vulnerable SOC compartments of the former topsoil macroaggregates may have already been decomposed before or during burial in deeper soil layers of depositional profiles, or the C sources

for the formation of macroaggregates in subsoils differ from those in topsoils and are more recalcitrant than topsoil sources. In contrast to the topsoil layers, the potential respiration for the subsoils was significantly and positively related to the clay/silt SOC ratio (Figure 33C). In other words, a higher abundance of silt over clay associated SOC results in lower respiration rates. This relation was even stronger for the microaggregate clay/silt SOC ratio (Figure 33B) and indicates that physical protection mechanisms play an important role in subsoil C dynamics (see further). The partial preservation of SOC in buried topsoil material discussed above is consistent with the observation that buried SOC is also stabilized in microaggregate and silt associated SOC (intermediate pool) and not only in the passive pool (Figure 31). Assuming that the in-situ subsoil SOC composition of the non-eroding and the depositional profile is similar, the burial efficiency for each pool can be calculated: on average 14% of the fast pool, 43% of the intermediate pool and 32% of the passive pool are preserved after burial and long-term decomposition processes. This finding and the abundance of aggregated SOC in depositional soils (Figure 32) suggests that: (i) physical protection plays a major role in depositional positions to stabilize SOC against decomposition also in the long-term and (ii) that the passive SOC pool will shrink as well facing long-term decomposition.

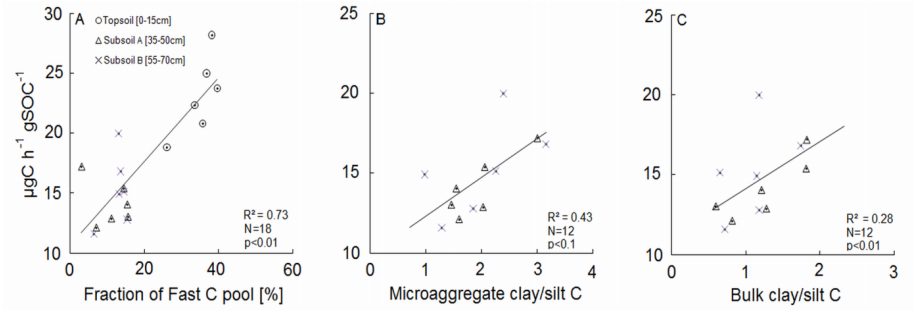

Figure 33: Observed respiration per unit C in relation to the abundance of the fast pool (hydrolyzable macroaggregate C) for top- and subsoil (A) and in relation to the ratio of silt/clay associated C in microaggregates (B) and bulk silt & clay (C) in subsoils.

6.4.7 SOC mean residence time and geomorphic position

The respiration results reflect the potential respiration for the fast and intermediate pools as the passive pool does not contribute to the respiration observed in these short-term incubations (Paul et al. 2001). Since the relative proportion of the passive pool in the total SOC pool was measured, the mean residence time (MRT) of the combined fast and intermediate pools can be estimated as a measure of the relative differences in turnover at different positions and soils depths. Differences in the MRT (relative to the non-eroding positions) and potential respiration for topsoil samples are not significant along the slope (Figure 34) and this is related to the similarity of their pool composition. In contrast, differences for subsoils are more pronounced: Subsoil C turnover is 1.7 times slower at depositional than non-eroding positions and this indicates a substantially higher stability of the fast and intermediate SOC pools in the subsoils of depositional profiles. This higher stability is consistent with the observation that depositional subsoils store more SOC in both microaggregate and silt-sized fractions compared to eroding profiles (Figure 32 & Figure 33). This implies that there is more physically protected SOC in depositional profiles relative to other positions. In eroding profiles, the stability of the intermediate and fast pool is significantly less and C turnover is 1.4 times faster than at non-eroding profiles (Figure 34).

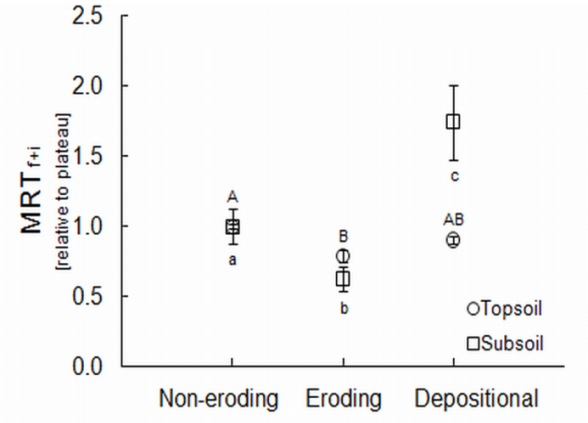

Figure 34: Mean Residence Time (MRT) for the fast + intermediate SOC pools derived from the incubation experiments and SOC fractionation for top- and subsoils as a function of the geomorphic position (non-eroding, eroding, and depositional). The figure expresses the MRT relative to the MRT of the stable positions. Same letters indicates no significant differences between different positions for the two depth classes ($p < 0.1$).

Here, significantly less SOC is physically stabilized in microaggregate and silt associated fractions. This can be explained by the fact that the C at eroding positions has been dynamically replaced and is therefore younger and less processed than the SOC that is stabilized in non-eroding profiles.
This is in accordance to findings from Berhe et al. (2008) who state that eroding profiles have higher SOC decomposition rates than depositional profiles and a 15 times higher rate of replacement of SOC with new photosynthates, indicating higher vulnerability and accelerated turnover in eroding landscape units.

6.4.8 Effects of soil redistribution on SOC quality

The higher abundance of aggregated SOC in the subsoil of depositional profiles is directly related to its origin: subsoil material in these positions is former topsoil material that has been buried. In topsoils, larger amounts of plant litter from recent crop residues are available and promote the formation of aggregates (Jastrow 1996; Angers and Giroux 1996; Golchin et al. 1996). The processes of decay and formation of physically protected SOC are in relative balance at the soil surface of flat, non-undulating landscapes. The stability of macroaggregates now depends further on a network of living root and hyphen and fresh, coarse plant litter. In deeper soil layers, the density of this network decreases. Consequently, once the topsoil is buried under freshly deposited material, macroaggregates will lose their structure and break up into more stable microaggregates and silt & clay fractions (e.g. Tisdall and Oades 1982; Oades 1984, Pulleman et al. 2005). The degradation of aggregates upon burial is further evidenced by the increase in $\delta^{13}C$ at depositional subsoils in microaggregates ($\delta^{13}C$ m eroding: -28.0 ± 0.6; depositional: -27.0 ± 0.4) and bulk silt SOC ($\delta^{13}C$ s eroding: -28.0 ± 1.2; depositional: -26.6 ± 0.3) (Table 15) (Tiunov 2007).
In summary, it was observed that SOC in both non-eroding and eroded soils, which are enriched in non-aggregated SOC, has a faster turnover than in depositional soils. This indicates that physical protection mechanisms play a key role in stabilizing SOC after burial and is consistent with findings of Moni et al. (2010) who identified protection within silt-sized aggregates to be important for different comparable soil types and Kleber et al. (2011) who state that the recalcitrance of SOC is not only a question of molecular structure and chemical composition but also depends on its physical environment.

6.4.9 Significance on larger scales and caveats

The majority of Europe's cropland is situated on gently rolling topographies where significant soil and SOC erosion/deposition has been observed. The area affected is at least 50 million ha within the EU25 and the size of the depositional SOC pool for this region is at least 4 Pg (Van Oost et al. 2007). Recent estimates of global agricultural erosion suggest an average soil erosion rate of 10.5 Mg ha^{-1} yr^{-1}, which results in the mobilization of 403.5 ± 201.8 Tg C yr^{-1} globally (Doetterl et al. 2012a). These numbers highlight the significance of SOC erosion and burial for C cycling and the need to develop spatially integrated approaches that specifically address processes that occur at the landscape scale. In order to do so, a careful analysis of erosion and deposition rates and patterns is necessary as well as detailed assessment what can be used as comparable reference sites. In this study, the CSR is used as a measure of erosion and deposition but this approach is subject to several drawbacks and assumptions might not be fully applicable at other sites. Soil development depth might not be constant along the hillslope and differ between profiles, as i.e. hydrology, one of the main variables fur subsoil weathering will differ along the slope as well. Even so no differences in hydromorphic features or drainage conditions were observed at the study sites here, this might not be the case for other hillslopes. Using radioisotopes such as ^{14}C or ^{137}Cs have shown their value to determine erosion and deposition patterns in former studies (i.e. Quine and Zhang 2002; Quine and Van Oost 2007; Trumbore 2009) and should be combined with a profound pedological and hydrological assessment of other study sites to overcome these drawbacks.

6.4.10 Soil aggregation vs. erosion

The observation that clay stabilized SOC is preferentially decomposed compared to silt or microaggregate SOC contrasts partly with the traditional view of high stability of SOC associated with minerals (e.g. Kaiser et al. 2002; Wattel-Koekkoek et al. 2003; Kahle et al. 2003; Mikutta et al. 2006; Sollins et al. 2006, 2009). The results highlight the importance of both aggregate formation and complexation of SOC with minerals for SOC stability and the need to account for geomorphic processes. At non-eroding positions, sequestration and release of SOC is unaffected by soil redistribution. At eroding positions, erosion leads to the removal of soil and the mixing of former subsoil into the topsoil. In this biologically active zone,

weathering processes lead to the formation of secondary minerals, which provide reactive surfaces to promote the complexation with organic material, e.g. through absorbance of SOC on mineral surfaces (Lehman et al. 2007). The processes of aggregate formation and complexation in subsoils, however, are, according to the findings presented here, slower than the geomorphic processes of erosion and subsoil mixing. Therefore, the fraction of SOC that becomes incorporated into microaggregates in subsoils remains small at eroding positions. The eroded soil is then transported downslope and buries the in-situ topsoil.

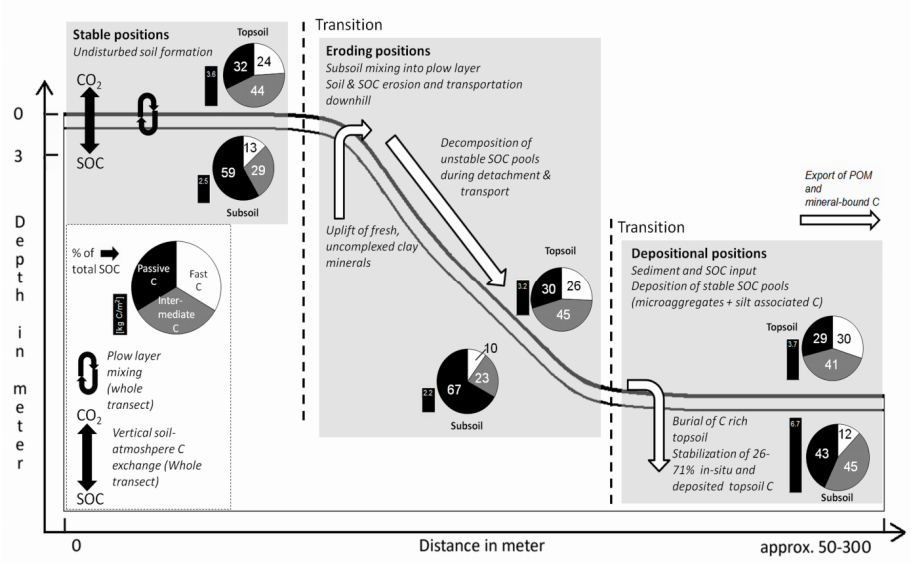

Figure 35: Summary figure describing the geomorphic controls on SOC pool composition and C stabilization mechanisms in eroding landscapes (Results aggregated from both hillslopes). Processes indicated at the non-eroding positions take place along the whole transect.

The data clearly showed that the buried SOC is stabilized in pools of intermediate turnover associated with microaggregates and silt sized particles. 40% of the SOC (Figure 35) was stabilized in passive pools, which stabilize SOC over longer timescales (see von Luetzow et al. 2007). Hence, further decomposition of a large part of the buried SOC, even so at a very low rate, is likely. The strength of the erosion-induced sink is therefore limited by (i) losses of SOC in burial positions, (ii) the capacity of soils to store intermediate and passive SOC pools in depositional subsoils and (iii) the C replacement efficiency at SOC-depleted eroding positions. For

understanding the strength of the erosion-induced sink over larger areas and longer timescales, more work needs to be done along geomorphic gradients, including colluvial, floodplain and aquatic settings, in order to better understand the environmental conditions that promote long-term stabilization.

6.4.11 Integration of lateral soil fluxes into SOC models

Previous studies on SOC pool changes related to land use conversion (e.g. Besnard et al. 1996; Cromack et al. 1999; DeGryze et al. 2004; Li et al. 2007) report that total SOC changes are mostly due to changes of the more vulnerable (free or occluded) particulate organic matter and only to a lesser extent (or restricted to specific conversions) due to changes in mineral associated organic matter. DeGryze et al. (2004) and Li et al. (2007) reported that changes were strongest in topsoils and decreased with soil depth. This is in contrast to the findings presented here from a several centuries old cropland system where soil redistribution is the main driver in SOC pool changes. Here, differences are strongest in the subsoil distribution of the intermediate and passive SOC pools. This implies that the response of SOC in eroding landscapes might be different than when SOC stock and SOC composition distributions are derived from non-eroding positions only. In conclusion, the results show the need for adapting and validating existing SOC models in systems were soil redistribution plays an important role. These models should not only take in-situ environmental conditions or land use changes into account, but also SOC pool composition changes related to soil redistribution, actively shifting SOC between sub- and topsoil layers and across different landscape units by lateral transport.

6.5 Conclusion

Here, the soil organic carbon (SOC) stock and pool distribution along geomorphic gradients were quantified and combined with data derived from soil organic matter fractionation and incubation experiments. The size and composition of the SOC pools were strongly related to geomorphic position: 1.6 to 6.2 times more SOC was stabilized in the subsoils (25-100 cm) of depositional profiles than in those of eroding profiles. Subsoil SOC of depositional profiles is predominantly associated with microaggregates and silt-sized particles which are associated with pools of intermediate stability.

A significantly higher mean residence time for the fast and intermediate turnover pools of buried SOC at depositional positions was observed, relative to non-eroding and eroding positions, resulting from the physical protection of SOC associated with microaggregates and silt particles. Conversely, significant amounts of SOC were replaced at eroding positions but the lower degree of decomposition and the lack of physically protected SOC, resulted in higher potential respiration rates. By considering C cycling at non-eroding, eroding and depositional positions, the findings show that the eroding landscapes studied store up to 10 % more SOC due to soil redistribution processes than non-eroding landscapes. This is the result of the stabilization of SOC in former subsoil at eroding positions and partial preservation of buried SOC in pools of intermediate turnover at depositional positions. However, the sink strength was limited by significant losses of buried SOC as only a small fraction of the SOC was associated with stable pools.

7 Mineralogical and pedogenic controls on spatial explicit SOC pools[5]

7.1 Outline

Soil fluxes are likely to affect soil properties which are crucial for predicting and understanding SOC dynamics by (i) relocating weathered soil material from eroding sites downslope and exposing less weathered subsoil to the surface and (ii) export or deposition and burial of the eroded sediment at the footslope. Soil properties in dynamic landscapes might therefore differ strongly from those in stable landscapes and affect SOC sequestration and stabilization in soils. Hence, it is evident that landscape scale processes must be considered in order to advance our understanding of SOC dynamics at the plot scale. Here, it is attempted to introduce a landscape scale perspective on plot scale observations of SOC dynamics and controls. In this chapter, the role of soil properties on the accumulation of SOC fractions along a geomorphic transect affected by soil redistribution is investigated. For this, a mineralogical characterization of three soil profiles along the same geomorphic transect used in Doetterl et al. (2012b) was carried out (Chapter 5). Soil profiles were chosen to give a contrasting view of different geomorphologic settings, including eroding and depositional sites, and soils from stable upslope plateaus unaffected by soil redistribution. The hypothesis that is tested here is that the soil redistribution history of a soil profile influences the weathering status of the soil material, and is therefore a primary control on the abundance and composition of the reactive soil phase in clay-sized minerals that are important for stabilization of SOC. The reactive soil phase and its potential to stabilize SOC should therefore be highly variable in space, i.e. horizontally in space along a slope transect and vertically with soil depth and in time, i.e. with ongoing soil redistribution. This hypothesis is tested by analyzing the interactions between clay-sized

[5] ***The content of this chapter has been submitted for publication as:*** Doetterl S., Cornelis, J-T. Six J., Quine T.A., Van Oost K. (*submitted*): The varying contribution of pedogenic oxides and clay minerals to stabilize carbon along a slope transect. *Journal of Geophysical Research-Biogeosciences.*

minerals and the reactive soil phase with SOC along slope transect positions and soil depths.

7.2 Material and methods

A detailed description of the location of the study site, the field sampling design, as well as well as the methods used to characterize the distribution of SOC fractions and potential turnover is given in chapter 4.2.1 and chapter 5.2 and only briefly described in the presented chapter where necessary. In this chapter, a description of the clay mineralogy of the bulk soil and the composition of the reactive solid soil phase of the bulk soil and the dominating SOC fractions is added to the former analysis. This information is complemented with measurements of the soil weathering stage defined by the total reserve in bases at different slope positions and depths. This analysis is based on 9 observations from different soil depths and slope positions.

7.2.1 Study site and sampling

The analysis was performed on soil samples that were collected in the study of Doetterl et al. (2012b) from a geomorphic transect on cropland. Soil samples were taken from a stable, non-eroding profile at the hilltop plateau, an eroding profile from the hillslope shoulder (200cm soil loss) and a depositional profile in the colluvial valley bottom (350cm soil gain). In order to quantify the vertical and horizontal distribution of SOC fractions, the soil cores were cut into slices in the following depth intervals: the topsoil (0-15 cm), the shallow subsoil (35-50 cm), and the deeper subsoil (55-70 cm). The study site is situated on cropland in the central Belgium Loessbelt (50°45’41.50’’N; 4°44’07.36”E) with a south/southeast facing slope. Soils are well drained and show no evidence of long lasting hydromorphic conditions. No detailed information about the long-term (i.e. several centuries) crop rotation or SOC input is available. However, this study focuses on the relative differences between geomorphic positions which were managed in the same way.

7.2.2 SOC fractionation

To derive functional SOC fractions, Doetterl et al. (2012b) used a method based on the conceptual SOC fraction model proposed by Six et al. (1998,

2002). The scheme (Figure 26, Chapter 6) consists of a series of chemical and physical fractionation techniques applied to isolate functional SOC fractions, differentiated by stabilization mechanisms (chemical, biochemical and physical) which can also be associated with different turnover times and SOC stability (see also von Luetzow et al. 2006).

7.2.3 Soil physico-chemical characterization

General. Soil profile descriptions (Doetterl et al. (2012b) were done using the WRB classification (IUSS Working Group WRB 2006). Soil pH values were determined as the mean of two measurements per sample after a response time of 30 min and 24 hours respectively in a 1:2.5 soil/solution ratio in 25 ml 0.01 M $CaCl_2$ potentiometrically with a glass electrode using a portable Multiparameter Meter HI9828 (Hanna Instruments US Inc., USA).

Soil weathering stage. The weathering stage of the soil material in the different depth layers of the investigated soils is estimated by measuring the Total Reserve in Bases (TRB, the sum of total content in Ca, Na, K, Mg, in $cmol_c.kg^{-1}$) following Herbillon et al. (1986). Total elemental content was determined by Inductively Coupled Plasma-Atomic Emission Spectrometry (ICP-AES) on the nine bulk soils and the parent loess material after borate fusion (Chao and Sanzolone 1992). The TRB can be used to compare soil horizons relative to the parent material to evaluate the weathering degree of soil material and to estimate the amount of weatherable minerals in the soil.

Sequential extraction of the reactive soil phase. A three-step sequential extraction scheme (Stucki et al. 1988) was carried out with sodium-pyrophosphate at pH 10 (Bascomb 1968), ammonium oxalate-oxalic acid at pH 3 (Dahlgren 1994) and dithionite-citrate-bicarbonate (DCB) at pH 8 (Mehra and Jackson 1960) to assess the contribution of Mn, Fe and Al-bearing phases in stabilizing organic carbon in the different SOC fractions through adsorption onto oxy-hydroxides and complexation/coprecipitation. The specific extraction was performed on the bulk soil of each sampling position, the (micro)aggregated (s+cm) and non-aggregated (s+c) silt and clay associated SOC fraction, and on the (micro)aggregated (sm) and non-aggregated (s) silt associated SOC fractions separately (Figure 26, Chapter 6). Due to insufficient sampling mass, the clay associated SOC fractions could not be analyzed separately. Each extract was analyzed for its Al, Fe, Mn content by ICP-AES.

Pyrophosphate ($_p$) extractable components are interpreted as predominantly organically complexed metals. Oxalate ($_o$) extractable components reflect the amorphous secondary Fe and Mn fractions oxides, and poorly crystalline aluminosilicates (imogolite-type materials, ITM). Oxalate extractable soil phases are generally assumed the most reactive group in many types of soils and presumably strong candidates for stabilizing SOC with minerals by adsorption on mineral surfaces (Huang et al. 1977; Kaiser and Guggenberger, 2003; Kleber et al. 2005; Eusterhues et al. 2005). Dithionite ($_d$) extractable components included partly poorly crystalline and predominantly crystalline oxy-hydroxides of Mn, Fe and Al. The presence of organic ligands in the soil solution has been shown to prevent the formation of crystalline Al and Fe oxy-hydroxides e.g. due to strong complexation gradients of fulvic acids with metals which prevent their complete hydroxylation (Kodama and Schnitzer 1980). Several authors could show that pyrophosphate extractable Al may not be attributable only to Al bound to organo-metallic complexes since the alkaline extractant could also extract Al from Al hydroxide phases and from poorly crystalline aluminosilicates (i.e. Schuppli et al. 1983; Kaiser and Zech 1996). The results of the sequential extraction must therefore be treated with caution due to uncertainty about the origin of the extracted Fe and Al. However, a significant amount of organic matter adsorbed onto minerals and complexed with metals is to be extractable by NH_4-oxalate and DCB solutions. Here, the analysis is limited to interpreting the abundance and spatial patterns of the various extractable components in the bulk soil and the SOC fractions and discuss the pedological implications of the observed carbon/mineral correlations.

Clay mineralogy. The mineralogy of the clay fraction was determined by X-ray diffraction (XRD, Cu Kα, D8, Brucker Advance) after K^+ and Mg^{2+} saturation, ethylene glycol solvation and thermal treatments at 300 and 550 °C (Robert and Tessier 1974). Clay minerals were then classified and identified according to Brindley and Brown (1980). The relative abundance of each clay mineral within a sample is described by comparison of the peak intensities of dominant clay minerals in each sample. In a second step, these results were then compared to equivalent samples along the geomorphic gradient, i.e. soil layers from the same depth across different positions or soil layers from different depths but the same profile, to find relevant trends.

7.2.4 Implementation and statistical analyses

All statistical analysis were conducted in SAS 9.3 (SAS Institute Inc., Cary, NC) and R 2.11.1 (R Development Core Team 2010). Differences between the means of classes have been performed using multi-group ANOVA Bonferroni corrections and Tamhane's T2. In addition, linear regressions were performed to test correlations between the abundance of the reactive soil phases and SOC in the bulk soil and for the isolated SOC fractions. All statistical tests were evaluated using $p<0.1$ as the level of significance.

7.3 Results

7.3.1 SOC fractions and SOC distribution

At the study site, 1.6 times more SOC is stored in the subsoil (30-100cm) of the depositional profile than in the stable or eroding profiles and the potential SOC turnover is 1.7 times slower at depositional than non-eroding, stable profile and this indicates a substantially higher stability of buried SOC (Doetterl et al. 2012b). This distribution pattern is related to the erosion and burial of former topsoil, and a high amount of SOC that is stabilized in aggregates at depositional profiles (Table 16). A clear change in the ratios of silt vs. clay associated SOC has been observed when comparing the eroding to the depositional profile of the transect: for both the aggregated and non-aggregated soil fraction, more SOC was associated with clay-sized particles in the subsoil of the eroding profile (clay/silt SOC ratio microaggregates: 2.1 / 1; non-aggregated: 1.3 / 1) than in the subsoil of depositional profile (clay/silt SOC ratio microaggregates: 1.2 / 1; non-aggregated: 0.8 / 1). Hence, the lower turnover rates in the depositional valley bottom derived from potential respiration experiments and the accumulation of SOC associated with silt-sized particles indicate that the C in this fraction is a very stable fraction. This stability is related to the protection of deposited and buried SOC from decomposition due to the presence of highly stable aggregates which provide physical protection (see chapter 6). Conversely, at the eroding hillslope, the abundance of clay associated SOC at SOC depleted subsoils of eroding sites suggests a high potential of clay to sorb quickly new C inputs, and the potential SOC turnover is 1.4 times faster than at non-eroding stable profile. The physical protection of SOC through aggregation is low at eroding sites because soil erosion continuously removes the most weathered and aggregated soil at the surface and less aggregated soil from

the subsoil gets mixed into the topsoil system. Hence, chemical protection mechanisms such as complexation/co-precipitation and adsorption of SOC with clay-sized minerals gain greater importance.

Table 16: Key soil properties and identified SOC fractions as described by Doetterl et al. (2012b) for the investigated soils at different slope positions and soil depths.

Parameter	**Units**	**Stable Plateau**			**Eroding hillslope**			**Depositional valley**		
Slope	[%]	3			10			4		
Total Erosion(-) & Deposition (+)	[cm]	±0			-200			350		
Depth	[cm]	0-15	35-50	55-70	0-15	35-50	55-70	0-15	35-50	55-70
Bulk BD	[g/cm^3]	1,58	1,56	1,59	1,52	1,63	1,51	1,55	1,64	1,58
pH [$CaCl_2$]		7.0	7.1	7.0	7.2	7.3	7.1	6.8	6.8	6.9
Bulk soil SOC	% SOC	1.0	0.3	0.2	0.9	0.2	0.2	1.2	0.7	0.4
Macroaggregate SOC	% SOC	1.4	0.3	0.4	1.2	0.3	0.5	1.4	0.8	0.6
Microaggregate SOC	% SOC	0.7	0.3	0.2	0.7	0.3	0.2	0.9	0.6	0.3
Free silt+ clay SOC	% SOC	0.8	0.2	0.2	0.7	0.2	0.2	0.9	0.7	0.3
Macroaggregate SOC	Relative % of total SOC	47	19	24	46	19	27	58	37	35
Microaggregate SOC	Relative % of total SOC	35	48	48	24	34	24	21	37	21
Free silt+ clay SOC	Relative % of total SOC	17	33	29	30	47	49	21	26	44
C stock	g/m^2/cm	152	40	38	136	35	32	180	110	62
Macroaggregate SOC	g/m^2/cm	72	8	9	63	7	9	105	40	22
Microaggregate SOC	g/m^2/cm	54	19	18	33	12	8	37	40	13
Free silt+ clay SOC	g/m^2/cm	26	13	11	41	16	16	39	29	27

7.3.2 Total reserve in bases and soil weathering status

The TRB for the loess parent material was 139 $cmol_c\ kg^{-1}$. For the different soil layers, TRB ranged between 101 and 118 $cmol_c\ kg^{-1}$, which represents a TRB loss of 15 to 27%. This is mostly related to decalcification (Table 17). These values are in the same range as reported for other Luvisol profiles in the region (Brahy et al. 2001). At the stable plateau and the eroding hillslope a significant trend ($p<0.1$) with lower TRB losses at greater depth can be observed, but with weaker increases of TRB with soil depth than reported

from similar soils (Brahy et al. 2001). In contrast, no effect of depth was observed in the depositional profile.

Table 17: Total content in Ca, K, Mg, Na and Total Reserve in Bases (TRB) values for the different soil profiles and depths and the loess parent material.

Parameter	Unit	**Stable Plateau**			**Eroding hillslope**			**Depositional valley**			**Loess**
Depth	cm	0-15	35-50	55-70	0-15	35-50	55-70	0-15	35-50	55-70	>100cm
Ca	cmolc kg^{-1}	14	13	13	15	12	14	15	13	13	70
K		46	46	48	47	50	46	42	41	43	32
Mg		15	20	19	17	19	19	14	14	16	18
Na		31	34	32	32	33	38	32	32	32	18
Total TRB sum		**107**	**113**	**112**	**111**	**115**	**118**	**103**	**101**	**103**	**139**
Relative diff. to parent material	*%*	*77*	*81*	*81*	*80*	*83*	*85*	*75*	*73*	*74*	*100*

7.3.3 Reactive soil phases

A*ggregated vs. non-aggregated soil***.** Pyrophosphate extractable components are largely abundant in microaggregates, especially as Fe(p) (1118±293 mg/kg soil) and Al(p) (1647±385 mg/kg soil) (Figure 36). The ratio of non-aggregated to aggregated pyrophosphate extracts in silt and clay is generally between 1:3 – 1:7 and shows a clear association of these components with soil microaggregates. This indicates that these components are potentially important compartments for the formation of microaggregates. These differences disappear when looking at the total (sum of Al, Fe and Mn in aggregated vs. non aggregated soil fraction) oxalate and DCB extractable components in both aggregated and non-aggregated soil fractions. Oxalate and DCB extractable phases do not show such a pattern between aggregated and non-aggregated soil samples. Approximately the same amount of oxalate extractable Al, Fe and Mn is present in aggregated (1648±400 mg/kg soil) and non-aggregated (2369±747 mg/kg soil) soil samples with c. five times more DCB extractable elements than oxalate in both soil compartments.

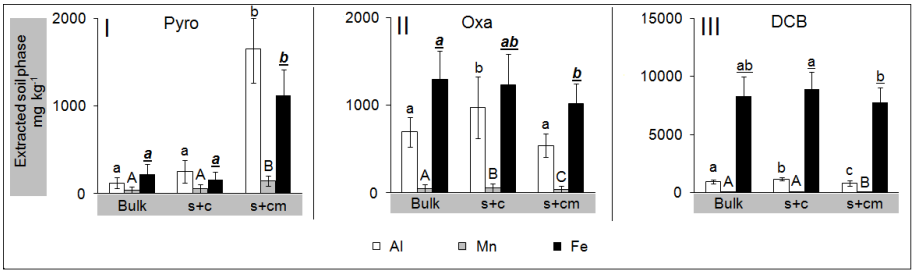

Figure 36: The distribution of pyrophosphate (I), oxalate (II) and dithionite (III) extractable Al, Mn and Fe between the Bulk soil and its compartments non-aggregated silt+clay (s+c) and aggregated silt+clay (s+cm). Same letter indicates no significant differences between the extracted element in the different SOC fractions ($p < 0.1$, tested for Figure I, II and III and the different elements separately as indicated by differences in font types).

Despite the small contribution of Mn(p) (40±36 mg/kg soil) to the total pyrophosphate extractable phase of the bulk soil compared to Al(p) (122±64 mg/kg soil) and Fe(p) (222±115 mg/kg soil), it is the only phase with a significant correlation (R^2=0,96, $p<0.1$, n=18) to SOC in the bulk soil across the whole slope transect (Figure 37).

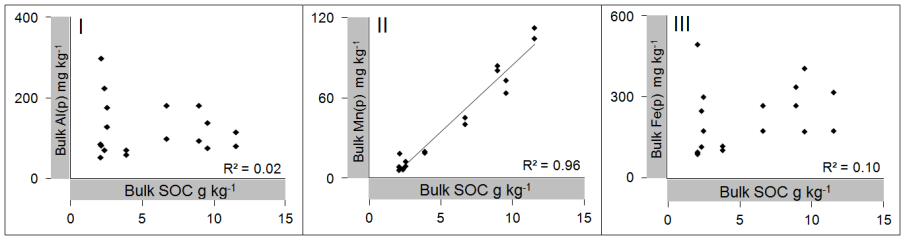

Figure 37: Correlation between SOC in the bulk soil and pyrophosphate extractable Al (I), Mn (II) and Fe (III).

Table 18 shows that the positive correlation of Mn(p) with SOC along the slope for the bulk soil is driven by the non-aggregated s+c fractions. In contrast to Mn(p), a correlation of Fe(p) and Al(p) with SOC could only be identified at the depositional site. Depth patterns of Al(p) and Fe(p) are not consistent for eroding and stable profiles, but a significant decrease with depth can be recognized at the depositional site. Mn(p), on the other hand, always decreases significantly ($p<0.1$) with depth. Despite their large selective abundance in microaggregates, only poor or negative correlations were found for all pyrophosphate extractable phases with SOC in microaggregate s+cm (Table 18).

Table 18: Correlations (Pearson r) between pyrophosphate extractable solid soil phases and soil SOC or soil depth (* = p <0.1; ** = p <0.05; *** p = <0.01) and the concentration range of the respective pyrophosphate extract.

SOC fraction	Element	Position	Soil phase and depth	Soil phase and SOC	Range mg kg^{-1}
Bulk soil	$Al_{(p)}$	Eroding	0.17	0.04	53-298
		Non-eroding	0.34	-0.37	70-223
		Depositional	-0.23	0.23	58-180
	$Fe_{(p)}$	Eroding	-0.12	0.34	91-498
		Non-eroding	-0.45	0.40	118-410
		Depositional	-0.67*	0.67*	106-320
	$Mn_{(p)}$	Eroding	-0.90***	0.99***	6-84
		Non-eroding	-0.95***	0.99***	6-73
		Depositional	-0.99***	0.99***	19-112
Non aggregated s+c	$Al_{(p)}$	Eroding	0.44	-0.27	87 - 568
		Non-eroding	0.61*	-0.47	106 - 403
		Depositional	-0.76**	0.76**	107 - 425
	$Fe_{(p)}$	Eroding	0.18	-0.06	46 - 362
		Non-eroding	0.05	0.20	67 - 252
		Depositional	-0.48	0.61*	73 - 271
	$Mn_{(p)}$	Eroding	-0.74**	0.72*	4 - 153
		Non-eroding	-0.88**	0.95***	10 - 107
		Depositional	-0.50	0.50	13 - 168
Aggregated s+cm	$Al_{(p)}$	Eroding	0.68*	0.57	1117 - 1954
		Non-eroding	0.80**	-0.96***	1290 - 1914
		Depositional	0.20	-0.27	1137 - 2685
	$Fe_{(p)}$	Eroding	0.39	0.71	681 - 1599
		Non-eroding	0.58	-0.76**	934 - 1189
		Depositional	0.37	-0.25	849 - 2021
	$Mn_{(p)}$	Eroding	-0.31	0.38	89 - 216
		Non-eroding	-0.69*	0.81**	62 - 170
		Depositional	0.43	0.01	58 - 221

Stabilizing SOC in silt fractions. While pyrophosphate extracts approximately 80% of total SOC in the bulk soil, the isolated silt fractions in the non-aggregated and aggregated soil show a different tendency. Only a small amount (25-30%) of SOC associated with the aggregated and non-

aggregated silt fraction could be extracted with pyrophosphate. This suggests a stronger importance of other components to stabilize SOC in these fractions. Unlike the source material (data not shown), positive correlations between the oxalate extractable phases could be found for the silt fractions between SOC and Fe(o) and Al(o) in the depositional soil and for Fe(o) also at the eroding profile (Table 19). No such correlation was found for Mn(o).

Table 19: Correlations (Pearson r) between oxalate extractable solid soil phases in the silt fractions and soil SOC or soil depth (* = p <0.1; ** = p <0.05; *** = p < 0.01) and the concentration range of the respective oxalate extract.

SOC fraction	Element	Position	Soil phase and depth	Soil phase and SOC	Range mg kg^{-1}
Non aggregated s	$Al_{(o)}$	Eroding	0.02	0.22	221-379
		Non-eroding	0.43	-0.20	340-477
		Depositional	-0.93***	0.93***	223-422
	$Fe_{(o)}$	Eroding	-0.89**	0.97***	303-733
		Non-eroding	-0.50	0.76*	338-1053
		Depositional	-0.85**	0.95*	352-647
	$Mn_{(o)}$	Eroding	0.91**	-0.86**	86-121
		Non-eroding	0.16	0.19	57-172
		Depositional	-0.23	-0.23	84-129
Aggregated sm	$Al_{(o)}$	Eroding	0.51	-0.78*	157-236
		Non-eroding	0.26	-0.52	117-215
		Depositional	-0.92**	0.92**	126-263
	$Fe_{(o)}$	Eroding	-0.76*	0.49	360-474
		Non-eroding	0.53	-0.68*	391-609
		Depositional	-0.91**	0.91**	274-599
	$Mn_{(o)}$	Eroding	0.68*	-0.90**	50-155
		Non-eroding	0.78*	-0.93***	37-106
		Depositional	0.20	-0.20	42-48

7.3.4 Clay mineralogy

The clay fraction of all investigated soils show the presence of illite, kaolinite and chlorite, partly inherited from the parent material as to be expected in luvisols of this region (Van Ranst et al. 1982). Several key changes in the abundance of different clay minerals have been identified

along the slope and for different soil depths (Figure 38). A relative enrichment of expandable 2:1 clay minerals associated with smectite at the eroding profile can be observed. In contrast, in the depositional profile, the smectite peak disappears and a relative enrichment of non expandable 2:1 clays associated with Illite is observable. This pattern is generally consistent for all depth layers, but most striking in the topsoil while the peak intensities are more similar between slope positions in the subsoil (data not shown).

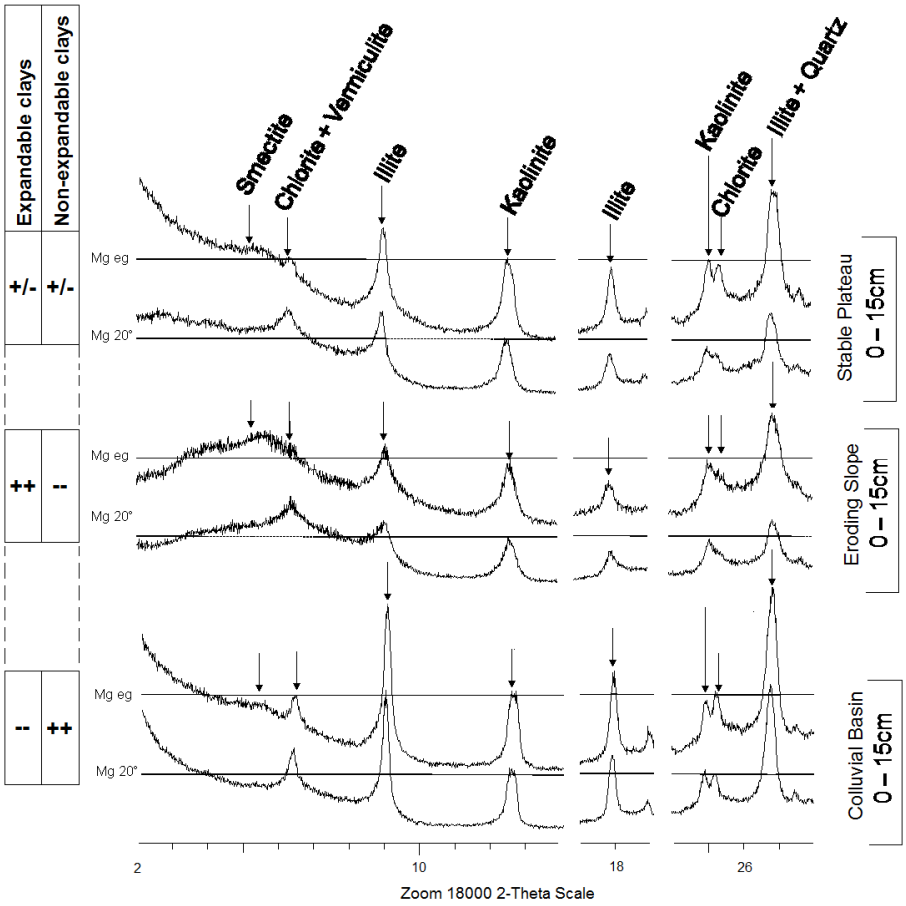

Figure 38: Clay spectra after preparation with Mg and Mg-ethylene glycol for the topsoil at the different slope positions. Horizontal black lines have been fitted through the kaolinite peak of the stable profile to ease the visualization of differences between the profiles. ++ indicate higher abundance, -- lower abundance of certain clay minerals in respect to the abundance at the plateau profile (+/-).

7.4 Discussion

7.4.1 Soil erosion as a soil rejuvenator

The strongest losses in TRB (Table 17), and hence the most advanced weathering stage, are observed for the deposited soils at the foothill (25 – 27 %), while the layers at the eroding hillslope have been facing the lowest losses, and hence the weakest weathering (15 -20 %). The results demonstrate the ongoing rejuvenation of the soil at the eroding hillslope by removing soil material and exposing less weathered material to the surface. The continuous removal of soil at the hillslope is acting at a faster rate than the natural soil weathering and this keeps the eroding profile TRB losses lower, and hence less weathered, than at the stable plateau site. This is consistent with the absence of a depth related trend in the TRB losses at the depositional site (Table 17) as this material is buried former topsoil, similar in TRB. Nevertheless, these differences are small compared to other soil types in the same region (Brahy et al. 2001) and indicate a rather small effect of soil redistribution on TRB.

7.4.2 Interactions of the reactive soil phase with SOC

Pyrophosphate extractable elements. The reactive soil phase, which has importance for SOC stabilization, seems to be largely extracted with pyrophosphate (Figure 37, Table 18): no strong correlation between oxalate extractable phases in the bulk soil, s+c or s+cm with SOC could be identified. DCB extractable elements are generally not significant or negatively correlated to SOC (data not shown) and this points to a minor importance of this extract, namely well crystallized oxides, for SOC stabilization at this site. This confirms earlier findings (Kodama and Schnitzer 1980; Kaiser and Zech 1996) that show that the presence of organic ligands prohibits the full crystallization of pedogenic oxides.

This result is interpreted in terms of the (i) specific soil conditions in the different profiles in which interactions between the reactive soil phase and SOC took place and (ii) to the varying mobility and thus potential of the extracted phases to stabilize SOC in those soils. First, the decreasing content of pyrophosphate extractable elements with soil depth is related to the fact that organo-mineral associations will make up a significant share of the pyrophosphate extract of the reactive soil phase where SOC is present in large quantities. Consequently, concentrations of the extracted elements, which are correlated to the abundance of SOC, will generally be higher in

SOC-rich topsoils than in SOC-depleted subsoils, as has been shown for non-aggregated Mn(p) along the slope and for non-aggregated Fe(p) and Al(p) at depositional sites.

Second, the pH-values in the soils analyzed here are near neutral pH (Table 16) and in the pH buffer zone, where Mn is highly mobile in the soil while the mobility of Fe and Al is strongly limited (Lindsay 1979). Therefore, at this study site, manganese (as ions or oxides) could influence significantly the dynamics of SOC in the investigated soil profiles by promoting the formation of organo-mineral complexes and by the redistribution of these complexes along the toposequence.

Third, the fact that pyrophosphate extractable elements are largely abundant in aggregates raises questions about the importance of the isolated elements for stabilizing SOC. One explanation could be that pyrophosphate extractable Fe and Al are important for aggregate stability as ligands between clay minerals, even without involving SOC, but not for SOC retention itself. Fe(p) and Al(p) could act as proxies for the formation of aggregates through the formation of organo-metallic complexes, but also through the formation of Fe, Al oxy-hydroxides (Kaiser and Zech 1996). This oxy-hydroxide formation then masks strong Fe(p) or Al(p) to SOC correlations. Pyrophosphate in that case might simply act as a strong reagent to disaggregate soil (Muneer and Oades 1989) and therefore the abundance of pyrophosphate extractable elements in aggregates does not point at an identifiable group of organo-mineral associations (Kaiser and Zech 1996).

Mobility and environment. Mn(p) does not show a similar accumulation in aggregates as Fe(p) and Al(p) (Table 18; Figure 36). In the bulk soil and non-aggregated soil, clear positive correlations between Mn(p) abundance and SOC can be found, which points at the predominant presence of organo-Mn complexes and to only a minor role of Mn oxy-hydroxides in the study site extracted with pyrophosphate. Finally, the high moisture content in colluvial profiles is well known to provoke redoximorphic processes, potentially affecting the spatial distribution of Mn, Fe and Al (Sposito 2008) by moving metals from reductive, and thus water saturated, to oxidative compartments of the soil to form oxy-(hydro)oxides that can be associated with water-soluble SOC (Eusterhues et al. 2011). It is possible that the annual hydrologic variability at depositional sites creates an environment for SOC to be adsorbed, coprecipitated or complexed with the reactive soil phase to a stronger degree than at eroding or stable sites. Even though the

measured pH values at the depositional profile are above the values necessary to mobilize Fe and Al (Schwertmann et al. 1987; Süsser and Schwertmann 1991), they are significantly lower ($p<0.1$) than at the stable or eroding profile (Table 16). Considering that the measured pH-values are always mean values of a homogenized soil section, the analysis ignores the natural variability of pH values between different compartments of the soil matrix. Hence, the changing hydromorphic conditions at the depositional site might create an micro-environment in parts of the soil where pH values are much lower, at least for part of the year, and in which SOC complexation not only takes place with Mn(p) but also with the less mobile Fe(p) and Al(p), so that the relative contribution of organo-metallic complexes in the Fe(p) and Al(p) extract begins to overpower the oxy-hydroxide signal at the depositional profile resulting in clear correlations between SOC and Fe(p) and Al(p).

Oxalate extractable elements. Some authors propose Ferrihydrite (Fh) as a prominent oxalate extractable soil compartment that stabilizes SOC over longer time scales by various types of SOC mineral associations, especially by adsorption (Tipping 1981; Eusterhues et al. 2005). The data presented here is supportive of this assumption. The results in Table 19 indicate a potential impact of amorphous Al and Fe oxides to stabilize SOC where physical protection of SOC by aggregation decreases: at eroding sites, the aggregation potential is small (Doetterl et al. 2012b) due to the continuous removal of aggregate-rich topsoil layers. At depositional sites, on the other hand, the burial of topsoil by soil that has been eroded uphill continuously moves the aggregate-rich topsoil out of the biological active zone of the soil into deeper soil horizons, where aggregates degrade slowly (Doetterl et al. 2012b) and SOC is released at a much slower rate to the atmosphere than under topsoil conditions (Van Oost et al. 2012). Interestingly, no such correlation was found for Mn(o) which confirms the earlier finding that Mn is mostly bound in organo-metallic complexes, extracted with pyrophosphate. However, the amount of all oxalate extractable Al and Fe phases is decreasing at the depositional profile with soil depth, indicating that, with burial and further aging/alteration of the soil material, the mechanism to stabilize SOC with poorly crystalline minerals is temporally limited.

7.4.3 Importance of the abundance of clay types

From the presented data, it is not possible to quantify the abundance of illite at the depositional profile and of smectite at the eroding profile (Figure 38). The mechanisms to explain the enrichment of some clay minerals as a function of the slope are still uncertain. Neo-formation of smectite from primary minerals at eroding sites could explain the relative enrichment but that is unlikely to be dominant processes under the given soil mineralogical and climatic conditions (Borchardt, 1989). Also the preferential mobilization of illite and its deposition at the foothill or neo-formation of illite at the depositional profile is a potential explanation for the differences between the clay spectra along the geomorphic gradient. Both mechanisms together could explain the low amount of aggregates at eroding sites but also the enrichment of aggregates at the depositional sites: at eroding sites, soil gets mobilized and eroded, mostly as aggregates (Wang et al. 2010). Smectite-dominated aggregates have been identified to be less stable due to shrinking and swelling of the smectite than kaolinite or illite-rich aggregates (Fan et al. 2008) or aggregates rich in amorphous and crystalline Al and Fe oxide (Goldberg 1989). The lower stability of smectite-dominated aggregates then leads to a preferential degradation of these aggregates during the transport to and burial at depositional sites. This gives a plausible explanation for the relative enrichment of non-expandable clays at the depositional site and is consistent with the observation of the preferential export of small particle sizes out of the catchment which are often dominated by smectite colloids (Gibbs 1967). Even though a direct quantification of its impact on stabilizing SOC is not possible with the analysis presented here, it is likely that the relative enrichment of expandable clay minerals at the eroding profile is part of the reason for the pre-dominant stabilization of SOC with the clay fraction in subsoils there as described by Doetterl et al. (2012b) and the disequilibrium of clay and silt associated SOC and aggregated vs. non-aggregated SOC along the slope's subsoil as described in section 6.3.1. Unlike non-expandable 2:1 and 1:1 layered minerals, smectite can provide a large specific surface area for interaction with SOC (Brady and Weil 2008 and references therein), which gives the clay fraction at the eroding profile a high potential to associate with SOC. The opposite effect can be observed at the depositional profile where silt associated SOC gains in importance compared to clay associated SOC. There, reactive surface area of clays is limited, as the widely abundant non-expandable clays (illite, kaolinite) can

only use limited surface area for interaction with C, which lowers the potential of the clay fraction to stabilize SOC.

7.4.4 Soil redistribution – A sink or source?

Agricultural activity has led to a maximum soil loss of 200cm at the hillslope and a maximum gain by deposition of 350cm (Table 16) at the depositional valley bottom over a period of at least 3000 years (Rommens et al. 2005). Rommens et al. (2005) proposed 2.30m as the average soil development depth of an undisturbed loess derived Holocene Luvisol in the region. This suggests that the originally developed loess profile has been almost completely removed from the eroding slope, and that the current soil profile is a result of soil weathering taking place over a much shorter period of only 3000 years, which explains the mineralogical similarity between the soil substrate at eroding sites and the loess parent material (Table 17). A meta-analysis of Alexandrovskiy (2007) suggests a mean soil development time of 0.1mm/yr in Luvisols, reaching a dynamic equilibrium between natural soil erosion and soil development after 2000-3000 years, but with a strong exponential decrease in weathering velocity after the initial centuries. This decrease is most likely the result of less physical and chemical weathering force on soil material at greater depths (Anderson et al. 2007) than at the surface and of the alteration of the soil material from easily weatherable to more stable soil material throughout the initial phase of soil weathering. This is supported by Egli et al. (2003) and Duemig et al. (2011), suggesting a similar weathering rate for soils in the Swiss Alps on granitic parent material and strongly decreasing weathering velocity with soil age.

Hence, based on TRB values, the mineralogical composition of the reactive soil phase and the clay fraction as well as the estimated erosion rates, the data clearly show that the current soil loss exceeds the current soil production rates, keeping eroding profiles from reaching an equilibrium state. However, this excess soil loss seems to be small enough to allow soil weathering to take place to such an extent to supply the soil with reactive soil minerals to form organo-mineral associations. This seems to favor SOC sequestration and supports the concept of the dynamic replacement of eroded SOC (Harden et al. 1999) as a local net atmospheric sink of C. Doetterl et al. (2012b) found no significant differences in the SOC depth distribution and SOC stocks between the stable and the eroding profile, suggesting that processes of C sequestration take place at the same rate as the removal of

SOC enriched topsoil. However, this sink function is temporally limited: About four meters of loess have been deposited and are available for soil formation at the study sites (Rommens et al. 2005; Doetterl et al. 2012b). From this layer, about two meters have been eroded from the investigated slope profiles. The loess covers less fertile Tertiary sand deposits (Wouter and Vandenberghe 1994) which have a substantially lower potential for C sequestration through the formation of organo-mineral associations (Torn et al. 1997; Feng et al. 2011) and lead to lower crop yields and hence C input to soils. Finally, the sink strength is also tied to the fate of the eroded and buried or exported SOC and also related to the fate of the additionally dissolved inorganic C from the eroding sites. Inorganic C in the unweathered loess parent material has been measured at 4-5% C. This corresponds to approx. 60 kg inorganic C per m^3 and largely exceeds the organic C stored in a similar soil volume at the study site (Table 18). Through soil removal the loess substrate at eroding sites is brought closer to surface and into a zone of faster soil weathering where it gets decalcified. The inorganic C of the substrate gets dissolved and re-precipitated elsewhere. Even so the dissolution of carbonates and its re-precipitation elsewhere is a CO_2 neutral process (Gislason 2005), a sink or source function of agricultural erosion will be decided by the stability of mobilized (organic and inorganic) C in its respective new environment.

7.5 Conclusion

The findings presented here constitute a major control on the distribution of measured SOC fractions and crucial to understand controls of SOC dynamics. Pyrophosphate extractable soil compartments, especially Mn(p) were identified as responsible for stabilizing SOC in the bulk soil and with non-aggregated silt and clay fractions. Pyrophosphate extractable Fe(p) and Al(p) components are largely abundant in aggregates, but show no strong correlation to SOC, indicating importance for aggregate stability but not for SOC retention. Oxalate extractable amorphous and poorly crystallized minerals were identified as a temporary but important compartment to stabilize SOC at the depositional profile, especially for the more recalcitrant silt associated SOC fractions; however, are of minor importance for SOC stabilization at other slope positions. Non-expandable clay minerals are relatively enriched at the depositional site and expandable clay minerals in

return at the eroding site. These changes in clay mineralogy along the slope are partly responsible for the abundance of silt or clay associated SOC. Current rates of soil erosion and the associated rejuvenation of soils at eroding sites and burial of soil at depositional sites provide a temporally limited local net sink for atmospheric C. The function of agricultural soil erosion as a global net sink or source for atmospheric C will be decided by the fate of mobilized (organic and inorganic) C.

8 Synthesis and general conclusion

8.1 Main findings

The aim of this thesis was to improve our understanding of the effects of soil redistribution on SOC dynamics. For this, a multi-scale analysis has been conducted covering different aspects of the SOC/Soil redistribution continuum. The work particularly focused on the identification of (soil) environmental controls on SOC dynamics and SOC distribution patterns along geomorphic gradients in landscapes affected by soil redistribution. This thesis postulated that (a) the influence of erosion and deposition along hillslopes is one of the major driver not only behind patterns of SOC quantity, but also for SOC quality on cropland and (b) that the analysis of local and regional topography is a suitable tool for studying SOC dynamics across scales if hydrological, climatic and pedological site parameters are known. The presented work particularly focused on (i) the identification of controls on C dynamics and C distribution patterns along geomorphic gradients in landscapes affected by soil redistribution, (ii) the different C stabilization mechanisms and (iii) the role of the mineral phase in stabilizing C.

The thesis began with an assessment of the importance of agricultural soil erosion for SOC dynamics on a global scale, including the identification of the most important factors controlling the magnitude of soil and SOC erosion. The main objective of this study was to test the assumptions underlying existing assessments and to reduce the uncertainty associated with global estimates of agricultural soil and SOC erosion. A global soil erosion rate of 10.5 Mg ha^{-1} yr^{-1} for cropland and 1.7 Mg ha^{-1} yr^{-1} for pastures was obtained. This corresponds to SOC erosion rates of 193 kg C ha^{-1} yr^{-1} for cropland and 40.4 kg C ha^{-1} yr^{-1} for eroding pastures, and results in a global flux of 20.5 (±10.3) Pg yr^{-1} of soil and 403.5 (±201.8) Tg C yr^{-1}. Although these estimates are lower than former assessments, the magnitude of soil fluxes illustrates the significance of soil redistribution for studies on SOC dynamics. The erosion-induced changes in topsoil SOC content, an average SOC loss of 22% in 50 years, show that agricultural soils should be considered to be dynamic systems that can change rapidly.

At the regional scale, the work focused on identifying environmental variables which act as controls on SOC stocks and examining how these variables can be used in a model to predict current SOC stocks (*Test of hypothesis H1*). Soil profile data was collected in two zones of differing soil texture (loam and clay-rich soils) in Luxembourg, in order to calibrate a linear mixed-effect model to predict the 3D SOC stock distribution on a regional scale for cropping systems, using a set of spatially-explicit hydrologic, climatic, pedologic and geomorphologic variables. A high spatial variability of SOC stocks could be demonstrated. Therefore, it is mandatory to consider various environmental processes to predict SOC accurately at a regional scale, especially in deeper soil layers, and to avoid simple depth extrapolation of topsoil SOC data as has been done earlier in flat landscapes. Using estimates of topsoil SOC contents covering a large area derived from hyperspectral remote sensing, spatial patterns of SOC stocks for cropland at a regional scale were predicted and were found to provide new insights into the spatial heterogeneity of soil C storage. The variability of SOC stocks in the two texture zones, expressed as values larger or smaller than the mean ± standard deviation, is lower in the loam zone (26.2%) than in the clay zone (38.7%). A mean SOC stock (to 100 cm soil depth) of 9.4±3.1 kg/m^2 for the clay-rich soils and 11.3±2.4 kg/m^2 for loamy soils were estimated. This represents the first regional estimate for SOC stocks to 1m soil depth for the research area using continuous spatial explicit datasets.

In the course of this regional scale analysis campaign, the limitations of current SOC sampling and analysis strategies, namely time, cost and labor intensity, became evident. To overcome this, a fully functional alternative to standard soil measurement methods was developed, combining percussion drilling with non-destructive Vis-NIR reflectance spectroscopic analyses of SOC distribution at a very high depth resolution on intact soil cores. The method was applied in the framework of a regional re-sampling campaign of historical cropland soil profiles along geomorphic gradients in the Belgian loambelt, with the aim of analyzing the spatial-dependent temporal changes of SOC depth distribution. Using a small but representative subset of the soil cores that were analyzed for SOC content with dry combustion, chemometric models were developed to interpolate observed SOC values to the entire dataset. It could be demonstrated that the approach allows to produce accurate (RMSE = ~1.2 g C kg^{-1}) and repeatable (SEL = 0.4 g C kg^{-1})

measurements of SOC content for the entire database. It provides very detailed SOC information at ~83% lower costs and reduces labor time by ~85% compared to a traditional approach at the same vertical resolution. The accuracy of spectroscopic predictions is comparable to standard soil analysis techniques and hence the approach can represent an operational alternative to reference methods of SOC analysis. However, the method is limited to soils with a low gravel content (<~5% gravel) and conditions where fine particles dominate the soil matrix.
The application of the method was exemplified on a regional sampling campaign of historical cropland soil profiles along a geomorphic gradient, with the aim of analyzing the spatial-dependent temporal changes in SOC depth distribution in relation to land management, geomorphology and pedology. These changes resulted in a net loss of ~20% SOC in the upper one meter of cropland soils in the study area between 1955/58 and 2011/12. This estimate is in the same range as former assessments using a non-topography related analysis approach on ΔSOC on cropland soils in the region. SOC losses can be largely related to changes in land management and dominating crop types. But also the local geomorphologic situation and soil redistribution regime play a role in controlling whether a soil profile accumulates or looses SOC. The presented data indicates a spatial diverse pattern of SOC losses related to topography. Soils with finer soil texture can hereby outbalance losses of SOC better than soils with coarser texture. However, an exact quantification of the influence of each of the outlined factors on ΔSOC was not possible with the given data for the here presented study due to methodological uncertainties related to the sampling position. Hence, an adapted sampling approach in future research is required.

The final part of the work presented here is a detailed investigation of the effects of soil redistribution on carbon quality at the hillslope scale, and an assessment of changing physico-chemical soil properties along the hillslope influencing SOC dynamics (*test of hypothesis H2 & H3*). The SOC stock and pool distribution along geomorphic gradients in the Belgian loambelt was quantified and combined with data derived from soil organic matter fractionation and incubation experiments. The size and composition of the SOC pools were strongly related to geomorphic position: 1.6 to 6.2 times more SOC was stabilized in the subsoils (25–100cm) of depositional profiles than in those of eroding profiles. Subsoil SOC of depositional profiles is

predominantly associated with microaggregates and silt-sized particles, which are themselves associated with pools of intermediate stability. A significantly higher mean residence time for the fast and intermediate turnover pools of buried SOC at depositional positions was observed, compared to non-eroding and eroding positions. This resulted from the physical protection of SOC associated with microaggregates and silt-sized particles. Conversely, significant amounts of SOC were replaced at eroding positions but the lower degree of decomposition and the lack of physically protected SOC, resulted in higher potential respiration rates. By considering SOC cycling at non-eroding, eroding and depositional positions, it was revealed that the eroding landscapes studied here store up to 10% more SOC due to soil redistribution processes than non-eroding landscapes. This is the result of the stabilization of SOC in advected former subsoil at eroding positions and partial preservation of buried SOC in pools of intermediate turnover at depositional positions. However, the long term sink strength is limited by significant losses of buried SOC, since only a small fraction of the SOC was associated with stable pools.

The chemical and mineralogical soil components involved in stabilizing carbon at various depths, slope positions and SOC fractions differ significantly. Pyrophosphate extractable soil compartments, especially Mn(p) are responsible for stabilizing SOC in the bulk soil and with non-aggregated silt and clay fractions. Pyrophosphate extractable Fe(p) and Al(p) components are largely abundant in aggregates, but show no strong correlation to SOC, indicating importance for aggregate stability but not for SOC retention. Oxalate extractable amorphous and poorly crystallized minerals are a temporary but important compartment for the stabilization of SOC at depositional sites, especially for the more recalcitrant silt associated SOC fractions, but are of minor importance for SOC stabilization at other slope positions. Non-expandable clay minerals experience a relative enrichment at the depositional site while expandable clay minerals are relatively enriched at the eroding site. These changes in clay mineralogy along the slope are partly responsible for the abundance of silt or clay associated SOC. Current rates of soil erosion and the associated rejuvenation of soils at eroding sites and burial of soil at depositional sites provide a temporally limited local net sink for atmospheric C by stabilizing SOC with minerals. However, the function of agricultural soil erosion as a global net

sink or source for atmospheric C will be decided by the fate of mobilized (organic and inorganic) C.

8.2 Soils and SOC in the geomorphic pump

More than a decade ago Stallard (1998) proposed the principle of a "geomorphic pump" in landscape scale studies of SOC. The concept states that SOC will be shifted by lateral transport from eroding to depositional settings, through erosional processes, and will be transferred from subsoil to topsoil at eroding positions and from topsoil to subsoil at depositional positions due to soil truncation and soil burial. This transport was postulated to have implications for the spatial pattern of SOC. Since then, various studies have shown that soil redistribution processes not only strongly affect the quantitative distribution patterns of SOC (i.e. DeGryze et al. 2008; Wang et al. 2010; Dlugoß 2011; Schwanghart and Jarmer 2011; Vandenbygaart et al. 2012; Nadeu et al. 2012) but also introduce qualitative changes (Gregorich et al. 1998; Berhe et al. 2008; 2012a; 2012b; Rumpel and Koegel-Knabner 2011) and provide support for this conceptual model. The findings of this thesis can now add further insight to this concept regarding (i) the environmental controls on SOC stocks and the (ii) spatial representation of these stocks in an agricultural landscape at a regional scale, (iii) the qualitative changes in SOC stocks with respect to SOC stability and chemico-physico characteristics of SOC fractions along geomorphic gradients and (iv) the pedogenic controls that are affected by transport processes and that are of importance to explain the observed qualitative and quantitative variability of SOC sequestration and SOC stabilization in soils along the same geomorphic transects.

A regional scale assessment in a landscape with strong geomorphic gradients and diverse soil redistribution patterns revealed the dominance of geomorphological processes over other environmental controls like pedology, hydrology or climate on SOC in sloping landscapes. The hillslope studies conducted for this thesis show that patterns of SOC distribution and quality are highly variable in sloping landscapes due to variability of (soil) environmental conditions and the history of soil redistribution processes, which transport SOC across the landscape to depositional environments and advect SOC depleted subsoil into the biologically active upper meter of the soil column at eroding sites. It is shown that processes acting on a landscape or regional scale will affect our understanding of SOC dynamics at the plot

scale and, vice-versa, knowledge on soil and SOC attributes at the plot scale are needed to come to solid estimates for SOC dynamics at the landscape level. Changes in SOC quality and soil parameters identified here are taking place over very long timescales and it is not possible to capture these changes in short-term manipulation experiments, as is the focus of many studies on SOC dynamics at the plot scale. Similarly, whether soils affected by soil redistribution act as a sink or source for atmospheric C largely depends on the considered timescale and long-term pedological and geomorphological site attributes. In the light of these findings, it is evident that the effects of landscape scale processes, acting on timescales of decades to centuries, must be considered in order to advance our understanding of SOC dynamics also at the plot scale. Hence, models of SOC turnover need to adopt a multi-scale perspective on SOC dynamics, and should integrate interactive effects of environmental controls on SOC to increase their predictive strength for future assessments on C dynamics.

The discussion about whether, or under which conditions, agricultural soils can act as a sink or source for atmospheric carbon is still ongoing and is a topic of vivid debate in the fields of soil management and tilling strategies (Baker et al. 2007) and erosion/deposition research (Smith et al. 2005; Van Oost et al. 2007, 2008; Lal and Pimentel 2008; Kuhn et al. 2009; Van Oost et al. 2012). This is partly due to the lack of data and model approaches available to verify findings from the hillslope at a larger scale. The work presented in this thesis can contribute to partly fill this gap by providing new methodological tools and understanding of the controls of SOC stocks at a regional scale.

At the study sites of this thesis in the Belgian Loambelt, under the given regime of soil rejuvenation at the eroding site and soil burial at the depositional site, the eroding site can provide a potential local net sink for atmospheric C for centuries due to constant supply of reactive minerals to form carbon-mineral associations. But this sink is substrate limited and so estimations on the long-term function of this sink must be treated with care and are highly localized as they largely depend on the spatial variability of fertile parent material for soil formation. The data shows that the eroded soil and SOC is transported and at least partly buried at depositional sites, or buries the in-situ SOC enriched topsoil there. This process of burial leads to a local net sink for carbon, since subsoil environments are generally less reactive than the equivalent topsoil and SOC can be stored there for

centuries. This sink, however is temporally limited, as shown in the delayed release of nearly all the buried C from colluvia within a timeframe of c. 500-700yrs after burial to the atmosphere by Wang (2011) and Van Oost et al. (2012).

The data presented in chapter 6 gives indication that the delayed loss of buried SOC on the scale of centuries (Van Oost et al. 2012; Wang 2011) is at least partly related to mineral alteration and the loss of SOC sorption potential, and not only to a slower reactivity of subsoil decomposer communities. Hence, depositional sites will slowly but steadily continue to release buried C into the atmosphere which might turn them from a sink to a source for atmospheric C. This release is spatially highly variable on a global scale, as the age of the mobilized soil sediment and, hence, deposited colluvia, as well as the amount of SOC stored in those colluvia is highly variable and can range from decades to millennia (Figure 39).

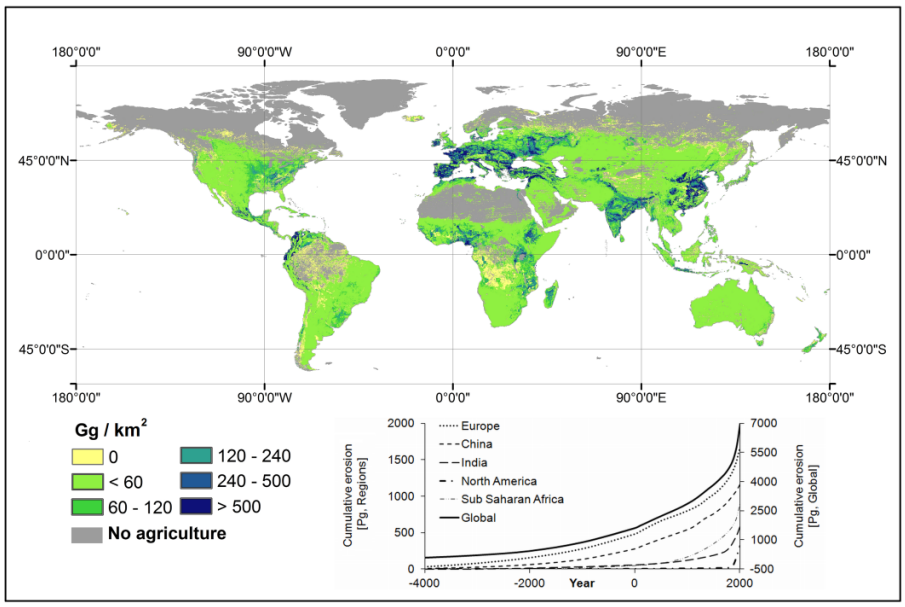

Figure 39: Cumulative agricultural erosion (water+tillage) and temporal patterns for selected world regions (as calculated for Van Oost et al. 2012).

Hence, the spatial variability of fertile soil substrate to provide a mineral-driven sink function at eroding sites due to (i) dynamic replacement of eroded C (Harden et al. 1999) and (ii) the spatial and temporally variability of deposition of soil and SOC in colluvia turns soil landscapes affected by soil redistribution into highly uncertain entities for long-term soil-

atmosphere C assessments. SOC dynamics in eroding landscapes are fundamentally different from those in stable landscapes, which are the basis for most SOC models. Nevertheless, improvements in model structure (Van Oost et al. 2005b; Billings et al. 2010; Dlugoß 2011) available data (FAO 2012) and assessment techniques (McBratney et al. 2006) might help to close this gap between our good understanding of soil carbon dynamics at the plot scale to coarse assessments on a global scale.

8.3 Final remarks – Scales, limitations and perspectives

This multi-scale research on SOC in dynamic landscapes showed that large gaps between our detailed understanding of C dynamics on the plot scale to coarse knowledge at larger scales exist. These gaps are largely driven by the unavailability of sufficient data at the respective scales to apply SOC models at a comparable level of quality, and by a limited understanding of interacting, multi-scale environmental controls on SOC dynamics. This thesis can contribute to solve these problems by linking SOC quality and quantity at the plot scale to pedological and geomorphological controls that act on the hillslope scale and which can be well represented with existing environmental datasets.

On the smallest scale processed in this thesis, the plot scale, sophisticated models and knowledge on different aspects of SOC dynamics are available (Von Luetzow et al. 2006, Totsche et al. 2010, Schmidt et al. 2011). On larger scales, such as continents or regions, a lack of tools to acquire sufficient data and a lack of availability of spatial explicit datasets at a high resolution is the most severe problem to develop similar models. Consequently, models to study carbon dynamics at these scales often have a very simplified structure or are of a more general nature in the framework of a holistic ecosystem model (Andrén and Kätterer 1997; Cox et al. 2000; Xenakis et al. 2008). This problem could not be solved with this thesis. But improvements in the resolution and accuracy of remote sensing devices and non-invasive soil analysis techniques lead to a larger spatial coverage of SOC datasets. Methodological advances and improved process understanding, as presented in this thesis, can lead to more complete datasets and, hence, be a basis for more sophisticated future models also on larger scales.

Many chapter in this thesis conclude that the information acquired from the experimental studies on spatial explicit patterns of SOC quality and quantity need to be integrated into models that can simulate both changes in soil environment and the anthropogenic forcing on this environment in which C stabilization takes place. However, a more general inclusion of the findings into a larger ecosystem context and into models has not yet been done. This section aims to outline a model structure that can fulfill this task in future research.

Effects on the stability of C in non-colluvial/non-sedimentary soil material are often considered only on the short-term and focus on labile SOC pools. Furthermore, in current C models (i.e. Century, Roth C) the soil mineral phase is often regarded as a steady-state system. These models are insensitive for changes in the mineral phase beyond soil textural changes, even so the importance of the mineral phase or various mechanisms to stabilize C has been long recognized (Torn et al. 1997; Kleber et al. 2011 Dungait et al. 2012). In consequence, these models cannot cover the effects of soil weathering and soil transport and the associated changes in soil physical and chemical parameters on soil carbon. In return, models including more complex soil forming or soil transportation processes often lack understanding of C stabilization mechanisms and SOC stability there is seen as function of its biochemical composition or not regarded in a qualitative matter (Dlugoß 2011; Yu et al. 2013). In agricultural soils, the soil weathering front (in deeper soil layers) and the core part of the soil C cycle (in topsoils) are brought into closer contact as soil erosion removes weathered soil from eroding slopes, while at colluvial sites the opposite effect will take place as weathered eroded material gets deposited and buries the *in-situ* soils, hence changing the mineral phase in contact with the C cycle. In consequence, the feedbacks between the soil weathering and the soil C Cycle will differ significantly between natural and disturbed systems. This represents a major gap in our understanding of the mechanisms that can stabilize carbon over longer timescales in systems with soil redistribution and represents the focus of the proposed model improvements.

A way to overcome this is to try combining existing models that can simulate the different discussed aspects into a holistic soil/SOC environmental model in three distinct steps: In a first step a basic C model will be modified to represent the identified functional pools outlined in this

thesis. The suggested basic C model applied hereby is the SOMPROF model (Braakhekke et al. 2011). SOMPROF is a vertically explicit C model, designed for implementation into large scale ecosystem and land surface models. The model dynamically simulates the vertical C profile and organic layer stocks based on mechanistic representations of bioturbation, liquid phase transport of organic matter, and vertical distribution of root litter input. In a second step, the modified model will then be implemented into a soil genesis model such as SoilGen (Finke and Hudson 2008), where it will replace its current soil C module, which is focused exclusively on biochemical recalcitrance of C as a tracer for its stability. SoilGen is a model for soil evolution at the pedon scale and simulates the change of soil properties over millennial timescales. Simulated processes comprise water flow, solute flow, heat flow, C-cycle, physical weathering, clay migration, weathering of primary minerals, solution and exchange chemistry, bioturbation and plant water and nutrient uptake. Soil processes are influenced by external forcings such as climate, vegetation, agricultural activities, topographic factors and erosion and sedimentation events starting from an (unconsolidated) parent material. In a third step, in order to reflect lateral fluxes, a soil C redistribution model, i.e. Speros-C (Van Oost et al. 2005), is linked to the modified model in order to develop a model that can simulate the effects of soil redistribution on the soil environment in which C sequestration, stabilization and transportation take place. Such an admittedly challenging model will advance former attempts to include depth-explicit differences in C quality and soil environmental factors. Insight in this topic can contribute largely to improve C turnover models at various scales and to clarify the response of the soil C cycle to disturbance. The innovative nature of model lies in the combination of concepts of soil formation, redistribution and soil C cycling acting at different temporal and spatial scales.

Finally, as is the case with all environmental parameters, SOC is connected to various mechanisms studied by a wide range of research schools, crossing geomorphology, pedology, (micro-)biology, hydrology and climatology. This thesis has been conducted in close cooperation with scientists from this diverse spectrum of research fields crossing from field and laboratory assessments to modeling with existing data. It is the author's conviction that future advances in understanding the importance of SOC in an ecosystem context will largely rely on cooperations between those different fields of

research, in order to overcome established paradigms and to look beyond individual perspectives as field, lab or modeling scientists. The next big advances in SOC research might not be made by adding more complexity and detail at the plot scale, but by finding ways to validate and transfer existing knowledge at this scale to the landscape or ecosystem level, which is the level of interest for policy makers and land use planners.

9 Bibliography

AGIV. 2003. Digitaal Hoogtemodel Vlaanderen. *Nieuwsbrief GIS-Vlaanderen*, **16**: 3-21.

Akaike H. 1973. Information theory and an extension of the maximum likelihood principle. *Second International Symposium on Information Theory*: 267-281.

Alexandrovskiy AL. 2007. Rates of soil-forming processes in three main models of pedogenesis. *Revista Mexicana de Ciencias Geologicas*, **24**(2): 283-292.

Anderson SP, von Blanckenburg F, White AF. 2007. Physical and Chemical Controls on the Critical Zone. *Elements* , **3**: 315–319.

Anderson DR., Burnham KP, et al. 1998. Comparison of Akaike information criterion and consistent Akaike information criterion for model selection and statistical inference from capture-recapture studies. *Journal of Applied Statistics*, **25**(2): 263-282.

Andrén O, Kätterer T. 1997. ICBM: The introductory carbon balance model for exploration of soil carbon balances. *Ecological Applications*, **7**: 1226-1236.

Angers DA, Giroux M. 1996. Recently deposited organic matter in soil water-stable aggregates. *Soil Science Society of America Journal*, **60**(5): 1547-1551.

ArcScripts. 2010. Topography Tools for ArcGIS (9.3,9.2,9.1/9.0), assembled by Dilt, T. Available at: *http://arcscripts.esri.com/details.asp?dbid=15996*..

Arya LM, Leij FJ, Shous PJ, Van Genuchten MT. 1999. Relationship between the hydraulic conductivity function and the particle-size distribution. *Soil Science Society of America Journal*, **63**(5): 1063-1070.

Aufdenkampe AK, Mayorga E, Raymond PA et al. 2011 Riverine coupling of biogeochemical cycles between land, oceans, and atmosphere. *Frontiers in Ecology and the Environment*, **9**(1): 53-60.

Baer SG, Meyer CK, Back EM, Klopf RP, Six J. 2010. Contrasting ecosystem recovery on two soil textures, implications for carbon mitigation and grassland conservation. *Ecosphere*, **1**(1), art5.

Baker JM, Ochsner TE, Venterea RT, Griffis TJ. 2007. Tillage and soil carbon sequestration – What do we really know? Agriculture, Ecosystems & Environment. 118(1-4): 1-5.

Bakker MM, Govers G, Rounsevell MDA. 2004. The crop-productivity-erosion relationship: an analysis based on experimental work. *Catena*, **57**(1): 55-76.

Balesdent J, Chenu C, Balabane M. 2000. Relationship of soil organic matter dynamics to physical protection and tillage. *Soil and Tillage Research*, **53**(3-4): 215-230.

Barnes RJ, Dhanoa MS, Lister SJ. 1989. Standard normal variate transformation and de-trending of near-infrared diffuse reflectance spectra. *Applied spectroscopy*, **43**(5): 772–777.

Bascomb, C.L. 1968. Distribution of pyrophosphate-extractable iron and organic carbon in soils of various groups. *Journal of Soil Science*, **19**: 251-268.

Batjes NH. 2006. ISRIC-WISE derived soil properties on a 5 by 5 arc-minutes global grid. Report 2006/02. ISRIC – World Soil Information. Wageningen.

Batjes NH. 2008. ISRIC-WISE Harmonized Global Soil Profile Dataset (Ver. 3.1). Report 2008/02. ISRIC-World Soil Information. Wageningen.

Batjes NH. 2000. Effects of mapped variation in soil conditions estimates of soil carbon and nitrogen stocks for South America. *Geoderma*, **97**(1-2): 135-144.

Batjes NH. 1996. Total carbon and nitrogen in the soils of the world. *European Journal of Soil Science*, **56**: 689-703.

Batlle-Aguilar J, Brovelli A, et al. 2011. Modelling soil carbon and nitrogen cycles during land use change. A review. *Agronomy for Sustainable Development*, **31**(2): 251-274.

BDSOL LU. 1969. "Soil profile database" property of: Ministère de l'agriculture, de la viticulture et du développement rural, Service de pédologie du Luxembourg, BP 75 L-9001 Ettelbruck, Luxembourg.

Ben-Dor E, Heller D, Chudnovsky A. 2008. A Novel Method of Classifying Soil Profiles in the Field using Optical Means. *Soil Science Society of America Journal*, **72**(4): 1113-1123.

Ben-Dor E, Irons J, Epema G. 1999. Soil Reflectance. p. 111–188. *In* Remote Sensing for the Earth Sciences: Manual of Remote Sensing. Wiley and Sons Inc. Rencz, A.N.

Berhe AA, Harte J, Harden J, Torn M. 2007. The significance of the erosion-induced terrestrial carbon sink. *Bioscience*, **57**: 337-346.

Berhe AA, Harden JW, Torn MS, Harte J. 2008. Linking soil organic matter dynamics and erosion-induced terrestrial carbon sequestration at different landform positions. *Journal of Geophysical Researc*h *G, Biogeosciences*, **113**(4).

Berhe AA. 2012a. Decomposition of organic substrates at eroding vs. depositional landform positions. *Plant and Soil*, **350**(1-2): 261-280.

Berhe AA, Harden JW, Torn MS, Kleber M, Burton SD, Harte J. 2012b. Persistence of soil organic matter in eroding versus depositional landform positions. *Journal of Geophysical Research, **117***, G02019, doi:10.1020/2011JG001790.

Besnard E, Chenu C, Balesdent J. 1996. Fate of particulate organic matter in soil aggregates during cultivation. *European Journal of Soil Science*, **47**(4): 495-503.

Beuselinck, L, Govers G, Poesen J, Degraer G, Froyen L. 1998 Grain-size analysis by laser diffractometry, comparison with the sieve-pipette method. *Catena*, **32:** 193-208.

Beven K J and Kirkby M J. 1979. A physically based, variable contributing area model of basin hydrology. *Hydrological Sciences Bulletin*, **24**: 43-69.

Bipfubusa M, Angers DA, Ndayegamiye AA, Antoun H. 2008. Soil aggregation and biochemical properties following the application of fresh and composted organic amendments. *Soil Science Society of America Journal*, **72**: 160-166.

Billings SA, Buddemeier RW, Richter DD, Van Oost K, Bohling G. 2010. A simple method for estimating the influence of eroding soil profiles on atmospheric CO2. *Global Biogeochemical Cycles*, **24**: GB2001.

Bird MI, Ascough PL. 2012. Isotopes in pyrogenic carbon: A review. *Organic Geochemistry*, **42:** 1529-1539.

Birkeland P. W. 1999. *Soils and Geomorphology, 3rd Edition*, 448p.

Blake GR, Hartge KH. 1986. Bulk Density. In: Methods of Soil Analysis, Part I. Physical and Mineralogical Methods, (ed Klute A), pp 363-375. SSSA Book Series 5, Madison.

Boardman J. 2006. Soil erosion science: Reflections on the limitations of current approaches. *Catena*, **68**(2-3): 73-86.

Braakhekke MC, Beer C, Hoosbeek MR, Reichstein M, Kruijt B, Schrumpf M, Kabat P. 2011. SOMPROF: A vertically explicit soil organic matter model. *Ecological Modelling*, **222**(10): 1712-1730.Brady NC and Weil RR. 2008. The nature and Properties of Soils., Pearson Education Inc., Upper saddle River, NJ. 975pp.

Breiman L. 2001. Random forests. *Machine learning*, **45**(1): 5–32.

Breiman L, Friedman JH, Olshen RA, Stone CJ. 1984. Classification and regression trees. Wadsworth International Group, Belmont, USA.

Bricklemeyer RS, Brown DJ. 2010. On-the-go VisNIR: Potential and limitations for mapping soil clay and organic carbon. *Computers and Electronics in Agriculture*, **70**(1): 209-216.

Brindley GW, Brown G. 1980. Crystal Structures of Clay Minerals and Their Identification. Mineralogical Society Monograph No. 5. Mineralogical Society, London. 495pp.

Brown DJ, Sheperd KD, Walsh MG, Dewayne Mays M, Reinsch TG. 2006. Global soil characterization with VNIR diffuse reflectance spectroscopy. *Geoderma*, **132**: 273-290.

Burnham KP and Anderson DR. 2001. Kullback-Leibler information as a basis for strong inference in ecological studies. *Wildlife Research*, **28**(2): 111-119.

Burt TP and Butcher DP. 1985. Topographic controls of soil moisture distributions. *Journal of Soil Science* **36**(3): 469-486.

Cantón Y, Solé-Benet A, Asensio C, Chamizo S, Puigdefábregas J. 2009. Aggregate stability in range sandy loam soils: Relationships with runoff and erosion. *Catena*, **77**(3): 192-199.

Cécillon L, Barthès BG. et al. 2009. Assessment and monitoring of soil quality using near-infrared reflectance spectroscopy (NIRS). *European Journal of Soil Science*, **60**(5): 770-784.

Cerdan O, Govers G, Le Bissonnais Y, Van Oost K, Poesen J, Saby N, Gobin A, Vacca A, Quinton J, Auerswald K, Klik A, Kwaad FJPM, Raclot D, Ionita I, Reijman J, Rousseva S, Muxart T, Roxo MJ, Dostal T. 2010. Rates and spatial variations of soil erosion in Europe: A study based on erosion plot data. *Geomorphology*, 122(1-2): 167-177.

Cerdan O, Poesen J, Govers G, Saby N, Le Bissonnais A, Gobin A, Vacca A, Quinton J, Auerswald K, Klik A, Kwaad FPM, Roxo MJ. 2006. Sheet and Rill Erosion. In: Boardman J and Poesen J (eds). Soil erosion in Europe. Wiley: New York; 501-513.

Chang CW, Laird DA, Mausbach MJ, Hurburgh CR. 2001. Near-infrared reflectance spectroscopy–Principal components regression analyses of soil properties. *Soil Science Society of America Journal*, **65**(2): 480–490.

Chao TT and Sanzolone RF. 1992. Decomposition techniques. *Journal of Geochemical Exploration*, **44**(1-3): 65-106.

Childs CW, Masue N, Yoshinaga N. 1991. Ferrihydrite in volcanic ash soils of Japan. *Soil Science and Plant Nutr*ion, **37**(2): 299-311.

Christensen BT. 2001. Physical fractionation of soil and structural and functional complexity in organic matter turnover. *European Journal of Soil Science*, **52**(3): 345-353.

Ciais P, Wattenbach M, Vuichard N, Smith P, Piao SL, Don A, Luyssaert S, Janssens IA, Bondeau A, Dechow R, Leip A, Smith PC, Beer C, Van der Werf GR, Gervois S, Van Oost K, Tomelleri E, Freibauer A, Schulze ED and CarboEurope Synthesis Team. 2010. The European carbon balance. Part 2: Croplands. *Global Change Biology*, **16**: 1409-1428.

Clark RN. 1999. Spectroscopy of rocks and minerals, and principles of spectroscopy. p. 3–58. *In* Manual of Remote Sensing. John Wiley & Sons Inc. Rencz, A.N., New York, USA.

Climatedata. 2012. Recent climate data for the city of Luxembourg (Luxembourg). Available at: http://www.climatedata.eu/climate.php?loc=luxx0003&lang=en# (Access retrieved 20 July 2012).

Coleman K, Jenkinson DS .1999. ROTHC-26.3. A Model for the Turnover of Carbon in Soil. Model Description and Users Guide. IACR, Rothamsted.

Coleman K, Jenkinson DS, et al. 1997. Simulating trends in soil organic carbon in long-term experiments using RothC-26.3. *Geoderma*, **81**(1-2): 29-44.

Compton JS, Herbert CT, Hoffman MT, Schneider RR, Stuut JB. 2010. A tenfold increase in the Orange River mean Holocene mud flux: implications for soil erosion in South Africa. *Holocene*, **20**(1): 115-122.

Conen F, Zimmermann M, Leitfeld J, Seth B, Alewell C. 2008. Relative stability of soil carbon revealed by shifts in delta N-15 and C : N ratio. *Biogeosciences*, **5**(1): 123-128.

Cox PM, Betts RA, Jones CD, Spall SA, Totterdell IJ. 2000. Acceleration of global warming due to carbon cycle feedbacks in a coupled climate model. *Nature*, **408**: 184-187.

Cromack K, Miller RE, Helgerson OT, Smith RB, Anderson HW. 1999. Soil carbon and nutrients in a coastal Oregon douglas-fir plantation with red alder. *Soil Science Society of America Journal*, **63**(1): 232-239.

Dahlgren RA. 1994. Quantification of allophane and imogolite. In: Zelazny LW, Amonette JE (eds). Quantitative methods in soil mineralogy. *Soil Science Society of America*, Madison. pp 430–451.

Davidson EA and Janssens IA. 2006. Temperature sensitivity of soil carbon decomposition and feedbacks to climate change. *Nature*, **440**(7081): 165-173.

DeGryze S, Six J, Bossuyt H, Van Oost K, Merckx R. 2008. The relationship between landform and the distribution of soil C, N and P under conventional and minimum tillage. *Geoderma*, **144**(1-2): 180-188.

DeGryze S. 2004. Soil organic carbon pool changes following land-use conversions. *Global Change Biology*, **10**(7): 1120-1132.

Del Galdo I, Six J, Peressotti A, Cotrufo MF. 2003. Assessing the impact of land-use change on soil C sequestration in agricultural soils by means of organic matter fractionation and stable C isotopes. *Global Change Biology*, **9**(8): 1204-1213.

Deng F, Knadel M, Peng Y, Heckrath G, Greve MH; Minasny B. 2012. Soil profile organic carbon prediction with visible-near infrared reflectance spectroscopy based on a national database. *5th Global Workshop on digital soil mapping*, 5: 409-413.

Denis A, Tychon B, Stevens A, Van Wesemael B. 2009. Improving Soil Organic Carbon (SOC) prediction by field spectrometry in bare cropland by reducing the disturbing effect of soil roughness. *International Geoscience and Remote Sensing Symposium*, **5**: 351-354.

De Vente J, Poesen J, Arabkhedri M, Verstraeten G. 2007. The sediment delivery problem revisited. *Progress in Physical Geography*, **31**(2): 155-178.

Den Biggelaar C, Lal R, Wiebke K, Breneman V. 2004. The global impact of soil erosion on productivity. *Advances in Agronomy*, **81**: 1-48.

Dlugoß V. 2011. Impacts of soil redistribution processes on soil organic carbon stocks and fluxes in a small agricultural catchment. PhD thesis. *Geographisches Institut der Universität zu Köln*. Köln. 143 pp.

Doetterl S, Van Oost K, Six J. 2012a. Towards constraining the magnitude of global agricultural sediment and soil organic carbon fluxes. *Earth Surface Processes and Landforms*, **37**(6): 642-655.

Doetterl S, Six J, Van Wesemael B, Van Oost K. 2012b. Carbon cycling in eroding landscapes, Geomorphic controls on soil organic C pool composition and C stabilization. *Global Change Biology*, **18**(7): 2218-2232.

Doetterl, S, Stevens A, Van Oost K, Quine TA, Van Wesemael B. (*submitted*). Spatially-explicit regional-scale prediction of soil organic carbon stocks in cropland using environmental variables and mixed model approaches. *Geoderma*.

Doetterl S., Cornelis, J-T. Six J., Quine T.A., Van Oost K. (*submitted*): The varying contribution of reactive soil phases to stabilize soil organic carbon along a slope transect. *European Journal of Soil Science*.

Doetterl S, Stevens A, Van Wesemael B, Van Oost K. (*submitted*): Using rapid closed tube sampling systems and VISNIR-spectroscopy for rapid landscape scale soil property assessments. *Agronomy Technical Bulletins.*

Don A, Scholten T, Schulze ED. 2009. Conversion of cropland into grassland, Implications for soil organic-carbon stocks in two soils with different texture. *Journal of Plant Nutrition and Soil Science*, **172**(1): 53-62.

Duiker SW, Rhoton FE, Torrent J, Smeck NE, Lal R. 2003. Iron (hydro)oxide crystallinity effects on soil aggregation. *Soil Science Society of America Journal*, **67**(2): 606-611.

Duemig A, Haeusler W, Steffens M, Koegel-Knabner I. 2012. Clay fractions from a soil chronosequence after glacier retreat reveal the initial evolution of organo-mineral associations. *Geochimica et Cosmochimica Acta*, **85:** 1-18.

Duemig A, Smittenberg R, Koegel-Knabner I. 2011. Concurrent evolution of organic and mineral components during initial soil development after retreat of the Damma glacier, Switzerland. *Geoderma*, **163**(1-2): 83-94.

Dungait JAJ, Hopkins DW, Gregory AS, Whitmore AP. 2012. Soil organic matter turnover is governed by accessibility not recalcitrance. *Global Change Biology*, **18**(6): 1781-1796.

European Comission. 2011. The European Soil Database. Available at: http://eusoils.jrc.ec.europa.eu/ESDB_Archive/ESDB/index.htm

EEA. 2012. Corine Land Cover 2006 raster data - version 16. Retrieved 20 July, 2012, available at: http://www.eea.europa.eu/data-and-maps/data/corine-land-cover-2006-raster-2.

Egli M, Mirabella A, Fitze P. 2003. Formation rates of smectites derived from two Holocene chronosequences in the Swiss Alps. *Geoderma*, **117**(1-2), 81-98.

Egli M, Nater M, Mirabella A, Raimondi S, Ploetze M, Alioth L. 2008. Clay minerals, oxyhydroxide formation, element leaching and humus development in volcanic soils. *Geoderma*, **143**(1-2): 101-114.

Ekschmitt K, Kandeler E, et al. 2008. Soil-carbon preservation through habitat constraints and biological limitations on decomposer activity. *Journal of Plant Nutrition and Soil Science*, **171**(1): 27-35.

Elementar GmbH. 2009. Solid-TOC with the elemental analyzer varioMAX. Application Report AB-C-170702-E-02: 1-3.

Eusterhues K, Rennert T, Knicker H, Totsche KU, Schwertmann U. 2011. Fractionation of organic matter due to reaction with Ferrihydrite, Coprecipiation versus Adsoprtion. *Environmental Science and Technology*, **45:** 527-533.

Eusterhues K, Wagner FE, Haeusler W, Hanzlik M, Knicker H, Totsche KU, Koegel-Knabner I, Schwertmann U. 2008. Characterization of ferrihydrite-soil organic matter coprecipitates by X-ray diffraction and Mössbauer spectroscopy. *Environmental Science and Technology*, **42**(21): 7891-7897.

Eusterhues K, Rumpel C, Koegel-Knabner I. 2005. Organo-mineral associations in sandy acid forest soils, importance of specific surface area, iron oxides and micropores. *European Journal of Soil Science*, **56**: 753-763.

Falkowski P, Scholes RJ, Boyle E, Canadell J, Canfield D, Elser J, Gruber N, Hibbard K, Hógberg P, Linder S, Mackenzie GT, Moore IIIB, Pedersen T, Rosenthal Y, Seitzinger S, Smetacek V, Steffen W. 2000. The Global Carbon Cycle: A Test of Our Knowledge Of Earth as a System, *Science,* **290**: 291-296.

Falloon P and Smith P. 2002. Simulating SOC changes in long-term experiments with RothC and CENTURY: Model evaluation for a regional scale application. *Soil Use and Management,* **18**(2): 101-111.

Falloon, P., P. Smith, et al. (2006). "RothCUK - A dynamic modeling system for estimating changes in soil C from mineral soils at 1-km resolution in the UK." *Soil Use and Management*, **22**(3): 274-288.

Fan Y, Lei T, Cai Q. 2008. Effects of wetting rate on soil surface strength and aggregate stability. *Transactions of the Chinese Society of Agricultural Engineering*, **24**(5): 46-50.

FAO/IIASA/ISRIC/ISSCAS/JRC, 2012. Harmonized World Soil Database (version 1.2). FAO, Rome, Italy and IIASA, Laxenburg, Austria.

Feng W, Plante AF, Six J. 2011. Improving estimates of maximal organic carbon stabilization by fine soil particles. *Biogeochemistry*. Doi, 10.1007/s10533-011-9679-7.

Finke P, Hutson JL. 2008. Modelling soil gensis in calcareous loess. *Geoderma*, **145**(3-4): 462-479.Fontaine S, Barot S, Barre P, Bdioui N, Mary B, Rumpel C. 2007. Stability of organic carbon in deep soil layers controlled by fresh carbon supply. *Nature*, **450**(7167): 277-280.

Forthofer RN, Lee ES, Hernandez M. 2006. Biostatistics, Second edition: A guide to Design, Analysis and Discovery. Elsevier Academic Press: Burlington.

Gesch DB, Verdin KL, Greenlee SK. 1999. New land surface digital elevation model covers the earth. Eos, Transactions, *American Geophysical Union,* **80**(6): 69-70.

Gibbs RJ. 1967. The geochemistry of the Amazon River system. Part I. The factors that control the salinity and the composition and concentration of the suspended solids. *Geolological Society of America Bulletin*, **78**: 1203-1232.

Goidts E, Van Wesemael B, Van Oost K. 2009a. Driving forces of soil organic carbon evolution at the landscape and regional scale using data from a stratified soil monitoring. *Global Change Biology*, **15**(12): 2981-3000.

Goidts E, Van Wesemael B, Crucifix M. 2009b. Magnitude and sources of uncertainties in soil organic carbon (SOC) stock assessments at various scales. *European Journal of Soil Science*, **60**: 723:739.

Goidts E and van Wesemael B. 2007. Regional assessment of soil organic carbon changes under agriculture in Southern Belgium (1955-2005). *Geoderma*, **141**(3-4): 341-354.

Golchin A, Clarke P, Oades JM. 1996. The heterogeneous nature of microbial products as shown by solid-state C-13 CP/MAS NMR spectroscopy. *Biogeochemistry*, **34**(2): 71-97.

Goldberg S. 1989. Interaction of aluminium and iron oxides and clay minerals and their effect on soil physical properties: A review. *Communications in Soil Science and Plant Analysis*, **20**(11-12): 1181-1207.

Gomez C, Viscarra Rossel RA, et al. 2008. Soil organic carbon prediction by hyperspectral remote sensing and field Vis-NIR spectroscopy: An Australian case study. *Geoderma*, **146**(3-4): 403-411.

González-Molina L, Etchevers-Barra JD, et al. 2008. Carbono en suelos de ladera: factores que deben considerarse para determinar su cambio en el tiempo. *Agrociencia*, **42**: 741-751.

Gregorich EG, Greer KJ, Anderson DW, Liang BC. 1998. Carbon distribution and losses, Erosion and deposition effects. *Soil and Tillage Research*, **47**(3-4): 291-302.

Grunwald S, Thompson JA, Boettinger JL. Digital Soil Mapping and Modeling at Continental Scales: Finding Solutions for Global Issues. *Soil Science Society of America Journal*, **75**: 1201-1213.

Guo Y, Gong P, Amundson R, Yu Q. 2006. Analysis of factors controlling soil carbon in the conterminous United States. *Soil Science Society of America Journal*, **70**(2): 601-612.

Guo LB and Gifford RM. 2002. Soil carbon stocks and land use change, A meta analysis. *Global Change Biology*, **8**(4): 345-360.

Harden JW, Sharpe JM, Parton WJ, Ojima DS, Fries TL, Huntington TG, Dabney SM. 1999. Dynamic replacement and loss of soil carbon on eroding cropland. *Global Biogeochemical Cycles*, **13**(4): 885-901.

Harris D., Horwath WR., van Kessel C. 2001. Acid fumigation of soils to remove carbonates prior to total organic carbon or carbon-13 isotopic analysis. *Soil Science Society of America Journal*, **65**(6): 1853-1856.

Haskard KA, Rawlins BG, et al. 2010. A linear mixed model, with non-stationary mean and covariance, for soil potassium based on gamma radiometry. *Biogeosciences*, **7**(7): 2081-2089.

Hassink J. 1997. The capacity of soils to preserve organic C and N by their association with clay and silt particles. *Plant and Soil*, **191**: 77–87.

Heckrath G, Halekoh U, et al. 2006. The effect of tillage direction on soil redistribution by mouldboard ploughing on complex slopes. *Soil and Tillage Research*, **88**(1-2): 225-241.

Herbillon AJ. 1986. Chemical estimation of wheatherable minerals present in the diagnostic horizons of low activity clay soils. In, Beinroth FH, Camargo MN, Eswaran H (eds). Proceedings of the eighth international soil classification workshop - Classification, Characterization and Utilization of Oxisols. Part 1 - Papers, 39-48.

Hiederer R, Köchyl M, 2012. Global soil organic carbon estimates and the harmonized world soil database. EUR 25225EN, Luxembourg.

Hijmans RJ, Cameron SE, Parra JL, Jones PG, Jarvis A. 2005. Very high resolution interpolated climate surfaces for global land areas. *International Journal of Climatology*, 25(15): 1965-1978.

Hoffmann T, Glatzel S, Dikau R. 2009. A carbon storage perspective on alluvial sediment storage in the Rhine catchment. *Geomorphology*, **108**(1-2): 127-137.

Holden PA & Fierer N. 2005. Microbial processes in the vadose zone. *Vadose Zone Journal*, **4**(1) : 1-21.

Hooke RL. 2000. On the history of humans as geomorphic agents. *Geology*, **28**(9): 843-846.

Houghton, R.A., 2007. Balancing the global carbon budget, Annual Review of Earth and Planetary Sciences. *Annual Review of Earth and Planetary Sciences*, pp. 313-347.

Huang PM, Wang TSC, Wang MK, Wu MH, Hsu NW. 1977. Retention of phenolic acids by non-crystalline hydroxy-aluminum and -iron compounds and clay minerals of soils. *Soil Science*, **123**: 213-219.

IPCC. 2007. Climate Change 2007 – Synthesis Report, 104 p. Available at: http://www.ipcc.ch/publications_and_data/publications_ipcc_fourth_assessment_report_synthesis_report.htm

IRM. 2011. Climatogramm for the period 1961-1990, Station 06447 (Uccle; Belgique). Retrieved 28.July.2011, 2011, available at: http,//www.meteo.be/meteo/view/fr/139844-Climatogrammes.html.

Ito A. 2007. Simulated impacts of climate and land-cover change on soil erosion and implication for the carbon cycle, 1901 to 2100. *Geophysical Research Letters*, **34**(9).

IUSS Working Group WRB. 2006. World reference base for soil resources 2006. 2nd edition. World Soil Resources Reports No. 103. FAO, Rome.

Jabro JD, Stevens WB, et al. 2010. Tillage depth effects on soil physical properties, sugarbeet yield, and sugarbeet quality. *Communications in Soil Science and Plant Analysis*, **41**(7): 908-916.

Jacinthe PA and Lal R. 2001. A Mass Balance Approach to Asssess Carbon Dioxide Evolution During Erosional Events. *Land Degradation & Development*, **12**(4): 329-339.

Jacinthe PA, Lal R, Kimble JM. 2001. Assessing Water Erosion Impacts on Soil Carbon Pools and Fluxes. In R. Lal R, Kimble JM, Follett RF, Stewart BA (eds). Assessment Methods for Soil Carbon. Lewis Publishers: Boca Raton: 427-450.

Jastrow JD. 1996. Soil aggregate formation and the accrual of particulate and mineral-associated organic matter. *Soil Biology & Biochemistry*, **28**(4-5): 665-676.

Jenness J. 2006. Topographic Position Index (tpi_jen.avx) extension for ArcView 3.x, v.1.2. Available at: http://www.jennessent.com/arcview/TPI.htm.

Jobbágy EG, Jackson RB. 2000. The vertical distribution of soil organic carbon and its relation to climate and vegetation. *Ecological Applications*, **10**(2): 423-436.

John B, Yamashita T, Ludwig B, Flessa H. 2005. Storage of organic carbon in aggregate and density fractions of silty soils under different types of land use. *Geoderma*, **128**(1-2): 63-79.

Kahle M, Kleber K, Torn MS, Jahn R. 2003. Carbon storage in coarse and fine clay fractions of illitic soils. *Soil Science Society of America Journal*, **67**(6): 1732-1739.

Kaiser K and Guggenberger G. 2007. Sorptive stabilization of organic matter by microporous goethite: sorption into small pores vs. surface complexation. *European Journal of Soil Science*, **58**(1): 45-59.

Kaiser K and Guggenberger G. 2003. Mineral surfaces and soil organic matter. *European Journal of Soil Science*, **54**(2): 219-236.

Kaiser K, Eusterhues K, Rumpel C, Guggenberger G, Koegel-Knabner I. 2002. Stabilization of organic matter by soil minerals - investigations of density and particle-size fractions from two acid forest soils. *Journal of Plant Nutrition and Soil Science*, **165**(4): 451-459.

Kaiser K, Guggenberger G, Haumeier L, Zech W. 1997. Dissolved organic matter sorption on subsoil and minerals studied by 13C-NMR and DRIFT spectroscopy. *European Journal of Soil Science*, **48**: 301-310.

Kaiser K. & Zech W. 1996. Defects in estimation of aluminum in humus complexes of podzolic soils by pyrophosphate extraction. *Soil Science*, **161**(7): 452-458.

Kalbitz K, Solinger S, Park JH, Michalzik B, Matzner E. 2000. Controls on the dynamics of dissolved organic matter in soils: A review. *Soil Science*, **165**(4): 277-304.

Kang S, Kim S, et al. 2000. Predicting spatial and temporal patterns of soil temperature based on topography, surface cover and air temperature. *Forest Ecology and Management*, **136**(1-3): 173-184.

Kang S, Doh S, et al. 2003. Topographic and climatic controls on soil respiration in six temperate mixed-hardwood forest slopes, Korea. *Global Change Biology*, **9**(10): 1427-1437.

Kennard RW, Stone LA. 1969. Computer aided design of experiments. *Technometrics*, **11**(1): 137–148.

Kleber M. 2010. What is recalcitrant soil organic matter? *Environmental Chemistry*, **7**(4): 320-332.

Kleber M, Nico PS, Plante A, Filley T, Kramer M, Swanston C, Sollins P. 2011. Old and stable soil organic matter is not necessarily chemically recalcitrant: implications for modeling concepts and temperature sensitivity. *Global Change Biology*, **17**: 1097–1107.

Kleber M, Sollins P, Sutton R. 2007. A conceptual model of organo-mineral interactions in soils: self-assembly of organic molecular fragments into zonal structures on mineral surfaces. *Biogeochemistry*, **85**: 9–24.

Kleber M., Mikutta R, Torn MS, Jahn R. 2005. Poorly crystalline mineral phases protect organic matter in acid subsoil horizons. *European Journal of Soil Science*, **56**(6): 717-725 .

Klein-Goldewijk K, Beusen A, Van Drecht G, De Vos M. 2010. The HYDE 3.1 spatially explicit database of human induced land use change over the past 12,000 years. *Global Ecology and Biogeography*, **20**(1): 73-86.

Knadel M, Thomsen A, Greve MH. 2011. Multisensor on-the-go mapping of soil organic carbon content. *Soil Science Society of America Journal*, **75**(5): 1799-1806.

Kodama A, and Schnitzer M. 1980. Effects of fulvic acids on the crystallization of aluminum hydroxides. *Geoderma*, **24**:195-205.

Koegel-Knabner I, Guggenberger G, Kleber M, Kandeler E, Kalbitz K, Scheu S, Eusterhues K, Leinweber P. 2008. Organo-mineral association in temperate soils: integrating biology, mineralogy and organic matter chemistry. *Journal of Plant Nutrition and Soil Science*, **171**: 61-82.

Krull ES, Skjemstad JO, Baldock JA. 2004. Functions of Soil Organic Matter and the Effects on Soil Properties. GRDC Australia Project No CSO 00029 ACT Report. 129pp.

Kuang B, Mouazen AM. 2011. Calibration of visible and near infrared spectroscopy for soil analysis at the field scale on three European farms. *European Journal of Soil Science*, **62**(4): 629–636.

Kuhn M, Wing J, Weston S, Williams A, Keefer C, Engelhardt A. 2012. Caret: classification and regression training. R package, v5.15. Available at http://cran.r-project.org/web/packages/caret/.

Kuhn NJ. 2007. Erodibility of soil and organic matter, independence of organic matter resistance to interrill erosion. *Earth Surface Processes and Landforms*, **32**(5): 794-802.

Kuhn NJ, Hoffmann T, Schwanghart W, Dotterweich M. 2009. Agricultural soil erosion and global carbon cycle, controversy over? *Earth Surface Processes and Landforms*, **34**(7): 1033-10.

Kummerer K, Held M, Pimentel D. 2010. Sustainable use of soils and time. *Journal of Soil and Water Conservation*, **65**(2): 141-149.

Kusumo BH, Hedley MJ, Tuohy MP, Hedley CB, Arnold GC. 2010. Predicting Soil Carbon and Nitrogen Concentrations and Pasture Root Densities from Proximally Sensed Soil Spectral Reflectance. In: Viscarra-Rossel et al. (eds.). Proximal Sensing. *Progress in Soil Science*, **1**:177-190.

Kutsch WL, Bahn M, Heinemeyer A. 2010. Soil Carbon Dynamics - An Integrated Methodology. Cambridge University Press: New York.

Lair GJ, Gerzabek MH, Haberhauer G. 2007. Sorption of heavy metals on organic and inorganic soil constituents. *Environmental Chemistry Letter*, **5**(1): 23-27.

Lal R. 2009. Challenges and opportunities in soil organic matter research, *European Journal of Soil Science*, **60**(2): 158-169.

Lal R. 2008. Sequestration of atmospheric CO2 in global carbon pools, *Energy and Environmental Science*, **1**: 86-100.

Lal R, Pimentel D. 2008. Soil erosion, A carbon sink or source? *Science*, **319**(5866): 1040-1042.

Lal R, Follett RF. Stewart BA, Kimble JM. 2007a. Soil carbon sequestration to mitigate climate change and advance food security. *Soil Science*, **172**(12): 943-956.

Lal R. 2007b. World soils and global issues. *Soil & Tillage Research*, **97**(1): 1-4.

Lal R. 2007c. Anthropogenic influences on world soils and implications to global food security. *Advances in agronomy*, **93**: 69-93.

Lal R. 2004. Ecology: Managing soil carbon. *Science*, **304**: 393

Lal R. 2003. Soil erosion and the global carbon budget. *Environment International*, **29**(4): 437-450.

Lannoo (ed). 2009. Le grand Atlas de Ferraris, Lannoo.

Leff B, Ramankutty N, Foley JA. 2004. Geographic distribution of major crops across the world. *Global Biogeochemical Cycles*, 18(1). GB1009, doi:10.1029/2003GB002108.

Lehmann, J., Kinyangi, J., Solomon, D. 2007. Organic matter stabilization in soil microaggregates, implications from spatial heterogeneity of organic carbon contents and carbon forms. *Biogeochemistry*, **85:** 45-47.

Lettens S, Van Orshoven J, et al. 2005. Soil organic carbon changes in landscape units of Belgium between 1960 and 2000 with reference to 1990. *Global Change Biology*, **11**(12): 2128-2140.

Li D, Niu S, Luo Y. 2012. Global patterns of the dynamics of soil carbon and nitrogen stocks following afforestation, A meta-analysis. *New Phytologist*, **195**(1): 172-181.

Liebens J. and VanMolle M. 2003. Influence of estimation procedure on soil organic carbon stock assessment in Flanders, Belgium. *Soil Use and Management*, **19**(4): 364-371.

Lindsay WL. (ed) 1979. Chemical equilibria in soils. The Blackburn Press, 450pp.

Li S, Lobb DA, Lindstrom MJ, Farenhorst A. 2008. Patterns of water and tillage erosion on topograpically complex landscapes in North American Great Plains. *Journal of Soil and Water Conservation*, **63**(1): 37-46.

Li XG, Li FM, Bhupinderpal S, Rengel Z, Zhan ZY. 2007. Soil management changes organic carbon pools in alpine pastureland soils. *Soil & Tillage Research*, **93**(1): 186-196.

LSP (Luxembourg Service de Pédologie). 1969. Carte des sols du Grand-Duché de Luxembourg. Compiled by Wagener, J., Ministère de l'Agriculture et de la Viticulture.

Liu SG, Bliss N, Sundquist E, Huntington TG. 2003. Modeling carbon dynamics in vegetation and soil under the impact of soil erosion and deposition. *Global Biogeochemical Cycles*, **17**(2): 1074.

Lu H, Prosser IP, Moran CJ, Gallant JC, Priestley G, Stevenson JG. 2003. Predicting sheetwash and rill erosion over the Australian continent. *Australian Journal of Soil Research*, **41**(6): 1037-1062.

Lvovich MI, Karasik GY, Bratseva NL, Medvedeva GP, Maleshko AV. 1991. Contemporary intensity of the world land intercontinental erosion. USSR Academy of Sciences, Moscow.

Mayor, A. G. and Bautista S. 2012. Multi-scale evaluation of soil functional indicators for the assessment of water and soil retention in Mediterranean semiarid landscapes. *Ecological Indicators*, **20**: 332-336.

McBratney AB, Minasny B, Rossel RV. 2006. Spectral soil analysis and inference systems: A powerful combination for solving the soil data crisis. *Geoderma*, **136**: 272-278.

McCarty GW, Ritchie JC. 2002. The Impact of soil movement on carbon sequestration in agricultural ecosystems. *Environmental Pollution*, **116**: 423-430.

McElroy B, Wilkinson B. 2005. Climatic control of continental physiography. *Journal of Geology*, **113**(1): 47-58.

McHale G, Newton MI, Shirtcliffe NJ. 2005. Water-repellent soil and its relationship to granularity, surface roughness and hydrophobicity, A materials science view. *European Journal of Soil Science*, **56**(4): 445-452.

McKenzie NJ and Ryan PJ. 1999. Spatial prediction of soil properties using environmental correlation. *Geoderma*, **89**(1-2): 67-94.

Meersmans J., Van Wesemael B, et al. 2009a. Changes in organic carbon distribution with depth in agricultural soils in northern Belgium, 1960-2006. *Global Change Biology*, **15**(11): 2739-2750.

Meersmans J, van Wesemael B, et al. 2009b. Modelling the three-dimensional spatial distribution of soil organic carbon (SOC) at the regional scale (Flanders, Belgium). *Geoderma*, **152**(1-2): 43-52.

Meersmans J, De Ridder F, Canters F, De Baets S, Van Molle M. 2008. A multiple regression approach to assess the spatial distribution of Soil Organic Carbon (SOC) at the regional scale (Flanders, Belgium). *Geoderma*, **143**(1-2): 1-13.

Mehra OP and Jackson ML. 1960. Iron oxide removal from soils and clays by a Dithionite-Citrate System Buffered with Sodium Bicarbonate. *Clays and Minerals,* **5**: 317-327.

Melillo JM, Steudler PA, et al. 2002. Soil warming and carbon-cycle feedbacks to the climate system. *Science*, **298**(5601): 2173-2176.

Milliman JD, and Syvitski JPM. 1992. Geomorphic tectonic control of sediment discharge to the ocean – The importance of small mountainous rivers. *Journal of Geology*, **100**(5): 525-544.

Mikutta R, Schaumann GE, Gildemeister D, Bonneville S, Kramer MG, Chorover J, Chadwick OA, Guggenberger G. 2009. Biogeochemistry of mineral-organic associations across a long-term mineralogical soil gradient (0.3-4100 kyr), Hawaiian Islands. *Geochimica Et Cosmochimica Acta*, **73**: 2034-2060.

Mikutta R, Kleber M, Torn MS, Jahn R. 2006. Stabilization of soil organic matter, Association with minerals or chemical recalcitrance? *Biogeochemistry*, **77**(1): 25-56.

Minasny B, McBratney AB. 2008. Regression rules as a tool for predicting soil properties from infrared reflectance spectroscopy. *Chemometrics and Intelligent Laboratory Systems*, **94**(1): 72–79.

Mishra U, Lai R, et al. 2010. Predicting the spatial variation of the soil organic carbon pool at a regional scale. *Soil Science Society of America Journal*, **74**(3): 906-914.

Moni C, Rumpel C, Virto I, Chabbi A, Chenu C. 2010. Relative importance of sorption versus aggregation for organic matter storage in subsoil horizons of two contrasting soils. *European Journal of Soil Science*, **61**: 959-969.

Montgomery DR. 2007. Soil erosion and agricultural sustainability. *Proceedings of the National Academy of Sciences of the United States of America,* **104**(33): 13268-13272.

Moulin AP, Anderson DW, et al. 1994. Spatial variability of wheat yield, soil properties and erosion in hummocky terrain. *Canadian Journal of Soil Science*, **74**(2): 219-228.

Mulder VL, de Bruin S, et al. 2011. The use of remote sensing in soil and terrain mapping - A review. *Geoderma***, 162**(1-2): 1-19.

Muneer M and Oades JM. 1989. The role of Ca-organic interactions in soil aggregate stability. III. Mechanisms and models. *Australian Journal of Soil Research*, **27**(2): 411-423.

Myers N. 1993. Gaia: An Atlas of Planet Management. Anchor Press: Garden City.

Nadeu E, Berhe AA, De Vente J, Boix-Fayos C. 2012. Erosion, deposition and replacement of soil organic carbon in Mediterranean catchments: A geomorphological, isotopic and land use change approach. *Biogeosciences*, **9**(3): 1099-1111.

National Land and Water Resources Audit (NLWRA). 2001. Australian Agriculture Assessment 2001. Available at: http://www.anra.gov.au/topics/agriculture/pubs/national/agriculture_soil_erosion.html.

Nearing MA. 1997. A single, continuous function for slope steepness influence on soil loss. *Soil Science Society of America Journal*, **61**(3): 917-919.

Noorbakhsh S, Schoenau J, et al. 2008. Soil properties, yield, and landscape relationships in south-central Saskatchewan Canada. *Journal of Plant Nutrition*, **31**(3): 539-556.

Nusser SM, Goebel JJ. 1997. The National Resources Inventory: A Long-Term Multi-Resource Monitoring Programme. *Environmental and Ecological Statistics*, **4**(3): 181-204.

Oades JM. 1984. Soil Organic-Matter and Structural Stability - Mechanisms and Implications for Management. *Plant and Soil*, **76**(1-3): 319-337.

Ogle SM, Breidt FJ, et al. 2007. An empirically based approach for estimating uncertainty associated with modelling carbon sequestration in soils. *Ecological Modelling*, **205**(3-4): 453-463.

Oldeman LR, Hakkeling RTA, Sombroek WG. 1991. World Map of the Status of Human-Induced Soil Degradation: An Explanatory Note. ISRIC. Wageningen and United Nations Programme, Nairobi.

O'Rourke SM, Holden NM. 2011. Optical sensing and chemometric analysis of soil organic carbon – A cost effective alternative to conventional laboratory methods? *Soil Use and Management*, **27**: 143-155.

Osterkamp WR, Hupp CR, Stoffel M. 2012. The interactions between vegetation and erosion: new directions for research at the interface of ecology and geomorphology. *Earth Surface Processes and Landforms*, **37**(1): 23-26.

Parsons AJ, Wainwright J, Powell DM, Kaduk J, Brazier RE. 2004. A conceptual model for determining soil erosion by water. *Earth Surface Processes and Landforms*, **29**(10): 1293-1302.

Parton WJ, Stewart JWB, Cole CV. 1988. Dynamics of C, N, P and S in grassland soils – A model. *Biogeochemistry*, **5**(1): 109-131.

Parton WJ, Schimel DS, et al. 1987. Analysis of factors controlling soil organic matter levels in Great Plains grasslands. *Soil Science Society of America Journal*, **51**(5): 1173-1179.

Paul EA, Morris SJ, Boehm S. 2001. The determination of soil C pool sizes and turnover rates: Biophysical Fractionation and Tracers. In: Assessment Methods for Soil Carbon (Advances in Soil Science). (eds Lal R, Kimble JM, Follett RF, Stewart BA), pp 193-206, CRC Press LLC, Boca Raton.

Paustian K, Cole CV, Sauerbeck D, Sampson N. 1998. CO2 mitigation by agriculture: An overview. *Climatic Change*, **40**(1): 135-162.

Peeters A. 2010. Country pasture / forage resource profile for Belgium. FAO, AGPC. Available at: http://www.fao.org/ag/AGP/AGPC/doc/Counprof/Belgium/belgium.htm.

Pimentel D, Harvey C, Resosudarmo P, Sinclair K, Kurz D, Mcnair M, Crist S, Shpritz L, Fitton L, Saffouri R, Blair R. 1995. Environmental and economic costs of soil erosion and conservation benefits. *Science*, **267**(5201): 1117-1123.

Pimentel D. 2000. Soil erosion and the threat to food security and the environment. *Ecosystem Health*, **6**(4): 221-226.

Pimentel D. 2006. Soil Erosion: A Food and Environmental Threat. *Environment, Development and Sustainability*, **8**: 119-137.

Pinheiro-Dick D and Schwertmann U. 1996. Microaggregates from Oxisols and Inceptisols, Dispersion through selective dissolutions and physicochemical treatments. *Geoderma*, **74**(1-2): 49-63.

Poesen JW, Torri D, Bunte K. 1994. Effects of rock fragments on soil erosion by water at different spatial scales – A review. *Catena*, **23**(1-2): 141-166.

Poesen J, Vandaele K, Van Wesemael B. 1996. Contribution of gully erosion to sediment production on cultivated lands and rangelands. In *Erosion and Sediment Yield:* Global and Regional Perspectives (Proceedings of the *Exeter Symposium.* July *1996*). IAHS Publ. no. 236.

Pulleman MM, Six J, van Breemen N, Jongmans AG. 2005 Soil organic matter distribution and microaggregate characteristics as affected by agricultural management and earthworm activity. *European Journal of Soil Science*, **56**(4): 453-467.

Quine TA, Van Oost K. 2007. Quantifying carbon sequestration as a result of soil erosion and deposition: retrospective assessment using caesium-137 and carbon inventories. *Global Change Biology*, **13**(12): 2610-2625.

Quine TA and Zhang Y. 2002. An investigation of spatial variation in soil erosion, soil properties, and crop production within an agricultural field in Devon, United Kingdom. *Journal of Soil and Water Conservation*, **57**(1): 55-65.

Quinlan JR. 1993. Combining instance-based and model-based learning. p. 236–243. *In* Proceedings of the Tenth International Conference on Machine Learning.

Quinton JN, Govers G, Van Oost K, Bardgett RD. 2010. The impact of agricultural soil erosion on biogeochemical cycling. *Nature Geoscience*, **3**(5): 311-314.

Rabbi FSM, Lockwood PV, Daniel H. 2010. How do microaggregates stabilize soil organic matter? 19th World Congress of Soil Science, Soil Solutions for a Changing World 1 – 6 August 2010, Brisbane, Australia. available at: http://www.iuss.org/19th_WCSS/Symposium/pdf/1617.pdf].

Ramankutty N and Foley JA. 1999. Estimating historical changes in global land cover: Croplands from 1700 to 1992. *Global Biogeochemical Cycles*, **13**(4): 997-1027.

Rawls WJ, Pachepsky YA, Ritchie JC, Sobecki TM, Bloodworth H. 2003. Effect of soil organic carbon on soil water retention. *Geoderma*, **116**: 61-76.

R Development Core Team. 2010. R: A Language and Environment for Statistical Computing. R Foundation for Statistical Computing. URL, http,//www.r-project.org [accessed November 2011.

Rees RM, Bingham IJ, Baddeley JA, Watson CA. 2005. The role of plants and land management in sequestering soil carbon in temperate arable and grassland ecosystems. *Geoderma*, **128**(1–2): 130-154.

Renard KG, Freimund JR. 1994. Using Monthly Precipitation Data to Estimate the R-Factor in the Revised USLE. *Journal of Hydrology*, **157**(1-4): 287-306.

Ritchie JC and McHenry JR. 1990. Application of radioactive fallout cesium-137 for measuring soil-erosion and sediment accumulation rates and patterns – a review. *Journal of Environmental Quality*, **19 :** 215–233.

Robert M and Tessier D. 1974. Méthode de préparation des argiles des sols pour des études minéralogiques. *Annals of Agronomy*. **25**: 859–882.

Rommens T, Verstraeten G, Poesen J, Govers G, Van Rompaey A, Peeters I, Lang A. 2005. Soil erosion and sediment deposition in the Belgian loess belt during the Holocene, establishing a sediment budget for a small agricultural catchment. *Holocene*, **15**(7): 1032-1043.

Rosenbloom NA, Harden JW, Neff JC, Schimel DS. 2006. Geomorphic control of landscape carbon accumulation. *Journal of Geophysical Research-Biogeosciences*, **111**(G01004), doi:10.1029/2005JG000077.

Rossel RAV. and Chen C. 2011. Digitally mapping the information content of visible-near infrared spectra of surficial Australian soils. *Remote Sensing of Environment*, **115**(6): 1443-1455.

Rumpel C and Koegel-Knabner I. 2011. Deep soil organic matter-a key but poorly understood component of terrestrial C cycle. *Plant and Soil*, **338**(1): 143-158.

Rustad LE, Campbell JL, et al. 2001. A meta-analysis of the response of soil respiration, net nitrogen mineralization, and aboveground plant growth to experimental ecosystem warming. *Oecologia*, **126**(4): 543-562.

Salomé C, Nunan N, Pouteau V, Lerch TZ, Chenu C. 2010. Carbon dynamics in topsoil and in subsoil may be controlled by different regulatory mechanisms. *Global Change Biology*, **16**(1): 416-426.

Sanchez PA, Ahamed S, Carré F, Hartemink AE, Hempel J, Huising J, Lagacherie P, McBRatney AB, McKenzie NJ, De Lourdes Mendonca-Santos M, Minasny B, Vågen TG, Vanlauwe B, Walsh MG, Winowiecki LA, Zhang GL. 2009. Digital soil map of the world. *Science*, **325**(5941): 680-681.

Savitzky A, Golay MJE. 1964. Smoothing and differentiation of data by simplified least squares procedures. *Analytical Chemistry*, **36**(8): 1627–1639.

Schjønning P, Thomsen IK, Møberg JP, De Jonge H, Kristensen K, Christensen BT. 1999. Turnover of organic matter in differently textured soils I. Physical characteristics of structurally disturbed and intact soils. *Geoderma*, **89**(3-4): 177-198.

Schmidt MWI, Torn MS, Abiven S, Dittmar T, Guggenberger G, Janssens IA, Kleber M, Koegel-Knabner I, Lehmann J, Manning DAC, Nannipieri P, Rasse DP, Weiner S, Trumbore SE. 2011. Persistence of soil organic matter as an ecosystem property. *Nature*, **478**(7367): 49-56.

Schmidt MWI, Gleixner G. 2005. Carbon and nitrogen isotope composition of bulk soils, particle-size fractions and organic material after treatment with hydrofluoric acid. *European Journal of Soil Science*, **56**(3): 407-416.

Schneckenberger K, Kuzyakov Y. 2007. Carbon sequestration under Miscanthus in sandy and loamy soils estimated by natural C-13 abundance. *Journal of Plant Nutrition and Soil Science*, **170**(4): 538-542.

Schnitzer M and Kodama H. 1992. Interactions between organic and inorganic components in particle-size fractions separated from four soils. *Soil Science Society of America Journal*, **56**: 1099-1105.

Schwanghart W and Jarmer T. 2011. Linking spatial patterns of soil organic carbon to topography - A case study from south-eastern Spain. *Geomorphology*, **126**(1-2): 252-263.

Schwarzenbach RP, Gschwend PM, Imboden DM. 1993. Environmental organic chemistry. New York, Wiley. 1000p.

Schuppli PA, Ross GJ, McKeague JA. 1983. The effective removal of suspended materials from pyrophosphate extracts of soils from tropical and temperate regions. *Soil Science Society of America Journal*, **47**: 1026-1032.

Schwertmann U, Süsser P, Nätscher L. 1987. Protonenpuffersubstanzen in Böden. *Journal of Plant Nutrition and Soil Science*, **144**: 289-305.

Seaber PR, Kapinos FP, Knapp GL. 1987. Hydrologic Unit Maps. U.S. Geological Survey Water-Supply Paper 2294.

Seybold CA, Mausbach MJ, Karlen DL, Rogers HH. 1997. Quantification of Soil Quality, In: Lal R, Kimble JM, Follett RF, Stewart BA. (eds.): Soil Processes and the Carbon Cycle, *Advances in Soil Sciences*: 387-404. CRC Press LLC.

Sherrod LA, Dunn G, Peterson GA, Kolberg RL. 2002. Inorganic Carbon Analysis by Modified Pressure-Calcimeter Method. *Soil Science Society of America Journal*, **66**: 299-305.

Singh N, Abiven S, Torn MS, Schmidt MWI. 2012. Fire-derived organic carbon in soil turns over on a centennial scale. *Biogeosciences*, **9**: 2847-2857.

Six J, Conant RT, Paul EA, Paustian K. 2002. Stabilization mechanisms of soil organic matter, Implications for C-saturation of soils. *Plant and Soil*, **241**(2): 155-176.

Six J, Guggenberger G, Paustian K, Haumaier L, Elliot ET, Zech W. 2001. Sources and composition of soil organic matter fractions between and within soil aggregates. *European Journal of Soil Science*, **52**(4): 607-618.

Six J, Elliott ET, Paustian K. 2000. Soil macroaggregate turnover and microaggregate formation: a mechanism for C sequestration under no-tillage agriculture. *Soil Biology & Biochemistry*, **32(**14): 2099-2103.

Six J, Elliott ET, Paustian K, Doran JW. 1998. Aggregation and soil organic matter accumulation in cultivated and native grassland soils. *Soil Science Society of America Journal*, **62**(5): 1367-1377.

Sleutel S, De Neve S, Singier B, Hofman G. 2007. Quantification of organic carbon in soils: A comparison of methodologies and assessment of the carbon content of organic matter. *Communications in Soil Science and Plant Analysis*, **38**: 2647-2657.

Smith P, Davies CA, Ogle S, Zanchi G, Bellarby J, Bird N, Boddey RM, McNamara NP, Powlson D, Cowie A, Van Noordwijk M, Davis SC, Richter DDB, Kryzankowski L, Van Wijk MT, Stuart J, Kirston A, Eggar D, Newton-Cross G, Adhya TK, Braimoh AK. 2012. Towards an integrated global framework to assess the impacts of land use and management change on soil carbon: Current capability and future vision. *Global Change Biology*, **18**(7): 2089-2101.

Smith P. 2008. Land use change and soil organic carbon dynamics. 2008. *Nutrient Cycling in Agroecosystems*, **81**(2): 169-178.

Smith P, Fang C, Dawson JJC, Moncrieff JB. 2008. Impact of Global Warming on Soil Organic Carbon. *Advances in Agronomy*, **97**: 1-43.

Smith SV, Sleezer RO, Renwick WH, Buddemeier RW. 2005. Fates of eroded soil organic carbon: Mississippi basin case study. *Ecological Applications*, **15**(6): 1929-1940.

Smith KA, Ball T, Conen F, Dobbie KE, Massheder J, Rey A. 2003. Exchange of greenhouse gases between soil and atmosphere: interactions of soil physical factors and biological processes. *European Journal of Soil Science*, **54**(4): 779-791.

Smith SV, Renwick WH, Buddemeier RW, Crossland CJ. 2001. Budgets of Soil Erosion and Deposition for Sediments and Sedimentary Organic Carbon Across the Conterminous Unites States. *Global Biogeochemical Cycles*, **15**: 698-707.

Smola AJ, Schölkopf B. 2004. A tutorial on support vector regression. *Statistics and Computing*, **14**(3): 199–222.

Soil Survey Staff. 2010. Keys to Soil Taxonomy. Eleventh ed. USDA - Natural Resources Conservation Services, Washington, DC.

Sollins P, Kramer MG, Swanston C, et al. 2009. Sequential density fractionation across soils of contrasting mineralogy: evidence for both microbial- and mineral-controlled soil organic matter stabilization. *Biogeochemistry*, **96**(1-3): 209-231.

Sollins P, Swanston C, Kleber M, et al. 2006, Organic C and N stabilization in a forest soil, Evidence from sequential density fractionation. *Soil Biology & Biochemistry*, **38**(11): 3313-3324.

Sollins P, Homann P, Caldwell BA. 1996. Stabilization and destabilization of soil organic matter: mechanisms and controls. *Geoderma*, **74**: 65-105.

Sposito G. (ed). 2008. The Chemistry of Soils. Oxford University Press, New York. 329pp.

Stallard RF. 1998. Terrestrial sedimentation and the carbon cycle: Coupling weathering and erosion to carbon burial. *Global Biogeochemical Cycles*, **12**(2): 231-257.

Steegen A, Govers G, Taken I, Nachtergaele J, Poesen J, Merckx R. 2001. Factors controlling sediment and phosphorus export from two Belgian agricultural catchments. *Journal of Environmental Quality*, **30**(4): 1249-1258.

Stern R, Ben-Hur M, Shainberg I. 1991. Clay mineralogy effect on rain infiltration, seal formation and soil losses. *Soil Science*, **152**: 455-462.

Stevens A, Udelhoven T, et al. 2010. Measuring soil organic carbon in croplands at regional scale using airborne imaging spectroscopy. *Geoderma*, **158**(1-2): 32-45.

Stewart CE, Paustian K, et al. 2007. Soil carbon saturation: Concept, evidence and evaluation. Biogeochemistry, **86**(1): 19-31.

Stucki JW, Goodman BA, Schwertmann U. 1988. Iron in Soils and Clay Minerals. Springer, Dordrecht, 893 p.

Süsser P and Schwertmann U. 1991. Proton buffering in mineral horizons of some acid forest soils. *Geoderma*, **49**: 63-76.

Suuster E, Ritz C, et al. 2012. Modelling soil organic carbon concentration of mineral soils in arable land using legacy soil data. *European Journal of Soil Science*, **63**(3): 351-359.

Syvitski JPM, Vorosmarty CJ, Kettner AJ, Green P. 2005. Impact of humans on the flux of terrestrial sediment to the global coastal ocean. *Science*, **308**(5720): 376-380.

Tipping E. 1981. The adsorption of aquatic humic substances by iron oxides. *Geochimica et Cosmochimica Acta*, **45**(2): 191-199.

Tisdall JM, Oades JM. 1982. Organic matter and water-stable aggregates in soils. *Journal of Soil Science*, **33**(2): 141-163.

Tiunov AV. 2007. Stable isotopes of carbon and nitrogen in soil ecological studies. *Biology Bulletin*, **34**(4): 395-407.

Thomsen IK, Schjønning P, Olesen JE, Christensen BT. 2003. C and N turnover in structurally intact soils of different texture. *Soil Biology and Biochemistry*, **35**(6): 765-774.

Torn MS, Trumbore SE, Chadwick OA, Vitousek PM, Hendricks DM. 1997. Mineral control of soil organic carbon storage and turnover. *Nature*, **389**(6647): 170-173.

Totsche KU, Rennert T, Gerzabek MH, Koegel-Knabner I, Smalla K, Spiteller M, Vogel HJ. 2010. Biogeochemical interfaces in soil, The interdisciplinary challenge for soil science. *Journal of Plant Nutrition and Soil Science*, **173**(1): 88-99.

Trumbore S. 2009. Radiocarbon and Soil Carbon Dynamics. *Annual Review of Earth and Planetary Sciences*, **37**: 47-66.

Trumbore SE, Czimczik CI. 2008. Geology - An uncertain future for soil carbon. *Science*, **321**(5895): 1455-1456.

U.S. Department of Agriculture. 2000. Summary Report: 1997 National Resources Inventory (revised December 2000). Natural Resources Conservation Service, Washington, DC, and Statistical Laboratory, Iowa State University, Ames, Iowa.

U.S. Geological Survey. 1996. GTOPO30 Global 30 Arc-Second Elevation Data Set. EROS Data Center (EDC) Distributed Active Archive Center (DAAC), Sioux Falls. Available at: http://edcdaac.usgs.gov/gtopo30/gtopo30.html.

Valentin C, Agus F, Alamban R, Boosaner A, Bricquet JP, Chaplot V, De Guzman T, De Rouw A, Janeau JL, Orange D, Phachomphonh K, Do Duy Phai, Podwojewski P, Ribolzi O, Silvera N, Subagyono K, Thiébaux JP, Tran Duc Toan, Vadari T. 2008. Runoff and sediment losses from 27 upland catchments in Southeast Asia: Impact of rapid land use changes and conservation practices. *Agriculture, Ecosystems and Environment,* **128**: 225-238.

Van de Vreken P, Beckers V, Jacxsens P, Van Meirvenne M, Van Orshoven J. 2011. Historiek van de bodemdatabank Aardewerk-Vlanderen-2010. 152p.

Vandenbygaart AJ, Kroetsch D, et al. 2012. Soil C erosion and burial in cropland. *Global Change Biology*, **18**(4): 1441-1452.

Van Hemelryck H, Govers G, Van Oost K, Merckx R. 2011. Evaluating the impact of soil redistribution on the in situ mineralization of soil organic carbon. *Earth Surface Processes and Landforms,* **36**(4): 427-438.

Van Oost K, Verstraeten G, Doetterl S, Notebaert B, Wiaux F, Broothaerts N, Six J. 2012. Eroding the C cycle, the legacy of human-induced C erosion and burial on soil-atmosphere C exchange. *Proceedings of the National Academy of Sciences of the United States of America*, **109**(47): 19492-7.

Van Oost K, Cerdan O, Quine TA. 2009. Accelerated sediment fluxes by water and tillage on European agricultural land. *Earth Surface Processes and Landforms*, **34**(12): 1625-1634.

Van Oost K, Quine TA, Govers G, DeGryze S, Six J, Harden JW, Ritchie JC, McCarty GW, Heckrath G, Kosmas C, Giraldez JV, Da Silva JRM, Merckx R. 2007. The impact of agricultural soil erosion on the global carbon cycle. *Science*, **318**(5850): 626-629.

Van Oost K, Govers G, De Alba S, Quine TA. 2006. Tillage erosion: A review of controlling factors and implications for soil quality. *Progress in Physical Geography*, **30**(4): 443-466.

Van Oost K, Govers G, Quine TA, Heckrath G, Olesen JE, DeGryze S, Merckx R. 2005a. Landscape-scale modeling of carbon cycling under the impact of soil redistribution: The role of tillage erosion. *Global Biogeochemical Cycles*, **19**(GB4014), doi:10.1029/2005GB002471.

Van Oost K, Quine TA, Govers G, Heckrath G. 2005b. Modelling soil erosion induced carbon fluxes between soil and atmosphere on agricultural land using SPEROS-C. In Roose EJ, Lal R, Feller C, Barthes B, Stewart BA (eds.) Advances in soil science – Soil erosion and carbon dynamics. CRC Press, Boca Raton. pp. 37-51.

Van Oost K, Govers G, Desmet P. 2000. Evaluating the effects of changes in landscape structure on soil erosion by water and tillage. *Landscape Ecology*, **15**: 577-589.

Van Orshoven J, Deckers JA, Vandenbroucke D, Feyen J. 1993. The completed database of Belgian soil profile data and its applicability in planning and management of rural land. *Bulletin des Recherches Agronomiques de Gembloux*, **28**(2-3): 193-212.

Van Orshoven J, Maes J, Vereecken H, Feyen J, Dudal R. 1988. A structured database of Belgian soil profile data, *Pedologie*, **38**(2): 191:206.

Van Ranst E, De Coninck F, Tavernier R, Langohr R. 1982. Mineralogy in silty to loamy soils of central and high Belgium in respect to autochthonous and allochthonous materials. *Bulletin de la Société Belge de Géologie*, **91**: 27-44.

Van Rompaey AJJ, Govers G. 2002. Data quality and model complexity for regional scale soil erosion prediction. *International Journal of Geographical Information Science*, **16**(7): 663-680.

Van Wesemael B, Paustian K, Meersmans J, Goidts E, Barancikova G, Easter M. 2010. Agricultural management explains historic changes in regional soil carbon stocks. *Proceedings of the National Academy of Sciences of the United States of America*, **107**(33): 14926-14930.

Verheijen FGA, Jones RJA, Rickson RJ, Smith CJ. 2009. Tolerable versus actual soil erosion rates in Europe. *Earth-Science Reviews*, **94**(1-4): 23-38.

Viscarra Rossel RA, Behrens T. 2010. Using data mining to model and interpret soil diffuse reflectance spectra. *Geoderma*, **158**(1-2): 46–54.

Von Luetzow M, Koegel-Knabner I, Ekschmitt K, Flessa H, Guggenberger G, Matzner E, Marschner B. 2007. SOM fractionation methods, Relevance to functional pools and to stabilization mechanisms. *Soil Biology & Biochemistry*, **39**(9): 2183-2207.

Von Luetzow M, Koegel-Knabner I, Ekschmitt K, Matzner E, Guggenberger G, Marschner B, Flessa H. 2006. Stabilization of organic matter in temperate soils, mechanisms and their relevance under different soil conditions - a review. *European Journal of Soil Science*, **57**(4): 426-445.

Walkley A and Black IA. 1934. An examination of the Degtjareff method for determining soil organic matter and a proposed modification of the chromic acid titration method. *Soil Science*, **37**: 29-37.

Walling DE. 2009. The Impact of Global Change on Erosion and Sediment Transport by Rivers: Current Progress and Future Challenges. Scientific Paper for the UNESCO-IHP International Sediment Initiative (ISI). UNESCO: France.

Wagai R and Mayer LM. 2007. Sorptive stabilization of organic matter in soils by hydrous iron oxides. *Geochimica et Cosmochimica Acta*, **71**(1): 25-35.

Walling DE, Webb BW. 1996. Erosion and sediment yield: A global overview. In Erosion and Sediment Yield: Global and Regional Perspectives (Proceeding of the Exeter Symposium, July 1996), IAHS. No. 236.

Walling DE, Webb BW. 1983. Patterns of sediment yield. In: Gregory KJ (ed). Background to palaeohydrology. Wiley: Chichester: 69-100.

Wang Z. 2011. Towards a better understanding of the fate of carbon mobilized by erosion. KUL, Leuven. Dissertation. 130pp.

Wang Z, Govers G, Steegen A, Clymans W, Van den Putte A, Langhans C, Merckx R, Van Oost K. 2010. Catchment-scale carbon redistribution and delivery by water erosion in an intensively cultivated area. *Geomorphology*, **124**(1-2): 65-74.

Wang Y, Amundson R, et al. 2000. Seasonal and altitudinal variation in decomposition of soil organic matter inferred from radiocarbon measurements of soil CO2 flux. *Global Biogeochemical Cycles*, **14**(1): 199-211.

Weiss A. 2001. Topographic Position and Landforms Analysis. ESRI User Conference, San Diego, CA.

Wetterlind J, Stenberg B. Near-infrared spectroscopy for within-field soil characterization: Small local calibrations compared with national libraries spiked with local samples. *European Journal of Soil Science*, **61**(6): 823-843.

Wilkinson BH and McElroy BJ. 2007. The impact of humans on continental erosion and sedimentation. *Geological Society of America Bulletin*, **119**(1-2): 140-156.

Wischmeier WH, Smith DD. 1978. Predicting rainfall erosion losses - A guide to conservation planning, United States Department of Agriculture, Agricultural Handbook 537.

Wold S, Sjöström M, Eriksson L. 2001. PLS-regression: a basic tool of chemometrics. *Chemometrics and Intelligent Laboratory Systems*, 58(2): 109–130.

Wouters, L., Vandenberghe, N. 1994. Géologie de la Campine. Essai de synthèse, ONDRAF.

Xenakis G, Ray D, Mencuccini M. 2008. Sensitivity and uncertainty analysis from a coupled 3-PG and soil organic matter decomposition model. *Ecological Modelling*, **219**: 1-16.

Xu HM, Jia HK, et al. 2005. A simulation model of net primary production at watershed scale in hilly area of Loess Plateau, China. *Acta Ecologica Sinica*, **25**(5): 1064-1074.

Yan FL, Shi ZH, et al. 2010. Wetting Rate and Clay Content Effects on Interrill Erosion in Ultisols of Southeastern China. *Pedosphere*, **20**(1): 129-136.

Yang DW, Kanae S, Oki T, Koike T, Musiake K. 2003. Global potential soil erosion with reference to land use and climate changes. *Hydrological Processes*, **17**(14): 2913-2928.

Yoo K, Amundson R, Heimsath AM, Dietrich WE. 2005. Erosion of upland hillslope soil organic carbon: Coupling field measurements with a sediment transport model. *Global Biogeochemical Cycles*, **19**(GB3003), doi:10.1029/2004GB002271.

Yoo K, Amundson R, Heimsath AM, Dietrich WE. 2006. Spatial patterns of soil organic carbon on hillslopes: Integrating geomorphic processes and the biological C cycle. *Geoderma*, **130**(1-2): 47-65.

Yu YY, Finke PA, WU HB, Guo ZT. 2013. Sensitivity analysis and calibration of a soil carbon model (SoilGen2) in two contrasting loess forest soils. *Geoscientific Model Development*, **6**: 29-44.

Zadorova T, Penizek V, Sefrna L, Rohoskova M, Boruvka L. 2011. Spatial delineation of organic carbon-rich Colluvial soils in Chernozem regions by Terrain analysis and fuzzy classification. *Catena*, **85**(1): 22-33.

Zhang S, Huang Y, et al. 2012. Spatial prediction of soil organic matter using terrain indices and categorical variables as auxiliary information. *Geoderma*, **171-172**: 35-43.

Zhang L, Zeng G, Tong C. 2011. A review on the effects of biogenic elements and biological factors on wetland soil carbon mineralization. *Shengtai Xuebao/ Acta Ecologica Sinica*, **31**(18): 5387-5395.

Ziegler A and Nogareda JS. 2009. Environmental management systems and technological environmental innovations: Exploring the causal relationship. *Research Policy*, **38**(5): 885-893.

Zuo X, Zhao X, et al. 2012. Scale dependent effects of environmental factors on vegetation pattern and composition in Horqin Sandy Land, Northern China. *Geoderma*, **173-174**: 1-9.

10 List of figures

Figure 1: The global carbon cycle in the 1990s. Units are in Pg C or Pg C yr^{-1}. Taken from Hougton (2007). 12

Figure 2: Box model concept of variables affecting SOC stability. To be viewed from center to periphery. Each level represents a different set of controls with decreasing direct influence on carbon stability. 14

Figure 3: Overview of recent estimates of soil erosion as a sink or source for atmospheric C, relative to soil systems that are unaffected by soil redistribution. Ranges of estimates are taken from articles listed on the right end (sources) or left end (sinks) of each horizontal bar. 16

Figure 4: Study concept: Soil erosion modifies soil profiles and introduces large lateral soil fluxes along a geomorphic gradient. These fluxes must leave a "footprint" in the distribution as well as on the quality and quantity of SOC stocks. Under similar climate, land use and pedology, topographical features determine SOC distribution and development. 20

Figure 5: Complete flow chart of the research project. 23

Figure 6: Scatter plots of erosion controlling factors derived from NRI and global databases. Data is aggregated at the HUC4 watershed level. 34

Figure 7: Scatter plots of NRI- and modeled water erosion estimates for US cropland and pastures. 37

Figure 8: Scatter plots of water erosion estimates taken from the Cerdan et al. (2010) study and modeled estimates for European cropland. Data is aggregated on a regular grid, using the mean HUC4 area estimate for the conterminous USA. 38

Figure 9: (a) Estimated water and tillage erosion rates for global cropland for the year 2000. (b) Estimated water erosion rates for global pastures for the year 2000. Only pastures in dry environments are considered to erode. 40

Figure 10: Frequency distributions of soil erosion and soil production derived from point observations (Montgomery 2007) and the estimates of cropland water erosion presented in this approach for the year 2000. 42

Figure 11: Simulated changes in topsoil SOC contents due to soil erosion for the period 2000–2050. Gains are related due to the inclusion of carbon rich subsoil. 45

Figure 12: Soil texture zones distributed on Luxembourg cropland (A), the location of study transect and study sites (B) and a conceptual view on the sampling design as well as typical horizontation as found in hillslope studies on cropland (C). 52

Figure 13:Mean SOC stocks for the two different soil texture zones and for different depths as derived from the profile data. Vertical bars represent the standard deviation from the mean in absolute numbers, numbers in percentage the relative standard deviation from the mean 59

Figure 14:Calibration points of predicted versus observed SOC stocks for the different depths and texture zones. The rRMSE values refer to results using the validation data. 60

Figure 15:Frequency (in % of data) histograms of the regional SOC stock estimates for different depth layers using the model structure presented here and HRS topsoil SOC data for the cropland covered by HRS. The data shows pronounced differences in SOC distribution for the deeper subsoil between the two regions. 64

Figure 16: Relative SOC stock differences of slope (eroding) and foothill/valley bottom (depositional) positions to the local stable plateau profile showing the variable impact of soil redistribution on SOC deposition (clay zones, deep soils) and strong erosion/ depletion on steep slopes (loam zones, deep soil). Same letter above nods indicate no significant difference in SOC stocks between eroding and depositional soil layers. ($p < 0.05$, tested separately for both texture zones and soil layers). 66

Figure 17:The study area in relation to its position in the Belgium Loambelt, its cropland coverage and the position of sampled soil profiles. 75

Figure 18:Illustration of the work steps for acquiring undisturbed samples for continuous spectroradiometric measurements; 1: Soil sampling with closed sampling systems; 2-4: Polishing and flattening of the soil surface of the sampled cores after the core has been dried; 5: Visual description of soil features and artifacts of the sample preparation. 76

Figure 19: Predicted versus observed SOC content (g C kg^{-1}) as produced by the best spectroscopic model. 79

Figure 20:Two soil cores with variable features and illustrating the precision and accuracy of the method. Figure 20a represents a complex profile covering C depleted (25-34cm; 65-87cm) and SOC enriched (0-25cm; 34-65cm) layers and rapid changes between loamy (0-65cm) and sandy soil textures (65-87cm). Figure 20b represents a profile with sharp boundaries between the Ap layer (0-24cm) and a redoximorphic loamy subsoil layer (24-66cm). 80

Figure 21: Nominal ranking of the defined topographic classes in terms of the dominating regime of soil redistribution. Profiles in the concave footslopes can be both in an eroding or depositing regime, depending on local site characteristics. 87

Figure 22:Mean SOC depth distribution in the AW database (Figure 22A) and the re-sampling campaign (Figure 22B) for each topographic class at the time of re-sampling. Vertical bars represent the standard error of the estimates. 88

Figure 23:Frequency distribution of slope steepness of the original and re-sampled Aardewerk profiles and Corine (100m res) – derived cropland in the research area. 90

Figure 24:Relationship of the Δ SOC with Δ Ap depth (Figure 24A) for all profiles in the Ap transition layer between 20-35cm soil depth and of the Δ SOC with soil texture (Figure 24B) for the layer 25-50cm soil depth in profiles at the convex slope shoulder ($p<0.05$). 92

Figure 25:Topographical transects and sampling point locations for both study sites. The soil profiles are classified according to IUSS Working Group WRB (2006). 96

Figure 26: Fractionation scheme used in the isolation of functional SOC fractions according to Six et al. (1998, 2002). 98

Figure 27: SOC depth distribution and stocks as a function of the geomorphic position. Significant differences between geomorphic positions for three depths (i.e., topsoil, subsoil, and total depth) are presented where the same letter indicates no significant difference between geomorphic positions ($p < 0.1$, tested for site 1 and 2 separately). 102

Figure 28: Observed respiration rates for top- and subsoil as a function of the geomorphic position (non-eroding, eroding and depositional). The respiration per unit soil (A) and per unit of C (B) is given. Same letter indicates no significant differences between different geomorphic positions for the two depth classes ($p < 0.1$, tested for Figure 28A & B separately). 104

Figure 29: Elemental and isotopic characterization of the measured SOC fractions. The key for the abbreviations is presented in Figure 26. Depth averaged values for C/N ratios and d13C for the measured SOC fractions indicate a clear distinction between non-hydrolyzable SOC fractions sources and other compartments. Same letter above bars indicate no significant differences between SOC fractions ($p < 0.1$, tested separated for both parameters and the different groups separated by the dashed lines). 105

Figure 30:Definition of the fast, intermediate and passive pools in relation to the measured functional SOC fractions. Note that non-hydrolyzable C from POM and mM fractions has not been isolated and is therefore not considered. 106

Figure 31: Distribution of SOC pools along the geomorphic gradient as a fraction of the total C in % (A) and absolute amount in g SOC per kg soil (B). Same letter indicates no significant differences between the pools and the geomorphic positions ($p < 0.1$, tested for Figure 31A & B and the top- and subsoil separately). 107

Figure 32:The changing contribution of different SOC fractions along the slope's subsoil. The fraction of microaggregate SOC (Figure 32A) and the contribution of silt associated SOC within this fraction (Figure 32C) and in the bulk silt and clay SOC (Figure 32D) is highest at depositional positions (high CSR values) while the non-aggregated SOC (Figure 32B) and clay associated SOC is highest at eroding sites (low CSR values). No such correlation was found for the slope's topsoil (data not shown). 108

Figure 33:Observed respiration per unit C in relation to the abundance of the fast pool (hydrolyzable macroaggregate C) for top- and subsoil (a) and in relation to the ratio of silt/clay associated C in microaggregates (b) and bulk silt & clay (c) in subsoils..... 112

Figure 34:Mean Residence Time (MRT) for the fast + intermediate SOC pools derived from the incubation experiments and SOC fractionation for top- and subsoils as a function of the geomorphic position (non-eroding, eroding, and depositional). The figure expresses the MRT relative to the MRT of the stable positions. Same letters indicates no significant differences between different positions for the two depth classes ($p < 0.1$). 113

Figure 35:Summary figure describing the geomorphic controls on SOC pool composition and C stabilization mechanisms in eroding landscapes (Results aggregated from both hillslopes). Processes indicated at the non-eroding positions take place along the whole transect..... 116

Figure 36:The distribution of pyrophosphate (I), oxalate (II) and dithionite (III) extractable Al, Mn and Fe between the Bulk soil and its compartments non-aggregated silt+clay (s+c) and aggregated silt+clay (s+cm). Same letter indicates no significant differences between the extracted element in the different SOC fractions ($p < 0.1$, tested for Figure I, II and III and the different elements separately as indicated by differences in font types). 126

Figure 37**:** Correlation between SOC in the bulk soil and pyrophosphate extractable Al (I), Mn (II) and Fe (III)..... 126

Figure 38:Clay spectra after preparation with Mg and Mg-ethylene glycol for the topsoil at the different slope positions. Horizontal black lines have been fitted through the kaolinite peak of the stable profile to ease the visualization of differences between the profiles. ++ indicate higher abundance, -- lower abundance of certain clay minerals in respect to the abundance at the plateau profile (+/-).. 129

Figure 39:Cumulative agricultural erosion (water+tillage) and temporal patterns for selected world regions (As calculated for Van Oost et al. 2012)..... 143

11 List of tables

Table 1: Comparison of global erosion estimates based on different methods taken from studies in the last two decades..... 26

Table 2: Step-wise linear regressions between NRI soil erosion estimates (A) and USLE factors aggregated at the HUC4 watershed level. R = rainfall erosivity factor, S=Slope percent, K= Soil erodibility factor, Cc= Crop cover factor, L=Slope length, P = support practice factor). Significance level p expressed as: 1% = **; not significant (p>0.1) = ^{ns}..... 32

Table 3: Cc factor estimates and differences in abundance for major croptypes..... 35

Table 4: Estimates for globally eroded sediment and linked SOC fluxes for cropland (C) and pastures (P) for the year 2000AD. Only Pastures in dry environments are considered to erode. 41

Table 5: Cropland C fluxes in the EU-25 compiled by Ciais et al. (2010) in relation to the estimate of C losses presented here due to erosion-induced dilution. 44

Table 6: Representativeness of US cropland and grasslands. 46

Table 7: Cropland area, mean slope of the research area and number of sampled profiles. Abbreviations for positions defined in Figure 12. 51

Table 8: Overview of the considered environmental covariates and their peculiarity. 55

Table 9: ^{137}Cs derived CV and SRI results for fields in the two different texture zones showing high rates of lateral soil fluxes transporting soil through the landscape. 59

Table 10: LMM performance parameters and SOC predictions for different depth layers..... 61

Table 11:Ranked explanatory variables for the SOC stocks of different depth layers in the two different texture zones. All variables are significant at p<0.05. Abbreviations: M=Mean; SD=Standard deviation; Nbh = Neighborhood. 62

Table 12: Running costs and time expenses for a traditional sampling campaign and a campaign using the proposed approach. Note the varying depth intervals between the low and high depth resolution scenario. $^{+}$ = Time is doubled as two operators are needed for field work. 82

Table 13: Mean slope steepness and depth of the plow layer in AW and the modern re-sampling campaign as well as soil texture distribution of the data. 89

Table 14:Study site description. Cumulative soil redistribution (CSR, cm), slope (%) and soil texture (% soil volume) values measured at different slope positions ranging from stable to eroding and depositional settings for site 1 and 2 (*=only one observation available). 101

Table 15:Significant correlations. Correlation coefficients of linear regressions between SOC concentration, soil depth or CSR and SOC parameters (**= p<0.05). 103

Table 16: Key soil properties and identified SOC fractions as described by Doetterl et al. (2012) for the investigated soils at different slope positions and soil depths. 124

Table 17:Total content in Ca, K, Mg, Na and Total Reserve in Bases (TRB) values for the different soil profiles and depths and the parent material. 125

Table 18:Correlations (Pearson r) between pyrophosphate extractable solid soil phases and soil SOC or soil depth (* = p <0.1; ** = p <0.05; *** p = <0.01) and the concentration range of the respective pyrophosphate extract.. 127

Table 19: Correlations (Pearson r) between oxalate extractable solid soil phases in the silt fractions and soil SOC or soil depth (* = p <0.1; ** = p <0.05; *** = p < 0.01) and the concentration range of the respective oxalate extract. 128